Eomesodermin governs the hemogenic competence of murine mesodermal progenitors



Luke Thomas Gilbert Harland

Sir William Dunn School of Pathology

University of Oxford

A thesis submitted for the degree of Doctor of Philosophy

Trinity College

Hilary Term 2020

For Gilbert Dickson Vinden,

your insatiable curiosity instilled in me a desire to pursue

a DPhil at Oxford in the biomedical sciences.

DECLARATION

I declare that the work presented in this thesis is my own unless otherwise stated. This thesis is based on an expanded version of a manuscript, written by myself in collaboration with Elizabeth J Robertson, Marella de Bruijn and Elizabeth K Bikoff, which is currently under review (see below). I have generated all the figures and performed all experiments and data analyses, except where indicated in figure legends and in the text.

Luke TG Harland, Claire S Simon, Anna D Senft, Ita Costello, Lucas Greder, Elizabeth K Bikoff, Catherine Porcher, Marella de Bruijn, Elizabeth J Robertson. The T-box transcription factor Eomesodermin governs hemogenic competence of yolk sac mesodermal progenitors.

ACKNOWLEDGEMENTS

I thank my gracious and knowledgeable supervisors, Elizabeth J. Robertson and Elizabeth K. Bikoff, for their constructive feedback and continuous support throughout my DPhil. You both provided me an optimal environment to develop as an independent scientist and for that I am truly grateful.

I would also like to thank all Robertson/Bikoff lab members, past and present, who created such an enjoyable and productive workplace. I am particularly thankful to Ita Costello, Claire Simon and Anna Senft for their mentorship, training and boundless excitement for the early mouse gastrula. I would also like to thank Maria-Eleni Xypolita and Thomas Clague for their help with mouse work and ChIP experiments. Finally, I am grateful to Arne Mould, Mubeen Goolam, Andrew Nelson, Andrew Robson, Alexandra Bisia and Jasha Trompf for their friendship and helpful feedback throughout my DPhil.

I thank my many collaborators in Oxford and Cambridge for their experimental advice and valuable discussions. I am particularly thankful to Marella de Bruijn for her sound advice and impressive knowledge of developmental haematopoiesis. I thank Ivan Imaz Rosshandler, John Marioni and Bertie Gottgens for help with scRNA-seq analyses. I thank Catherine Porcher and Doug Higgs for helpful feedback and encouragement. I also thank Michal Maj and Line Eriksen for help with FACS experiments and Joey Riepssame for advice regarding CRISPR-Cas9 targeting strategies. Finally, I thank the Wellcome Trust, Trinity College and the Clarendon Fund for their generous funding support.

I am thankful for the many friends from Trinity College and OUGC with whom I have enjoyed countless meals, convivial conversations and blustery rounds of golf. I am indebted to my parents Stephen and Rachel, my sister Victoria and my extended family including my in-laws (James and HA) who have all loved, supported and encouraged me. Finally, to my wife Emily Penner, you have been an endless source of comfort, joy and encouragement throughout my DPhil. We will always cherish this Oxford adventure that we have done, each step of the way, together. Your steadiness and love have carried me through.

ABSTRACT

During mouse gastrulation pluripotent epiblast cells traverse the primitive streak (PS) and diversify into mesoderm and endoderm subtypes. The T-box transcription factor Eomesodermin (Eomes) is expressed during PS formation and is critical for the development of the cardiac mesoderm and definitive endoderm lineages. The earliest wave of progenitors to traverse the posterior PS give rise to extraembryonic mesoderm (ExM) that differentiates into the endothelium and hematopoietic progenitors of the yolk-sac (YS). How a specific subset of ExM becomes committed to a hematopoietic fate remains unclear. Here we report that Eomes is transiently expressed in Flk-1+ ExM progenitors that generate virtually all YS hematopoietic and endothelial cells. Using an embryonic stem cell differentiation model of YS hematopoiesis, we find Eomes activity is essential for the production of primitive erythrocytes and pro-definitive hematopoietic progenitors but dispensable for the development of endothelial cells. Single-cell RNA-seq experiments demonstrate that in the absence of Eomes function Flk-1^{hi}/PdgfRa^{-} hematoendothelial progenitors are specified but fail to transition into hematopoietic cells.

Strikingly, Eomes regulates Runx1 expression in the hemogenic endothelial (HE) lineage. Furthermore, ATAC-seq experiments demonstrate that the accessibility of enhancers, that SCL normally utilizes to specify primitive blood cells, are governed by Eomes functional activity. ChIP-seq experiments suggest that Eomes coordinates the development of hematopoietic mesoderm in the context of Activin/Nodal and Tead-Yap signalling. Finally, the potencies of Eomes+ progenitors that arise during gastrulation remain ill-defined; therefore, I additionally generate two temporally regulatable Eomes.CreERT2 lines that will be used for clonal lineage tracing experiments in the future. Collectively, these results demonstrate that

Eomes promotes hemogenic competence of the YS mesodermal lineage by regulating Runx1 expression and SCL functional activity at the outset of gastrulation. These findings suggest that hemogenic competence is endowed earlier during murine embryogenesis than previously appreciated and have widespread implications for the generation of HE from pluripotent stem cell sources.

,

TABLE OF CONTENTS

Declaration ***2***

Acknowledgements ***3***

Abstract ***5***

List of Figures ***12***

List of Tables ***15***

Abbreviations ***16***

Chapter 1 : Introduction ***17***

1.1 Mouse Development **17**

1.1.1 Pre-Implantation Mouse Development 17

1.1.2 Post-Implantation Mouse Development 17

1.2 Experimental Approaches **19**

1.2.1 Embryonic Stem Cell Technology 19

1.2.2 Genome Wide Approaches 21

1.2.3 Lineage Tracing 22

1.3 Murine Gastrulation **24**

1.3.1 Cell Fate Allocation 24

1.3.2 Signals Driving Fate Decisions during Gastrulation 25

1.4 Developmental Hematopoiesis **26**

1.4.1 Waves of Hematopoiesis 26

1.4.2 Ontogeny of Hematopoietic Progenitors 27

1.4.2 Hemangioblast 28

1.4.4 Hemogenic Endothelium 29

1.5 Modelling Murine Hematopoiesis In Vitro 30

1.6 Essential Genes for Hematopoietic and Endothelial Development 31

1.6.1 Flk-1 32

1.6.2 ER71 32

1.6.3 SCL 33

1.6.4 Runx1 34

1.7 Eomesodermin 35

1.8 Aims of Thesis 37

Question #1: Is Eomes functionally required for the development of the extraembryonic mesodermal lineage? 37

Question #2: What is the transcriptional heterogeneity of Eomes expressing progenitors and what are their potencies during mouse gastrulation? 37

Chapter 2 : Eomes governs the hemogenic competence of mesodermal progenitors 39

2.1 Introduction 39

2.2 Results 40

2.2.1 Eomes, T and Flk-1 expression during mouse gastrulation 40

2.2.2 Eomes expressing cells give rise to ExM and YS hematopoietic and endothelial cells 43

2.2.3 Eomes is functionally required for ExM development *in vivo* 46

2.2.4 Eomes, Scl and Runx1 expression kinetics during hematovascular development 46

2.2.5 Eomes functional loss disrupts primitive and pro-definitive haematopoiesis 50

2.2.6 Transcriptional characterization of Flk-1/PdgfRa mesodermal populations generated in Eomes loss-of-function cultures 52
2.2.7 scRNA-seq analysis of Eomes mutant Flk-1^{hi}/PdgfRa^{-} *cells* 59
2.2.8 Eomes is non-essential for the expression of SCL during hematovascular development *in vitro* 64
2.2.9 Eomes is essential for the development of Runx1+ HE 67
2.2.10 Runx1 re-expression in Eomes-/- EHT cultures rescues EHT and the production of pro-definitive blood cells 71
2.2.11 Eomes influences chromatin accessibility at SCL bound enhancers in hematovascular mesoderm 75
2.2.12 Inspecting changes in chromatin accessibility in the Eomes-/- PdgfRa+ paraxial mesoderm population 78
2.2.13 Generating Eomes-V5 ESCs to identify Eomes genomic targets using ChIP-seq 82
2.2.14 Eomes, Tead4 and Smad2/3 bind regions transiently marked by H3K27Ac during early stages of hematopoieitc development 88
2.2.15 Comparing Eomes ChIP peaks with Eomes-dependent SCL bound cis-regulatory regions 90
2.2.16 The Generation of an Eomes$^{iCre\text{-}nLacZ}$ Reporter Allele 92
2.2.17 An Experimental System to Address the Timing of Eomes Activity During the Primitive and Definitive Waves of Hematopoiesis 95

2.3 Summary of Findings 98

Chapter 3 : transcriptional diversity and potency of Eomes expressing cells during gastrulation 101

3.1 Introduction 101

3.2 Results 102

3.2.1 Production of targeted ESCs for clonal lineage tracing of Eomes progenitors.... 102

3.2.2 Isolation of Eomes.GFP+ progenitors from mouse embryos 105

3.3 Summary of Findings 107

Chapter 4 : General Discussion.....108

4.1 Discussion and Future Work 108

4.1.1 Reconciling the differences between in vitro and in vivo Eomes loss-of-function experiments..... 108

4.1.2 Eomes sits upstream of SCL functional activity..... 109

4.1.3 Eomes regulates Runx1 expression in the HE lineage..... 111

4.1.4 Eomes is essential for the generation of primitive erythrocytes 112

4.1.5 Eomes binds cis-regulatory regions at the Runx1 locus and regulates the accessibility of Runx1 enhancers..... 113

4.1.6 A hemogenic signaling niche during gastrulation 114

4.1.7 A strategy to uncouple primitive and pro-definitive hematopoietic progenitors ... 115

4.1.8 Does Eomes regulate Runx1 expression in the HSC lineage?..... 116

4.1.9 Resolving the potencies of Eomes+ progenitors during gastrulation 116

4.1.10 Eomes and the development of paraxial meosderm 117

4.2 Concluding Remarks..... 118

Chapter 5 : Materials and Methods.....119

5.1 Methods..... 119

5.1.1 Mouse strains and genotyping 119

5.1.2 Immunostaining 120

5.1.3 Whole-mount in situ hybridization and LacZ staining 120

5.1.4 ESC maintenance and differentiation 121
5.1.5 CRISPR modification of ESCs 122
5.1.6 Hematopoietic progenitor colony assays 125
5.1.7 Flow cytometry, cell sorting and MACS 125
5.1.8 RNA isolation and quantitative RT-PCR 126
5.1.9 RNA-seq 126
5.1.10 RNA-seq analysis 127
5.1.11 scRNA-seq 127
5.1.12 scRNA-seq analysis 128
5.1.13 ATAC-seq 129
5.1.14 ATAC-seq analysis 130
5.1.15 ChIP-seq 131
5.1.16 ChIP-seq analysis 131
5.2 Materials 133
5.2.1 Antibodies 133
5.2.2 CRISPR Reagents 134
5.2.3 Primers 135
5.3 Gene Lists 136
5.3.1 scRNA-seq 136
5.3.2 ChIP-seq 137
References 138

LIST OF FIGURES

Figure 1.1 Mouse development: blastocyst to gastrulation 19

Figure 1.2 Mesodermal cell fate allocation during gastrulation 26

Figure 1.3 Multiple waves of hematopoiesis during mouse embryogenesis 28

Figure 1.4 Long and short mRNA Eomes isoforms 35

Figure 2.1 Eomes, T and Flk-1 expression patterns at the outset of mouse gastrulation..... 42

Figure 2.2 Eomes expressing progenitors generate YS mesodermal cells 44

Figure 2.3 Eomes.iCre+ progenitors generate YS endothelial and hematopoietic cells 45

Figure 2.4 Eomes, SCL and Runx1 expression kinetics during hematovascular development *in vitro* and *in vivo* 49

Figure 2.5 Eomes loss-of-function disrupts primitive and pro-definitive hematopoiesis 53

Figure 2.6 Eomes loss-of-function disrupts EHT 55

Figure 2.7 Comparing the transcriptional profiles of various Flk-1/PdgfRa mesodermal populations that form in wildtype and Eomes-loss-of-function EBs..... 57

Figure 2.8 Expression of *in vivo* cell type markers in Eomes-/- and WT day 4 Flk1/PdgfRa EB populations..... 58

Figure 2.9 scRNA-seq suggests that hematoendothelial progenitors are still specified in the absence of Eomes function but blood progenitors are lost 61

Figure 2.10 Mapping WT and Eomes-/- Flk1^{hi}/Pdgfra^{-} cells generated *in vitro* onto the *in vivo* mouse gastrulation atlas 63

Figure 2.11 Eomes-/- cells do not transition from hematoendothelial progenitors into blood progenitors..... 65

Figure 2.12 Eomes is not required for SCL expression 66

Figure 2.13 Eomes is required for the expression of Runx1 68

Figure 2.14 Eomes is essential for the generation of Runx1+ HE 70

Figure 2.15 Eomes is required cell autonomously for Runx1 expression..... 71

Figure 2.16 Eomes-/- endothelium immunophenocopies Runx1-null endothelium 73

Figure 2.17 Re-expression of Runx1 in Eomes loss-of-function EHT cultures rescues pro-definitive hematopoiesis..... 74

Figure 2.18 Assessing changes in chromatin accessibility in the Flk-1^{hi}/PdgfRa^{-} hematovascular mesoderm population generated in Eomes loss of function cultures 77

Figure 2.19 Eomes regulates chromatin accessibility at SCL bound regulatory regions nearby hematopoietic regulators..... 79

Figure 2.20 Assessing changes in chromatin accessibility in the Flk-1-/PdgfRa+ paraxial mesoderm population generated in Eomes loss of function cultures 81

Figure 2.21 Generation of an ES cell line expressing N-terminally V5-tagged Eomes..... 83

Figure 2.22 Generation of an ES cell line expressing C-terminally V5-tagged Eomes..... 84

Figure 2.23 Expression pattern of Eomes-V5 during hematovascular differentiation..... 85

Figure 2.24 ChIP-Western demonstrates that crosslinked Eomes-V5 complexes can be immunoprecipitated..... 86

Figure 2.25 Assessing Eomes' genomic targets in day 4 bulk EB cultures..... 87

Figure 2.26 Genomic regions marked transiently by H3K27Ac are bound by Eomes, Tead4 and Smad2/3 during early stages of hematopoietic mesoderm development..... 89

Figure 2.27 Eomes binds numerous genomic regions surrounding the Runx1 locus..... 91

Figure 2.28 Comparing Eomes bound ChIP-seq peaks with the subset of ATAC-seq peaks that are Eomes-dependent and normally bound by SCL at various stages of hematopoietic differentiation 93

Figure 2.29 Generation of an Eomes.iCre-LacZ allele for fate mapping 94

Figure 2.30 Eomes.iCre-LacZ expressing cells give rise to hematopoietic and endothelial cells at sites of definitive hematopoiesis..... 95

Figure 2.31 Regulating Eomes expression during hematovascular differentiation..... 97

Figure 2.32 Eomes regulates the generation of primitive erythrocytes upstream of SCL functional activity and EHT upstream of Runx1 expression in the HE lineage..... 100

Figure 3.1 Generation of an Eomes.CreERT2 mouse strain for lineage tracing 104

Figure 3.2 Generation of an Eomes.CreERT2-LacZ mouse strain for lineage tracing 105

Figure 3.3 Isolation of Eomes.GFP+ progenitors from early PS stage mouse embryos..... 106

LIST OF TABLES

Table 1. List of antibodies 133

Table 2. Sequence for CRISPR Reagents 134

Table 3. List of qRT-PCR primers 135

Table 4. Differentially expressed genes in the Seurat clusters 136

Table 5. Conserved markers in the Seurat clusters..... 136

Table 6. Eomes-V5 bound genomic regions..... 137

ABBREVIATIONS

APS	anterior primitive streak
ATAC	assay for transposase-accessible chromatin
BI	blood islands
BMP	bone morphogenic protein
bp	base pairs
Cas9	CRISPR associated protein 9
cDNA	complementary deoxyribonucleic acid
ChIP	chromatin immunoprecipitation
CRISPR	clustered regularly interspaced short palindromic repeats
DE	definitive endoderm
DNA	deoxyribonucleic acid
dNTP	deoxynucleotide triphosphate
E	embryonic day
EB	embryoid body
Epi	epiblast
EHT	endothelial to hematopoietic transition
EMT	epithelial to mesenchymal transition
Eomes	eomesodermin
ES	embryonic stem
ExM	extraembryonic mesoderm
FACS	fluorescent activated cell sorting
GFP	green fluorescent protein
gRNA	guide RNA
HE	hemogenic endothelium
kb	kilobase
LacZ	E. Coli beta-galactosidase
Neo	neomycin phosphotransferase
PS	primitive streak
RNA	ribonucleic acid
sc	single cell
seq	sequencing
ssODN	single stranded donor oligonucleotide
T	brachyury
TK	thymidine kinase
TSS	transcriptional start site
YS	yolks sac

CHAPTER 1 : INTRODUCTION

1.1 MOUSE DEVELOPMENT

1.1.1 Pre-Implantation Mouse Development

Mouse development involves a complex series of molecular, cellular and morphogenetic events that transform a single cell, the zygote, into a complex multicellular organism. At the outset of mouse embryogenesis, the zygote undergoes a series of cellular divisions and differentiation steps that results in the production of a spherical blastocyst (Arnold and Robertson, 2009; Beddington and Robertson, 1999). The blastocyst is composed of an outer layer of trophectoderm and an inner cell mass that is made up of the epiblast and primitive endoderm **(Figure 1.1, a)** (Beddington and Robertson, 1999). The trophectoderm gives rise to the extra-embryonic placenta (Arnold and Robertson, 2009), which nourishes and protects the embryo as it develops. The chorion and yolk-sac, two extra-embryonic membranes, arise from primitive endoderm derived lineages. Finally, the pluripotent epiblast gives rise to all somatic tissues of the adult mouse (Arnold and Robertson, 2009; Beddington and Robertson, 1999).

1.1.2 Post-Implantation Mouse Development

At approximately E4.5, the blastocyst implants in the maternal uterine epithelium and elongates along the proximal-distal axis, forming a bi-layered cup often referred to as the egg cylinder (Arnold and Robertson, 2009). Around two days later, at E6.5, the process of gastrulation commences which generates the three embryonic germ layers, namely mesoderm, endoderm and ectoderm. Gastrulation begins when, in response to local signaling cues, epiblast cells on the prospective posterior side of the embryo are induced to

undergo an epithelial-to-mesenchymal transition (EMT)(Arnold and Robertson, 2009) **(Figure 1.1, b)**. These nascent epiblast-derived mesenchymal cells delaminate and initiate migration within a transient structure called the primitive streak (PS). Over the course of the next 24 hours the PS elongates towards the distal tip of the embryo. During PS elongation the conceptus increases substantially in size as subsequent waves of epiblast-derived mesenchymal cells traverse the PS and produce mesoderm and endoderm.

Migratory mesoderm forms a layer between the visceral endoderm and the epiblast referred to as the mesodermal wings. Mesodermal wings migrate laterally from the PS in both directions and meet on the anterior side of the embryo, forming the mid-line. In contrast, the definitive endoderm intercalates onto the surface of the embryo to partially displace the overlying visceral endoderm (Kwon et al., 2008). Mesodermal progenitors diversify into vascular, hematopoietic, cardiac and skeletal muscle lineages while the definitive endoderm gives rise to the gut tube and its associated organs. Anterior epiblast cells that do not undergo EMT form the neuroectoderm which gives rise to the epidermis and nervous system (Arnold and Robertson, 2009). Resolving the inductive signals, gene-regulatory networks, and epigenetic modifications that direct cell fate specification during gastrulation is an area of active research. Recent advances in genome editing, lineage tracing, microscopy and genome-wide sequencing technologies provide scientists an unprecedented opportunity to shed light on the molecular mechanisms that direct gastrulation.

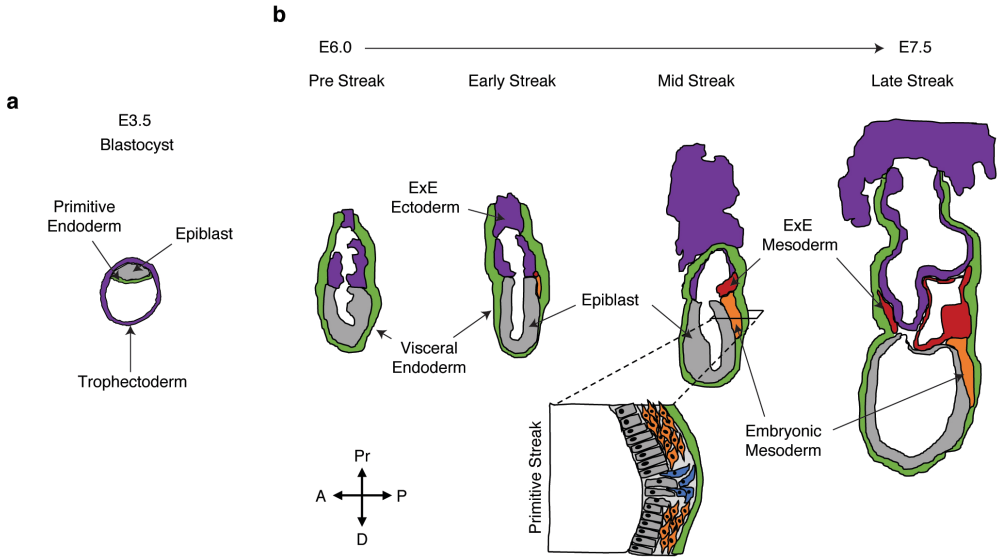


Figure 1.1 Mouse development: blastocyst to gastrulation
(a) The spherical blastocyst arises at embryonic day 3.5 (E3.5) and is made up of three distinct cell lineages: the trophectoderm (purple), primitive endoderm (green) and epiblast (grey). **(b)** After implantation, gastrulation commences at approximately E6.0. During gastrulation epiblast cells undergo EMT and traverse a transient structure called the PS (see cross-section at mid-streak stage). PS cells generate migratory layers of embryonic (orange) and extraembryonic (red) mesoderm that becomes sandwiched between the visceral endoderm (green) and epiblast (grey). A = anterior; P = posterior; D = distal; Pr = proximal. Adapted from (Pereira et al., 2011).

1.2 EXPERIMENTAL APPROACHES

1.2.1 Embryonic Stem Cell Technology

Mouse embryonic stem (ES) cells, were first derived from the epiblast of the mouse blastocyst in the 1980's, and have properties which enable their indefinite propagation in culture (Evans and Kaufman, 1981). Shortly after their discovery, it was proven that genetically modified mouse strains can be generated via blastocyst injections of genetically modified ES cells (Schwartzberg et al., 1989). The development of ES cell technology

opened up an entirely new field of research, enabling embryologists to assess which genes play essential roles during murine embryonic development by performing gain- and loss-of-function experiments. Loss-of-function studies involve the removal of a protein coding sequence. In contrast, gain-of-function experiments test the effects of ectopic expression of a particular protein. Genetic recombination techniques, such as the Cre-LoxP and FLP-FRT systems, can be exploited to perform functional studies in specific lineage contexts. Recent advances in directed genome editing technologies, using TALENS and CRISPR-Cas9, has markedly increased the rate at which scientists can generate genetically modified ES/mouse lines (Wang et al., 2013).

ES cells can also be differentiated into specialized cell types of the three germ layers *in vitro* (Evans and Kaufman, 1981). The differentiation pathways that ES cells follow *in vitro* are very similar to those which occur naturally during *in vivo* development; that is, epiblast-like ES cells transition through PS and mesoderm/endoderm cellular states as they differentiate into specialized cell types *in vitro* (Murry and Keller, 2008). As such, ES differentiation cultures serve as a useful model of murine embryogenesis. Researchers initially used different serum batches to preferentially drive the differentiation of particular cell types, such as hematopoietic or cardiac cells, from ES cells (Keller, 2005; Murry and Keller, 2008). More recently, sophisticated serum free strategies have been developed that involve the addition of specific cytokines, small molecules and growth factors, in a staged fashion, to selectively drive the development of particular lineages (Kattman et al., 2011; Murry and Keller, 2008; Nostro et al., 2008). A major benefit of the ES model system, over *in vivo* studies, is that it provides unlimited access to extremely rare and highly transient developmental populations for molecular studies. A major drawback of the ES model system is the loss of positional information in the developing embryo.

1.2.2 Genome Wide Approaches

DNA molecules, housed within the nucleus of each cell, encode tens of thousands of genes. Genes are transcribed into RNA molecules, which are subsequently translated into strings of amino acids that fold together into proteins. The different types of proteins expressed within a single cell endow it with a capacity to perform a specific set of functions. Thus, cellular diversity is underpinned by the differential expression of genes and their final protein products during development. A particularly important group of proteins are transcription factors (TF) that bind to specific DNA sequences, promoters and enhancers, to regulate gene expression and coordinate cell fate specification. The recent development of next-generation-sequencing technologies has birthed a new field of genomic techniques that have transformed the study of gene regulation during embryogenesis.

Combining next-generation-sequencing technology with traditional molecular biology techniques has enabled researchers to study gene regulation at a genome-wide scale. RNA sequencing (RNA-seq) provides information about the quantity and type of RNA molecules expressed in a pool of cells (Kukurba and Montgomery, 2015). ChIP-seq technology identifies protein-DNA interactions and assays such as DNase1 hypersensitivity (Boyle et al., 2008) and ATAC-seq (Buenrostro et al., 2013) provide chromatin accessibility information. Integrating genomics data from these various techniques can be utilized to uncover direct genomic targets of TFs, identify *cis*-regulatory regions, and reveals relationships between histone marks and transcriptional activity across the genome (Buecker and Wysocka, 2012; Jiang and Mortazavi, 2018; Klemm et al., 2019). These technologies, however, require inputs from tens of thousands to millions of cells and therefore generate data that provides ensemble averages and lacks information about underlying cellular heterogeneity. More recently, single-cell RNA-seq (scRNA-seq) and

single-cell chromatin accessibility (scATAC-seq) techniques have been developed that allow genome-wide sequencings experiments to be performed on inputs from single cells (Buenrostro et al., 2015; Shapiro et al., 2013; Thurman et al., 2012). As cell fate decisions occur at the level of individual cells, these new single-cell technologies will be particularly useful for the field of developmental biology.

1.2.3 Lineage Tracing

Lineage tracing experiments involve identification of a single cell and all of its future progeny over a developmental time-course. These types of experiments enable the construction of fate maps and lineage trees that describe cellular hierarchies. Historically, it has been challenging to perform lineage tracing experiments during mouse gastrulation and organogenesis as these stages necessitate support from a maternal environment. Genetic tools, however, have been developed that allow lineage tracing studies to be performed that do not require removal of mouse embryos from their maternal environment (Kretzschmar and Watt, 2012). Additionally, culture conditions that allow short term development of mouse embryos *ex vivo* have been identified (Kinder et al., 1999). Confocal imaging and light-sheet microscopy are particularly useful in this context as they allow researchers to follow fluorescently labelled cells and their progeny in real-time with cellular/sub-cellular resolution (Amat and Keller, 2013; Ichikawa et al., 2014). An ultimate goal of the field is the construction of a high-resolution lineage tree that encompasses all fate transitions that occur during mouse gestation.

Genetic recombination systems have been particularly useful for lineage tracing experiments. In these systems the expression of a conditional reporter allele is induced via

the activity of a recombinase enzyme. A recombination event leads to the permanent genetic labelling of a founder cell and all of its progeny. The Cre-loxP and FLP-FRT site specific recombinase systems have been widely used to perform lineage tracing in the mouse and other species (Kretzschmar and Watt, 2012). In these systems, expression of a Cre/FLP recombinase is placed under the control of a tissue- or cell-type specific promoter and recombination occurs at LoxP and FRT sites, respectively. Commonly these recombination events remove a stop codon to induce the expression of a reporter allele, such as GFP or LacZ, located in the safe harbor ROSA26 locus (Soriano, 1999; Srinivas et al., 2001). The development of estrogen receptor (ER) tagged versions of Cre recombinase allows an added layer of temporal regulation of Cre activity (Feil et al., 1996; Feil et al., 1997; Metzger et al., 1995). Cre-ER is normally localized to the cytoplasm where it is bound by a heat-shock protein. The diffusion of an ER ligand, such as tamoxifen, into the cytoplasm induces a conformational change that causes CreER to be released from the heat-shock protein and shuttled into the nucleus. Once in the nucleus CreER recombinase is active and able to induce the expression of a reporter allele.

The development of single cell DNA sequencing technology has birthed a new wave of experimental approaches to ascertain lineage relationships during murine development (McKenna and Gagnon, 2019). These new technologies all rely on DNA sequence changes accumulating over time. Algorithms are utilized to make inferences about lineage histories based on the DNA sequence similarities of a large number of single cells. Cells that share more similar lineage histories will have more similar DNA sequences. Low levels of DNA mutations occur naturally during murine development; therefore, whole genome sequencing of individual cells can be used to generate a lineage tree. This method, however, is expensive and as such methods that capture sequence specific regions of the genome, called barcodes, have been developed. Lineage reconstruction depends on the creation of

mutations at these barcode regions via the activity of recombinase enzymes (Pei et al., 2019; Peikon et al., 2014) (Cre/Frt) or CRISPR-Cas9 induced DNA strand breaks. Clever methods that modulate the rate of mutations induced by Cas9 at barcode regions have been developed and these techniques are being used in combination with scRNA-seq to generate molecular recordings of murine embryogenesis (Chan et al., 2019).

1.3 MURINE GASTRULATION

1.3.1 Cell Fate Allocation

Dye labelling and cell transplantation studies, completed over thirty years ago, suggest that the timing and positioning of epiblast migration along the anterior-posterior axis of the elongating PS is predictive of cell fate (Kinder et al., 1999; Tam et al., 1997). The very first cells to ingress through the most posterior aspect of the PS generate extraembryonic mesoderm that gives rise to the blood islands (BI) of the visceral yolk-sac (YS) **(Figure 1.2)**. The YS BIs contain hematopoietic, endothelial and smooth muscle cells. Interestingly, erythrocyte precursors traverse the posterior PS prior to ingression of endothelial fated cells, which has led to the concept of fate allocation of YS lineages in the epiblast prior to EMT. Slightly later, at mid streak stages, cells that traverse the posterior, middle and anterior aspects of the PS give rise to extraembryonic, cardiac/cranial and paraxial mesoderm, respectively **(Figure 1.2)**. At late streak stages the most posterior cells continue to move into the extraembryonic region and generate mesoderm of the allantois which gives rise to the umbilical cord **(Figure 1.2)**. Intermediate and posterior regions of the PS at late streak stages generate lateral-plate and paraxial mesoderm, respectively **(Figure 1.2)**. Finally, cells that traverse the most anterior aspect of the PS give rise to definitive endoderm and axial mesoderm (node, notochord and prechordal plate) **(Figure 1.2)**.

1.3.2 Signals Driving Fate Decisions during Gastrulation

Manipulation of signaling pathways in ES cell differentiation cultures (Murry and Keller, 2008) and *in vivo* loss-of-function experiments suggest that graded TgfB/Wnt signals play a critical role for cell fate allocation during gastrulation (Arnold and Robertson, 2009; Tam and Loebel, 2007). Loss of nodal signaling leads to absence of anterior PS derivatives such as the definitive endoderm and axial/paraxial mesoderm (Beck et al., 2002; Episkopou et al., 2001; Hoodless et al., 2001; Yamamoto et al., 2004). Additionally, high concentrations of Activin A induce the formation of definitive endoderm in ES differentiation cultures (Kubo et al., 2004). In contrast extraembryonic mesodermal lineages that arise from the posterior aspect of the PS require high levels of BMP signaling. BMP4 is secreted from the extraembryonic ectoderm which sits next to the posterior PS and BMP4-/- embryos lack extraembryonic/hematopoietic mesoderm (Winnier et al., 1995). Conversely, deletion of the Bmpr1a results in the excessive generation of paraxial mesoderm (Miura et al., 2006). Wnt signaling is required for the generation of mesoderm *in vitro* (Gadue et al., 2006) and Wnt3a-/- embryos contain ectopic neuroectoderm in place of paraxial mesoderm (Yoshikawa et al., 1997). Altogether, these results suggest that different levels of BMP, Nodal and Wnt signaling guide cell fate allocation along the anterior-posterior axis during PS formation **(Figure 1.2)**.

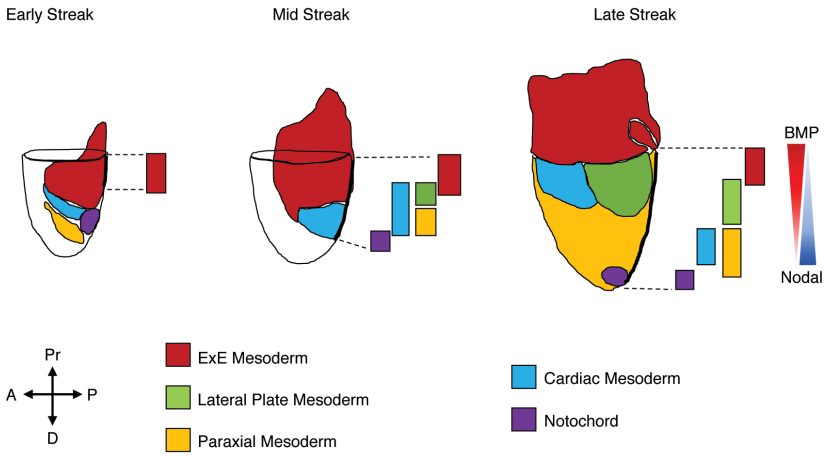


Figure 1.2 Mesodermal cell fate allocation during gastrulation
The site and timing of epiblast ingression through the PS is predictive of mesodermal fate. Rectangular boxes indicate the mesodermal fates of cells traversing the PS. The cells that traverse the most posterior aspect of the PS give rise to ExE mesoderm at early, mid and late streak stages. The middle portion of the PS gives rise to cardiac, lateral plate and paraxial mesoderm at mid and late streak stages. The most anterior portion of the PS generates the notochord at mid and late streak stages. Cells traversing different areas of the PS rely on graded levels of BMP and Activin A signalling to diversify into different endoderm and mesoderm subtypes. ExE = extraembryonic. Adapted from (Kinder et al., 1999) and (Murry and Keller, 2008).

1.4 DEVELOPMENTAL HEMATOPOIESIS

1.4.1 Waves of Hematopoiesis

Blood cell formation occurs in three sequential waves (primitive, pro-definitive and definitive) during mouse embryogenesis (Ditadi et al., 2017; Dzierzak and Speck, 2008) **(Figure 1.3)**. The first wave of hematopoiesis, called primitive hematopoiesis, begins at E7.25 in the blood islands (BI) of the visceral YS (Ferkowicz and Yoder, 2005; Palis et al., 1999). The BIs contain endothelial cells and primitive hematopoietic progenitors that give rise to primitive erythrocytes, macrophages and megakaryocytes. Primitive erythrocytes express embryonic

forms of hemoglobin, are larger than definitive erythrocytes and are nucleated when they enter circulation (Palis, 2014). Approximately a day later two additional hematopoietic progenitor pools arise in the YS, erythro-myeloid (EMP) and lympho-myeloid primed (LMPP) progenitors (Ditadi et al., 2017) that constitute the second wave of pro-definitive hematopoiesis (Frame et al., 2016; McGrath et al., 2015a; McGrath et al., 2015b). EMPs form at E8.25, express the cell surface markers c-kit, CD41 and CD16/32, and give rise to definitive erythrocytes, megakaryocytes and granulocytes (McGrath et al., 2015a; Palis et al., 1999). LMPPs, arise slightly later at E9 and generate myeloid and lymphoid cells but lack erythroid potential (Boiers et al., 2013; Yoshimoto et al., 2012). Finally, at E10.5 a third wave of multipotent hematopoietic progenitors arise in arterial vessels that includes the definitive hematopoietic stem cell (HSC)(de Bruijn et al., 2000). HSCs are defined functionally by their capacity to reconstitute the hematopoietic system of a lethally irradiated adult mouse. The most well characterized site of HSC production is the ventral side of the dorsal aorta located in the AGM region (Boisset et al., 2010; de Bruijn et al., 2000). Additionally, there is evidence for *de novo* generation of HSCs in the vasculature of the head, YS and placenta (Gekas et al., 2005; Li et al., 2012; Ottersbach and Dzierzak, 2005).

1.4.2 Ontogeny of Hematopoietic Progenitors

Unravelling the developmental origins of the different waves of hematopoietic progenitors has been a long-standing goal of developmental hematologists. Primitive and pro-definitive hematopoietic progenitors are derived from extraembryonic mesodermal cells that traverse the posterior PS at the outset of gastrulation (Clements and Traver, 2013; Kinder et al., 1999). In contrast, the dorsal aorta where the HSC is formed at E10.5 arises from lateral plate mesoderm that traverses more anterior aspects of the PS. Much work over the past

four decades has focused on refining our understanding of how these mesodermal populations transition into hematopoietic cells. Lineage hierarchy studies have uncovered a

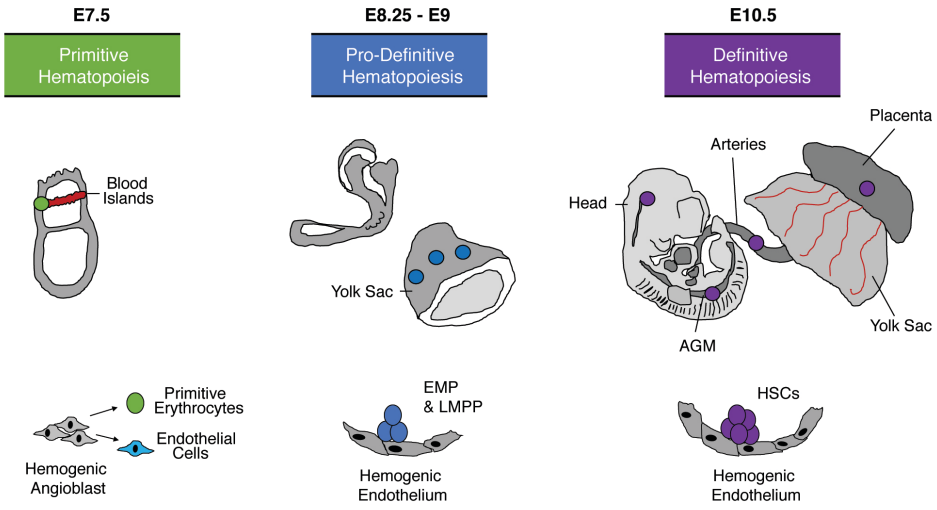


Figure 1.3 Multiple waves of hematopoiesis during mouse embryogenesis
Primitive hematopoietic progenitors arise from hemogenic angioblasts and give rise to primitive erythrocytes beginning at E7.5 in the YS BIs. Pro-definitive hematopoietic progenitors (EMPs and LMPPs) are derived from hemogenic endothelium (HE) and arise at E8.25-E9 in the YS vasculature. The definitive HSC is formed *de novo* beginning at E10.5 from HE that is located in the dorsal aorta of the AGM, as well as in the vasculature of the head, placenta and umbilical arteries. AGM = aorta-gonad-mesonephros. Adapted from (Ditadi et al., 2017).

close relationship between the development of both vascular and hematopoietic cells, which has led to concepts of mesoderm derived progenitors called hemangioblasts and hemogenic endothelium.

1.4.2 Hemangioblast

The term hemangioblast was initially coined at the turn of the 20th century when anatomists visualized the simultaneous formation of red blood cells and vascular cells in a variety of mammalian species, including the mouse (Murray, 1932; Sabin, 1920). In the late 1990's the

Keller lab demonstrated that a bipotent cell can be isolated from ES cell differentiation cultures that gives rise to both hematopoietic and endothelial cells (Choi et al., 1998). Shortly thereafter a similar progenitor was isolated from the posterior PS in E7.0 mouse gastrulas. In both cases these vascular/hematopoietic precursors express the mesodermal marker T and the cell surface receptor Flk-1 (Huber et al., 2004). Together, these findings led to the concept of the hemangioblast – a multipotent mesodermal cell that gives rise to endothelial, hematopoietic and vascular smooth muscle cells. As previously mentioned, seminal fate mapping studies suggested that YS primitive erythrocyte and endothelial fates arise in separate epiblast populations prior to mesoderm formation (Kinder et al., 1999). More recent lineage tracing studies corroborate these previous fate mapping results (Padron-Barthe et al., 2014; Ueno and Weissman, 2006), bringing into question the existence of an *in vivo* hemangioblast.

1.4.4 Hemogenic Endothelium

In the past decade mounting evidence from live imaging and fate mapping studies strongly suggests that EMPs, LMPPs, and HSCs all arise from a specialized subset of endothelial cells called hemogenic endothelium (HE) (Boisset et al., 2010; Frame et al., 2016). At sites of pro-definitive and definitive hematopoiesis, HE cells differentiate into hematopoietic progenitors via a process termed the endothelial-to-hematopoietic transition (EHT) (Boisset et al., 2010; de Bruijn and Dzierzak, 2017; Kissa and Herbomel, 2010; Yoshimoto et al., 2012). During EHT endothelial cells round up, detach from the endothelial layer and enter the blood stream. During this differentiation process an endothelial program is downregulated and a hematopoietic transcriptional program is upregulated. In contrast, primitive hematopoietic progenitors arise in the YS blood islands, prior to the formation of a proper vascular plexus and HE, from localized cell masses that express low levels of

endothelial markers that do not yet line the interior of blood vessels (Lacaud and Kouskoff, 2017).

1.5 MODELLING MURINE HEMATOPOIESIS IN VITRO

Due to the small size and inaccessibility of the post-implantation mouse gastrula it is challenging to study the molecular events that regulate the onset of developmental hematopoiesis. The unlimited self-renewal and differentiation capacity of ES cells, however, provides developmental biologists and stem cell scientists a useful tool to model hematopoiesis *in vitro*. Numerous research groups have developed staged ES differentiation protocols that efficiently generate primitive erythrocytes and multipotent progenitors that give rise to definitive erythrocytes and myeloid cells (Keller, 2005; Murry and Keller, 2008). Similar strategies have also been used to produce cells of the lymphoid lineage, such as T-cells (Clarke et al., 2013; Irion et al., 2010). A robust protocol, however, that allows routine generation of HSCs without genetic manipulation of ES cells has not yet been published. For this reason, it is thought that many of the differentiation protocols developed thus far mimic YS-like primitive and pro-definitive hematopoiesis rather than intra-embryonic definitive hematopoiesis (Cook, 2014; Lacaud and Kouskoff, 2017).

Efficient generation of primitive and pro-definitive hematopoietic progenitors *in vitro* has been accomplished via the addition of signaling pathway agonists and antagonists in staged approaches that mimic *in vivo* development (Keller, 2005; Murry and Keller, 2008). Hematopoietic colony forming assays, flow cytometry and RNA/protein expression assays are used throughout differentiation protocols to monitor the efficiency of hematoendothelial development. ES cells are often initially dissociated in these protocols and placed in culture

conditions that allow the formation of spherical aggregates called embryoid bodies (EB), which have properties similar to the post-implantation mouse epiblast. Primitive streak and mesoderm formation can then be induced in EBs via the activation of BMP, Activin/Nodal and Wnt signaling (Gadue et al., 2006; Irion et al., 2010; Kattman et al., 2011; Nostro et al., 2008). Different concentrations of BMP4 and Activin A can be used to selectively generate Flk1/PdgfRa expressing mesodermal populations that arise from different sites along the anterior-posterior axis of the PS (Kattman et al., 2011). High amounts of BMP4 and lower amounts of Activin A have been shown to enhance the production of a Flk-1^{hi}/PdgfRa^{-} population that is enriched for hemogenic potential and likely represents extraembryonic mesoderm and/or lateral plate mesoderm (Kattman et al., 2011). Additionally, kinetic analyses have demonstrated that primitive and pro-definitive hematopoietic progenitors arise in ES cultures in a chronological order that mimics YS hematopoiesis (Keller, 2005; McGrath et al., 2015a). An early wave of Flk-1+ cells predominantly generate primitive erythrocyte colonies (Irion et al., 2010). In contrast, Flk-1+ cells that arise later on generate HE that gives rise to hematopoietic cells found at sites of pro-definitive hematopoiesis (Clarke et al., 2013; Irion et al., 2010). These protocols, therefore, allow researchers to study both primitive hematopoiesis and YS-like HE specification *in vitro*.

1.6 ESSENTIAL GENES FOR HEMATOPOIETIC AND ENDOTHELIAL DEVELOPMENT

Understanding the transcriptional hierarchy that guides hematopoiesis during embryogenesis is essential for the generation of hematopoietic progenitors from pluripotent stem cell sources *in vitro*. A number of genes, including Flk-1 and ER71, have been identified that play essential roles during vascular and hematopoietic specification from mesoderm. At later stages of hematopoietic differentiation, transcriptional regulators that

impact hematopoietic output from HE, without disturbing endothelial development, have also been uncovered. These TFs include SCL and Runx1 and investigations into their molecular activities have significantly refined our understanding of hematopoietic development at early embryonic stages (de Bruijn and Dzierzak, 2017; Porcher et al., 2017).

1.6.1 Flk-1

The cell surface receptor tyrosine kinase, Flk-1, as previously mentioned, marks the hemangioblast and is expressed on extraembryonic and lateral plate mesodermal precursors that give rise to primitive, pro-definitive and definitive hematopoietic progenitors (Choi et al., 1998; Huber et al., 2004; Lugus et al., 2009). Additionally, Flk-1 is expressed on cardiac mesoderm and paraxial mesoderm (Lugus et al., 2009). Cardiac/paraxial mesodermal progenitors, however, also express the cell surface marker PdgfRa that is not expressed on hemogenic mesoderm (Craft et al., 2013; Kattman et al., 2011; Koyano-Nakagawa and Garry, 2017). Strikingly, Flk-1-/- embryos lack YS blood islands and die between E8.5 and E9.5 due to defects in vascular and hematopoietic development (Shalaby et al., 1995). Additionally, Flk-1-/- ES cells do not contribute to the hematopoietic lineage in blastocyst chimeras which demonstrates that Flk-1 is required cell autonomously for the development of hematopoietic progenitors (Shalaby et al., 1997). These findings reveal a very early role for Flk-1 during mouse hematopoietic development.

1.6.2 ER71

ER71 (also referred to as Etv2) is an ETS TF and is one of the earliest known transcriptional regulators required for the development of endothelial cells and hematopoietic progenitors

during mouse embryogenesis (Koyano-Nakagawa and Garry, 2017; Zhao et al., 2017). ER71 is expressed in Flk-1+/PdgfRa- extraembryonic and lateral plate mesoderm *in vivo* (Koyano-Nakagawa and Garry, 2017) and its expression is essential for the development of Flk-1+/PdgfRa- hemangiogenic mesodermal cells *in vitro* (Liu et al., 2012*)*. ER71 is not essential, however, for the development of Flk-1+/PdgfRa+ cardiac mesoderm or Flk-1-/PdgfRa+ paraxial mesoderm. Interestingly, ER71-/- embryos die due to severe blood vessel defects reminiscent of Flk-1 mutants (Lee et al., 2008). Furthermore, forced expression of ER71 in Flk-1 mutant EBs rescues hematoendotheilal development *in vitro* (Rasmussen et al., 2013). ER71 is functionally required prior to the onset of Flk-1 expression as conditional deletion of ER71 using a Flk-1:Cre deleter strain does not disrupt hematopoiesis (Wareing et al., 2012). Finally, chimera experiments demonstrate that ER71 is required cell autonomously for the development of hematopoietic progenitors (Lee et al., 2008).

1.6.3 SCL

SCL (also known as Tal1) is a basic helix-loop-helix TF that is required for the specification of the hematopoietic fate from Flk-1+ mesoderm (D'Souza et al., 2005; Porcher et al., 2017). Unlike ER71 mutants, SCL-/- ES cells robustly generate Flk-1+/PdgfRa- hemogenic mesoderm (Chagraoui et al., 2018). SCL mutant embryos, however, completely lack hematopoietic progenitors and die at around E9.5 (Shivdasani et al., 1995). Chimera experiments demonstrate that SCL activity is required cell autonomously for the acquisition of the blood cell fate, however, SCL is not required for the development of other mesodermal subsets or endothelial cells (Pijuan-Sala et al., 2019). Evidence has mounted more recently which suggests that SCL not only activates a hematopoietic program but also actively suppresses the acquisition of a cardiac cell fate (Chagraoui et al., 2018; Org et al., 2015; Van Handel et al., 2012). In line with this, CD31+ YS endothelial cells that form in SCL

mutant embryos express cardiac genes such as Nkx2-5 and cTNT (Van Handel et al., 2012). SCL functions downstream of ER71 as re-expression of SCL in ER71-/- mesodermal cells is sufficient to restore hematopoiesis (Kataoka et al., 2011) and ER71 binds the SCL locus (Kataoka et al., 2011). SCL-/- ES cells are able to form endothelial and smooth muscle cells *in vitro* (D'Souza et al., 2005), however, they do not generate a Tie2+/cKit+ compartment that has been associated with HE (Lancrin et al., 2009). Finally, deletion of SCL in endothelial cells, using a Tie2:Cre deleter strain, does not block the formation of HSCs but impedes erythroid and megakaryocytic maturation (Schlaeger et al., 2005). Together, these results suggest that SCL is functionally required for hematopoietic development during the transition of hematopoietic mesoderm into HE.

1.6.4 Runx1

Runx1, a runt-domain TF, is often described as the master regulator of definitive hematopoiesis. In contrast to ER71, SCL and Flk-1, Runx1 mutant embryos die later on at E12.5 due to hemorrhaging (Wang et al., 1996). Runx1 is non-essential for the development of primitive erythrocytes and primitive megakaryocytes (de Bruijn and Dzierzak, 2017). Runx1 is, however, absolutely essential for EHT and the generation of all pro-definitive and definitive hematopoietic cells. Elegant conditional deletion experiments demonstrate that Runx1 is required for the development of hematopoietic progenitors from Cdh5:Cre expressing endothelial cells (Chen et al., 2009). Deletion of Runx1 in nascent hematopoietic cells, however, using a Vav1:Cre deleter does not impact hematopoiesis (Chen et al., 2009). Together these results reveal that Runx1 is functionally required for hematopoietic development within a narrow developmental time window in the HE lineage.

ChIP-seq experiments suggest that Runx1 initiates EHT via activating a hematopoietic transcriptional program and downregulating endothelial genes (de Bruijn and Dzierzak, 2017; Tanaka et al., 2012). This is accomplished via Runx1 activating Gfi1/1b, TFs that suppress the endothelial cell fate and regulate EHT (Lancrin et al., 2012; Thambyrajah et al., 2016). A number of *cis*-regulatory regions, including a +23 enhancer that specifically marks HE, have been discovered that drive Runx1 expression at sites of pro-definitive and definitive hematopoiesis (Schutte et al., 2016; Swiers et al., 2013). The precise upstream signals and transcriptional regulators that coordinate Runx1 expression within the HE lineage, however, remain ill-defined.

1.7 EOMESODERMIN

The successful cloning and sequencing of brachyury, T, during the 1990's revealed its role as a nuclear transcription factor (Herrmann et al., 1990). Soon after brachyury's discovery an entire family of related proteins was uncovered, now known as the T-box protein family. T-box proteins are characterized by a highly conserved T-box DNA binding motif (Papaioannou, 2014). Numerous studies have revealed crucial roles for T-box proteins during vertebrate development (Naiche et al., 2005). Of the seventeen T-box proteins, Eomesodermin (Eomes) is thought to be expressed at the earliest stages of mouse development. In the mouse, Eomes mRNA is alternatively spliced into a long form (Eomes-long) and a shorter form (Eomes-short) which lacks 19 amino acids in exon 6 **(Figure 1.4)**.

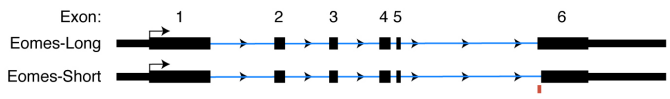


Figure 1.4 Long and short mRNA Eomes isoforms

***Figure legend 1.4 continued*;** Exons are shown as thick black blocks and untranslated regions are shown as thinner black blocks. The translational start site is indicated by the black arrow. The red block highlights the 19 amino acids missing from the shorter isoform of Eomes. Eomes-Long, 707 amino acids. Eomes-short, 688 amino acids.

Eomes is first expressed in the trophectoderm of the blastocyst and subsequently in the extraembryonic ectoderm (Ciruna and Rossant, 1999). Eomes loss-of-function causes lethality shortly after implantation due to defects in trophoblast stem cell maintenance (Strumpf et al., 2005). At later stages, from E5.75 to E7.5, Eomes is expressed on the posterior side of the embryo in the developing primitive streak (PS) and nascent mesoderm (Ciruna and Rossant, 1999; Hancock et al., 1999). Prior to overt PS formation, conditional inactivation of Eomes in the epiblast disrupts EMT and blocks migration of nascent mesoderm from the PS (Arnold et al., 2008). In this context, Eomes is required for specification of cardiac mesoderm upstream of the basic helix-loop-helix TF Mesp1 (Costello et al., 2011; Van Den Ameele et al., 2012). Additionally, Eomes expression in the epiblast is required for the specification of the definitive endoderm lineage (Arnold et al., 2008). These functional roles for Eomes are conserved throughout mammalian evolution as the specification of cardiac mesoderm and definitive endoderm also rely on Eomes functional activity in human ES cell cultures (Pfeiffer et al., 2018; Teo et al., 2011). Finally, conditional inactivation of Eomes in the visceral endoderm results in failure of specification and migration of the anterior visceral endoderm and consequently causes improper anterior-posterior axis formation (Nowotschin et al., 2013).

1.8 AIMS OF THESIS

My DPhil focuses on answering two overarching questions: firstly, what functional role does Eomes play during murine hematopoiesis and secondly, how diverse are the transcriptomes and potencies of Eomes expressing progenitors during gastrulation.

Question #1: Is Eomes functionally required for the development of the extraembryonic mesodermal lineage?

Preliminary experiments performed by Claire Simon, a previous DPhil student in the Robertson lab, suggest that Eomes coordinates the development of extraembryonic mesoderm and the differentiation of hematopoietic cells. In line with these results, another group has found that Eomes plays an important role during the generation of Flk-1+ hemangiogenic mesoderm downstream of FoxH1 (Zhao and Choi, 2017). The first aim of my thesis was to thoroughly evaluate the functional role Eomes plays during murine hematopoietic and vascular development. To accomplish this, I performed a number of loss- and gain-of-function experiments utilizing *in vitro* ES models of YS hematopoiesis and a variety of genome wide sequencing experiments.

Question #2: What is the transcriptional heterogeneity of Eomes expressing progenitors and what are their potencies during mouse gastrulation?

Retrospective fate mapping studies demonstrate contribution of Eomes expressing progenitors to mesodermal derivates (extraembryonic, cardiac/cranial, lateral plate) and the definitive endoderm (Arnold et al., 2008; Costello et al., 2011; Pimeisl et al., 2013). These

arise from different portions of the PS (Kinder et al., 1999; Tam et al., 1997). Therefore, it seems likely that discrete Eomes+ progenitors traverse the PS at different times and in different locations. The second aim of my thesis is to determine the potencies and transcriptional heterogeneity of individual Eomes+ progenitors during mouse gastrulation. To accomplish this, I will perform clonal lineage tracing experiments and scRNA-seq of Eomes+ progenitors during mouse gastrulation.

CHAPTER 2 : EOMES GOVERNS THE HEMOGENIC COMPETENCE OF MESODERMAL PROGENITORS

2.1 INTRODUCTION

Hematopoiesis commences during mouse gestation in the visceral YS. An initial wave of blood progenitors arise in the YS BIs at E7.25 that generate primitive erythrocytes, primitive macrophages and primitive megakaryocytes (Ferkowicz and Yoder, 2005). Shortly thereafter, at E8.25, a second wave of pro-definitive blood progenitors arise in the YS from a specialized subset of endothelial cells, called hemogenic endothelium (HE). HE derived pro-definitive blood progenitors, in contrast to the definitive HSC that arises at E10.5, have restricted hematopoietic potential, generating either definitive-erythro-myeloid cells (EMPS) or lymphoid-myeloid lineages (LMPP). Both the vascular and hematopoietic lineages of the YS are derived from extraembryonic mesoderm (ExM) that traverses the posterior aspect of the PS during gastrulation and expresses the cell surface receptor Flk-1. How specific subsets of ExM become committed to primitive and pro-definitive hematopoietic fates, however, remains ill-defined.

The development of ES differentiation protocols that model YS hematopoiesis *in vitro* has significantly aided researchers in studying the transcriptional hierarchy that directs murine hematopoiesis. How HE is specified is of particular interest as this represents a critical early step in the generation of definitive hematopoietic cells, including the HSC. Only a few transcriptional regulators, such as SCL and Runx1, however, have been uncovered that specifically impact hematopoietic output from HE (de Bruijn and Dzierzak, 2017; Porcher et al., 2017). SCL is required for the specification of HE and the production of all hematopoietic

cells during gestation. In contrast, Runx1 is not required for the generation of HE or primitive erythrocytes/megakaryocytes but is essential for the production of all definitive hematopoietic stem and progenitor cells as Runx1 governs EHT.

At the outset of mouse gastrulation, the earliest progenitor populations to traverse the PS generate the extraembryonic mesoderm, cardiac/cranial mesoderm and definitive endoderm lineages (Kinder et al., 1999; Tam et al., 1997). Previous studies by our lab and others have demonstrated that Eomes is essential for the specification of the cardiac mesoderm and definitive endoderm lineages (Arnold et al., 2008; Costello et al., 2011; Van Den Ameele et al., 2012). Although previous fate mapping studies indicate that Eomes expressing cells generate YS vasculature (Costello et al., 2011; Pimeisl et al., 2013), whether Eomes plays an essential role during extraembryonic mesoderm development has not been extensively evaluated. The first aim of my DPhil was therefore to determine whether or not Eomes functional activity is essential for the specification of extraembryonic mesoderm and/or the subsequent differentiation of hematopoietic and endothelial lineages that arise in the murine yolk-sac. To accomplish this, I utilized an *in vitro* model of YS hematopoiesis and performed a number of genome wide sequencing experiments.

2.2 RESULTS

2.2.1 Eomes, T and Flk-1 expression during mouse gastrulation

ExM is generated from the first wave of mesodermal progenitors to traverse the posterior region of the primitive streak at the outset of gastrulation (Ferkowicz and Yoder, 2005; Kinder et al., 1999) **(Figure 2.1, a)**. ExM progenitors migrate proximally, displace the overlying extraembryonic ectoderm and alongside the extraembryonic visceral endoderm

differentiate into hematopoietic and endothelial cells, generating the YS BIs where the first two waves of hematopoiesis occur in the mouse conceptus **(Figure 2.1, a)**. Previous fate mapping studies have demonstrated that all hematopoietic and endothelial cells of the developing YS are derived from mesoderm that expresses the cell surface receptor tyrosine kinase, Flk-1 (Lugus et al., 2009). Furthermore, the tri-potent hemangioblast that can be isolated from E7.0 mouse embryos is marked by the expression of Flk-1 and the T-box transcription factor brachyury (T) (Huber et al., 2004).

Immunostaining experiments were performed in collaboration with Claire Simon and Ita Costello to assess the expression patterns of Eomes, T and Flk-1 at the outset of mouse gastrulation **(Figure 2.1, b-e)**. Eomes and T are expressed within the epiblast, PS and nascent mesoderm E6.5 **(Figure 2.1, b,c)**. At early/mid streak stages Eomes is more broadly expressed than T in the epiblast and PS region **(Figure 2.1, b,c)**. Unlike T, Eomes is also expressed in the extraembryonic ectoderm **(Figure 2.1, b,c, white arrow)**. A population of Flk-1+ migratory mesoderm co-expressed Eomes at early streak stages **(Figure 2.1, d, white arrow)**. At mid/late streak stages Flk-1+ cells located in the developing YS blood islands lacked Eomes expression **(Figure 2.1, e, white arrow)**, however, Eomes was expressed at this stage in Flk-1+ anterior embryonic mesoderm **(Figure 2.1, e, orange arrow)**. These results suggest that Eomes is expressed prior to overt T expression within an early wave of migratory ExM.

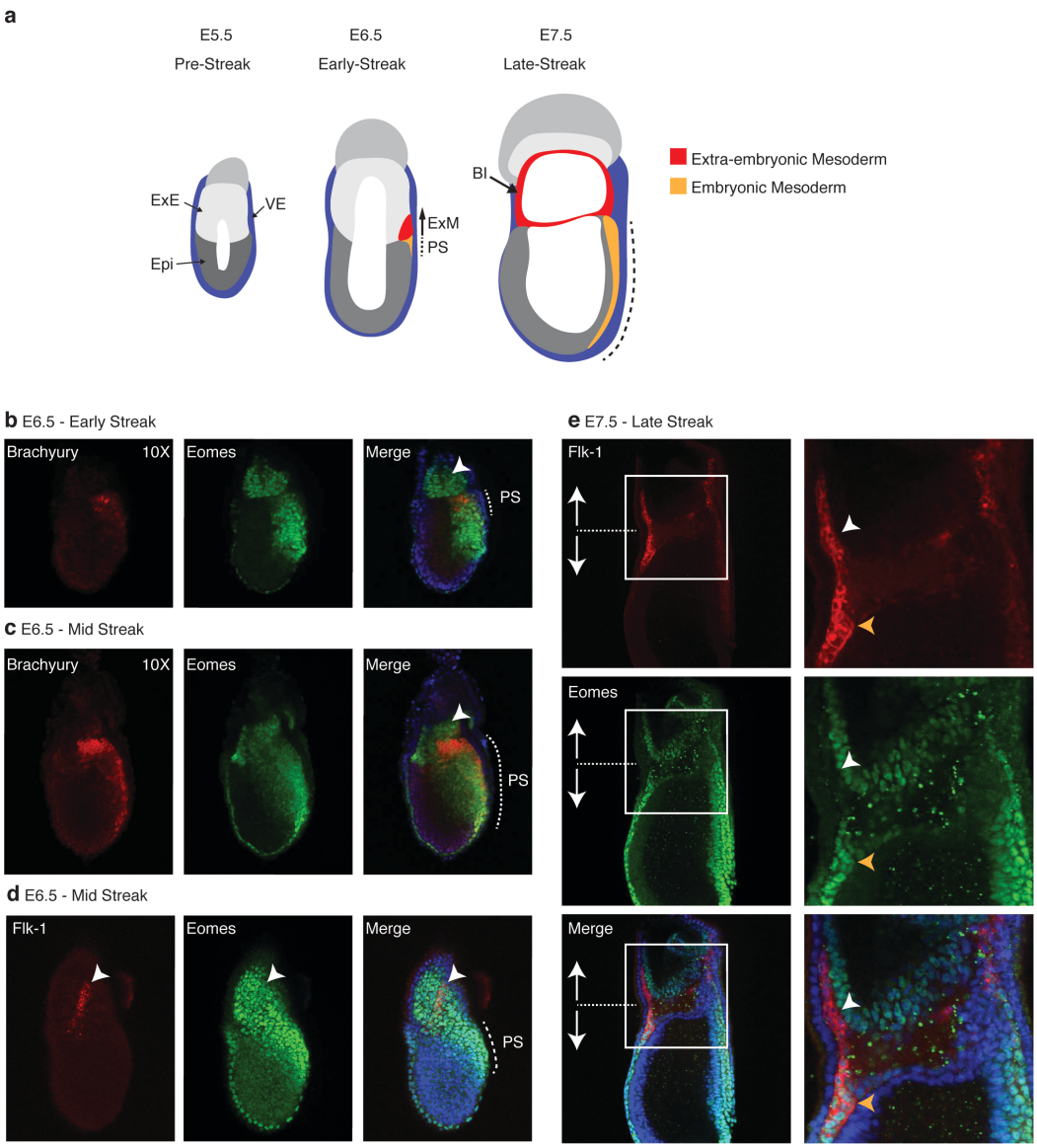


Figure 2.1 Eomes, T and Flk-1 expression patterns at the outset of mouse gastrulation

(a) Schematic representation of mouse gastrulation. ExM progenitors migrate proximally from the PS (dotted line) giving rise to the BIs of the developing YS. (ExE = extraembryonic ectoderm, Epi = epiblast, VE = visceral endoderm, PS = primitive streak). **(b, c)** Early/mid streak stage embryos (E6.5) stained for Brachyury (red) and Eomes (green) and counterstained with DAPI (blue). The length of the PS is denoted by the dotted line. **(d)** Early streak stage embryos (E6.5) stained for Flk-1 (red) and Eomes (green) and counterstained with DAPI (blue). The length of the PS is denoted by the dotted line. **(e)** Late streak stage embryos (E7.5) stained for Flk-1 (red) and Eomes (green) and counterstained with DAPI (blue). Dotted white lines indicate the extraembryonic/embryonic boundary. White boxes denote the zoomed in areas displayed in the right-hand panels. White arrows highlights Flk-1+/Eomes- ExM and the orange arrows highlight Flk1+/Eomes+ anterior embryonic mesoderm. *Immunostaining was performed by Claire Simon and Ita Costello.*

2.2.2 Eomes expressing cells give rise to ExM and YS hematopoietic and endothelial cells

To evaluate the contribution of Eomes expressing cells to the ExM of the developing YS we utilized an $Eomes^{GFP/+}$ reporter strain (Arnold et al., 2009). At E7.5, the stage when the blood islands begin to develop in the YS, $Eomes^{GFP/+}$ embryos were stained for the ExM/hematopoietic marker Runx1 and the ExM/endothelial marker Flk-1 **(Figure 2.2, a,b)**. GFP+ cells co-expressed Runx1/Flk-1 in the ExM cell population that lines the extra-embryonic visceral endoderm **(Figure 2.2, a,b, white arrows)**. At this stage Eomes protein was expressed in the anterior PS, nascent embryonic mesoderm and the chorionic layer in the extra-embryonic region of the embryo. However, Eomes protein was not expressed in GFP+ ExM cells **(Figure 2.2, c, white arrows)**. Therefore, the $Eomes^{GFP/+}$ mouse strain can be utilized for short-term lineage tracing due to GFP perdurance in the ExM lineage. These results demonstrate that Eomes expressing cells generate ExM.

To assess the contribution of Eomes expressing cells to the YS at later developmental stages Claire Simon generated an $Eomes^{iCre}$ reporter allele and performed longer-term fate mapping studies **(Figure 2.3, a)**. $Eomes^{iCre}$ male mice were crossed with female $ROSA26^{LacZ}$ (Friedrich and Soriano, 1991; Soriano, 1999) mice and the resulting embryos were stained for LacZ activity. At E8.5 and E9.5 the vast majority of mesoderm derived cells of the visceral yolk-sac, including hematopoietic and endothelial cells, are LacZ+ **(Figure 2.3, a)**. Altogether, these results demonstrate that the entire YS mesodermal lineage is derived from precursors that express Eomes.

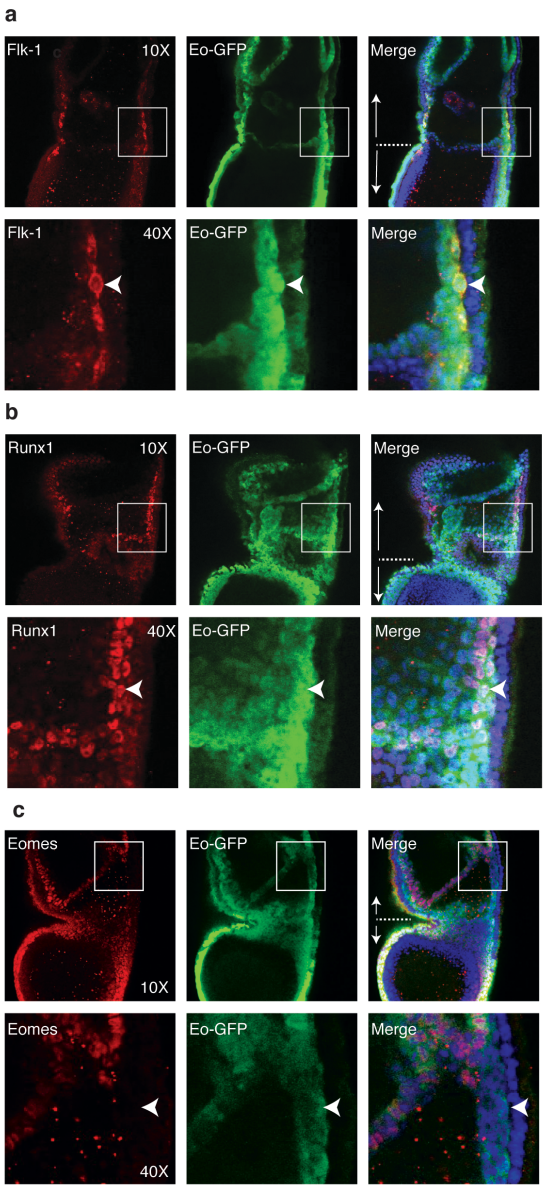


Figure 2.2 Eomes expressing progenitors generate YS mesodermal cells

(a-c) Immunofluorescence staining of E7.5 Eomes $^{GFP/+}$ embryos for Flk-1(red, **a**), Runx1(red, **b**) or Eomes (red, **c**) and Eomes-GFP (green). Nuclei are stained with DAPI (blue). Dotted white lines indicate the extraembryonic/embryonic boundary. White arrows indicate Eomes-GFP+ ExM cells. White boxes denote the zoomed in areas displayed in the lower panels. *Immunostaining experiments were performed by Ita Costello.*

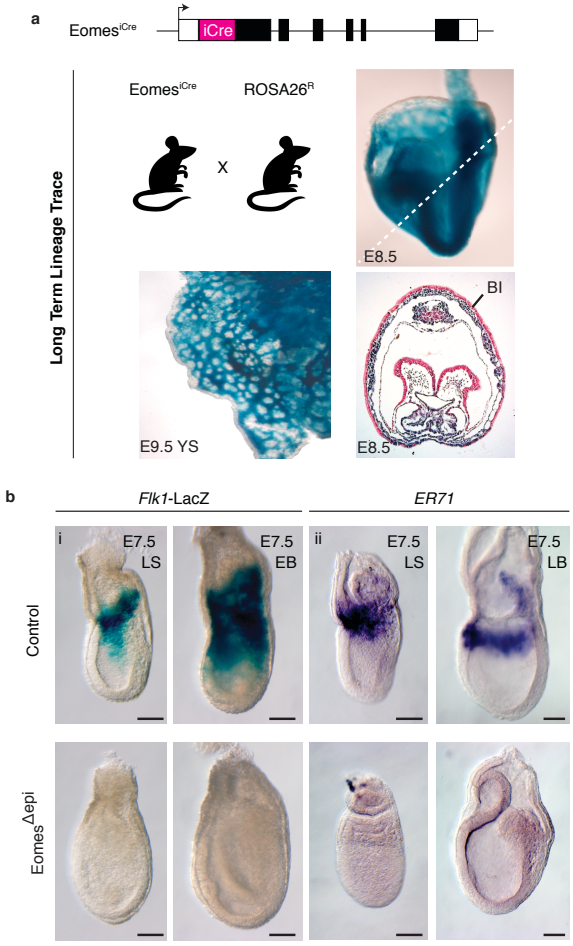


Figure 2.3 Eomes.iCre+ progenitors generate YS endothelial and hematopoietic cells

(a) Descendants of Eomes^{iCre} expressing cells give rise to hematopoietic and endothelial cells of the YS BI. Mice carrying an improved Cre recombinase (iCre) inserted into the ATG start site at the Eomes locus were crossed to ROSA26^{R} reporter mice that express LacZ upon Cre induced recombination. Wholemount X-gal staining was performed on E8.5 and E9.5 embryos and sections were counterstained with nuclear fast-red to highlight non-labelled cells. (BI = blood islands, YS = yolk-sac) **(b)** Eomes conditional inactivation in the epiblast (Eomes$^{\Delta epi}$) disrupts expression of extra-embryonic mesodermal markers. (i) Wholemount X-gal staining of E7.5 control (top) and mutant Eomes$^{\Delta epi}$ (bottom) embryos carrying a Flk-1-LacZ reporter allele. (ii) Wholemount in-situ hybridization analysis of ER71 expression in control (top) and mutant Eomes$^{\Delta epi}$ (bottom) embryos. Scale bars, 100 μm. (LS = late streak, EB = early allantoic bud stage). *Fate mapping/WISH/LacZ staining experiments were performed by Claire Simon.*

2.2.3 Eomes is functionally required for ExM development in vivo

Next, to assess whether or not Eomes is functionally required for the development of ExM the expression of Flk-1-LacZ and ER71 were evaluated in embryos in which Eomes was conditionally inactivated in the epiblast ($Eomes^{\Delta epi}$)(Arnold et al., 2008). Flk-1 and ER71 are essential for normal vasculogenesis and haematopoiesis to occur within the developing YS (Koyano-Nakagawa and Garry, 2017; Lee et al., 2008; Shalaby et al., 1995). Control embryos express Flk-1-LacZ and ER71 in the ExM, YS and allantois at E7.5 **(Figure 2.3, b)**. In striking contrast, equivalent stage $Eomes^{\Delta epi}$ embryos lack expression of Flk-1 and ER71 **(Figure 2.3, b)**. These results suggest that ExM specification relies on Eomes functional activity. Nascent mesoderm generated in $Eomes^{\Delta epi}$ embryos, however, does not properly delaminate and migrate from the PS (Arnold et al., 2008). Therefore, a block in ExM specification may occur in $Eomes^{\Delta epi}$ embryos as a consequence of morphogenetic defects rather than cell intrinsic requirements for Eomes during ExM specification.

2.2.4 Eomes, Scl and Runx1 expression kinetics during hematovascular development

To circumvent the problems associated with studying Eomes functional requirements *in vivo* I opted to utilize an *in vitro* differentiation system that models YS hematopoietic and vascular development (Clarke et al., 2013; Irion et al., 2010; Kattman et al., 2011; Nostro et al., 2008). Briefly, mESCs grown in 2i + LIF were dissociated and cultured in suspension on an orbital shaker overnight to promote the generation of spherical aggregates called embryoid bodies (EB). Two days later BMP4, Activin A and VEGF were added to the EB suspension cultures to promote the generation of $Flk1^{hi}/PdgfRa^{-}$ hematovascular mesoderm **(Figure 2.4, a)**. To monitor the efficiency of PS, mesoderm and hematopoietic induction we evaluated the

expression patterns of various cell surface markers (EpCAM, CD56, Flk-1, PdgfRa, CD41) from day 3-5 of EB culture **(Figure 2.4, b-d)**. Additionally, utilizing various mESC reporter lines ($Eomes^{GFP/+}$, $SCL^{mCherry/+}$, $Runx1^{Venus/Venus}$) (Arnold et al., 2009; Chagraoui et al., 2018) we also concurrently assessed the expression kinetics of Eomes as well as the hematopoietic master regulators SCL and Runx1 **(Figure 2.4, b-d)**. The $Runx1^{Venus}$ line was a gift from Marella de Bruijn, which has not yet been published.

The epithelial cell adhesion molecule (EpCAM) is initially expressed in the epiblast but downregulated during Flk-1+ mesoderm commitment *in vivo* and *in vitro* (Sarrach et al., 2018). Cell adhesion molecule (CAM) switching, downregulation of EpCAM and upregulation of N-CAM (CD56), occurs during an EMT like process in a human ES model of mesoderm development (Evseenko et al., 2010). In our *in vitro* differentiation system Eomes-GFP is initially expressed in an $EpCAM^{hi}$ population at day 3 **(Figure 2.4, b)**. At day 4 a PS-like/nascent mesodermal population of cells arise that downregulate EpCAM, induce high levels of CD56 expression and are predominantly EoGFP+ **(Figure 2.4, b)**. By day 5 the majority of EB cells no longer express EoGFP and are $EpCAM^{lo/-}$ and $CD56^{hi}$, indicating that CAM switching and an EMT like process has occurred efficiently in our EB cultures **(Figure 2.4, b)**.

To assess mesodermal generation in our cultures we assessed the expression of Flk-1 and PdgfRa, cell surface receptors that have been previously shown to distinguish hematovascular ($Flk\text{-}1^{hi}/PdgfRa^{-}$), cardiac ($Flk\text{-}1^{+}/PdgfRa^{+}$), and paraxial ($Flk\text{-}1^{-}/PdgfRa^{+}$) enriched mesoderm subpopulations (Izumi et al., 2007b; Kattman et al., 2011; Koyano-Nakagawa and Garry, 2017). Additionally, at day 5 we stained for the surface receptor CD41 which is the earliest known marker of hematopoietic progenitors (Ferkowicz et al., 2003;

Mikkola et al., 2003; Mitjavila-Garcia et al., 2002). In our culture system Eomes-GFP+ cells were first detectable at day 3, prior to the expression of Flk-1/PdgfRa **(Figure 2.4, c)**. A day later the majority of cells, including the Flk-1^{hi}/PdgfRa^{-} hematovascular mesoderm enriched compartment are Eomes-GFP+ **(Figure 2.4, c)**. At day 5, EomesGFP^{+} cells comprise roughly half the Flk-1^{hi}/PdgfRa^{-} compartment, however, developing CD41^{+} hematopoietic cells are predominantly Eomes-GFP- **(Figure 2.4, c,d)**. In contrast, SCL-mCherry and Runx1-Venus expression are first detectable within the Flk-1^{hi}/PdgfRa^{-} compartment at day 4 **(Figure 4, c)**. SCL-mCherry is expressed in nearly all Flk-1^{hi}/PdgfRa^{-} cells at day 4/5 whilst Runx1-Venus expression is restricted to a subset of this population that only weakly expresses Flk-1 **(Figure 2.4, c)**. Maturing hematopoietic cells co-express CD41 and SCL-mCherry/Runx1-Venus, are PdgfRa- and downregulate Flk-1 expression at day 5 **(Figure 2.4, c,d)**.

Consistent with our *in vitro* flow cytometry analysis and our *in vivo* lineage tracing and immunofluorescence studies, differentiation trajectories constructed using scRNAseq data from E6.5 to E8.5 mouse embryos (Pijuan-Sala et al., 2019) reveal dynamic Eomes transcript expression during hematoendotheilal development *in vivo* **(Figure 2.4, e)**. Eomes is expressed transiently in a population of mixed mesoderm and hematoendothelial progenitors that upregulate ER71 and Flk-1, downregulate PdgfRa and give rise to endothelial and hematopoietic cells **(Figure 2.4, e)**. Concurrent with downregulation of PdgfRa expression hematoendothelial progenitors upregulate expression of SCL **(Figure 2.4, e)**. Finally, developing hematopoietic cells downregulate expression of Flk-1, maintain SCL expression and upregulate Runx1expression **(Figure 2.4, e)**. Collectively these results highlight the similarities between our *in vitro* differentiation system and hematovasular development *in vivo*. In both instances, Eomes is transiently expressed prior to the onset of SCL and Runx1 expression during the development of the hematovascular lineage.

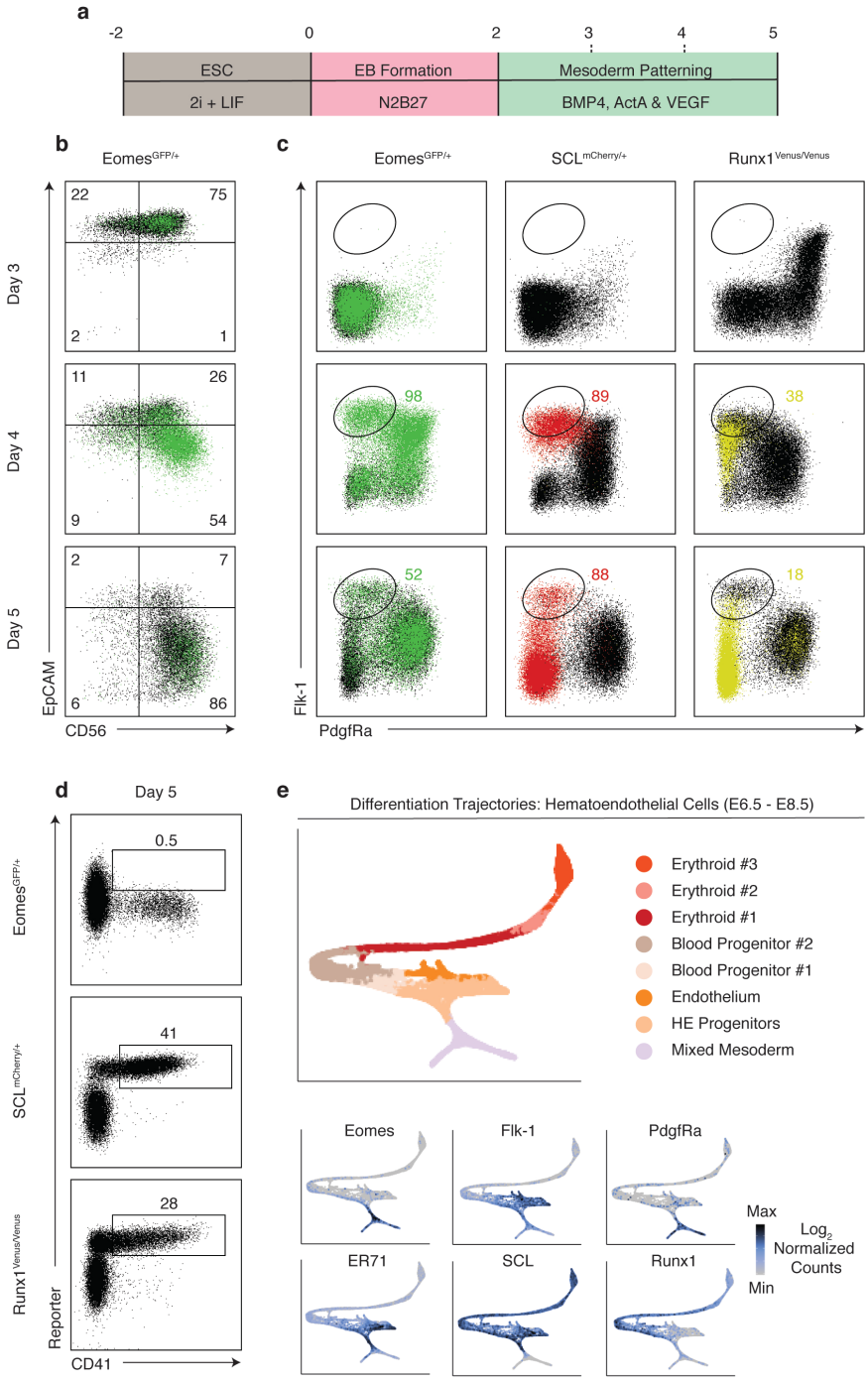


Figure 2.4 Eomes, SCL and Runx1 expression kinetics during hematovascular development *in vitro* and *in vivo*

(a) Schematic representation of the ESC differentiation protocol used to generate hematovascular mesoderm. **(b)** Flow cytometry analysis for CD56 and EpCAM expression of day 3-5 EB cultures generated from Eomes$^{GFP/+}$ ES cells. Green dots are Eomes-GFP+ and black dots are Eomes-GFP- (representative FACS plots from n=2 Eomes$^{GFP/+}$ clones). **(c)** Flow cytometry analysis of EB cultures generated from Eomes$^{GFP/+}$, SCL$^{mCherry/+}$ and Runx1$^{Venus/Venus}$ ESC reporter ESC lines. Cells expressing the indicated fluorescent reporters are shown by

***Figure legend 2.4 continued*;** coloured dots (Eomes-GFP+ = green, SCL-mCherry+ = red, Runx1-Venus+ = yellow). The percentages of reporter positive cells within the circled Flk-1^{hi}/PdgfRa^{-} cell population are also indicated. (FACS plots from n=1 independent differentiation). **(d)** Analysis of day 5 EBs showing fluorescent reporter activity and expression of the hematopoietic marker CD41. (FACS plots from n=1 independent differentiation). **(e)** Force-directed graph layout of cells isolated from E6.5 to E8.5 embryos associated with the blood/endothelial lineage, adapted from: (Pijuan-Sala et al. 2019). Top plot highlights various sub-clusters (HE = hematoendothelial) that are generated along the hematovascular lineage trajectory as mesoderm differentiates into endothelial and hematopoietic cells. Bottom plots are overlaid with Log_2 normalized gene expression levels.

2.2.5 Eomes functional loss disrupts primitive and pro-definitive haematopoiesis

Next, I examined the ability of Eomes-loss-of-function ESCs (Eomes-/-)(Arnold et al., 2008; Costello et al., 2011) to differentiate into hematovascular mesoderm *in vitro* **(Figure 2.5, a)**. Eomes-/- ESCs are able to generate an EpCAM$^{lo/-}$/CD56^{hi} population by day 5, suggesting that an EMT-like process occurs *in vitro* even in the absence of Eomes functional activity **(Figure 2.5, b)**. These findings are in line with a previous study that demonstrated that *ex vivo* Eomes$^{\Delta epi}$ PS outgrowths can downregulate EpCAM and undergo migration (Arnold et al., 2008). Efficiency of mesodermal generation was evaluated in Eomes-/- cultures by staining day 4/5 EBs for Flk-1 and PdgfRa expression **(Figure 5, c)**. In line with the known role for Eomes during cardiac mesoderm specification, day 4 Eomes-/- EBs lack a Flk-1^{+}/PdgfRa^{+} cell population and express lower levels of the known Eomes target and master regulator of cardiac lineage specification, Mesp1(Costello et al., 2011; Van Den Ameele et al., 2012) **(Figure 2.5, c,d)**. Interestingly, day 4 Eomes-/- EBs contain higher proportions of Flk-1^{-}/PdgfRa^{+} cells and lower levels Flk-1^{hi}/PdgfRa^{lo} cells compared to wildtype EBs (Figure 2.5, c). Consistent with these results day 4 qPCR analysis of bulk Eomes-/- EBs reveals that they express higher levels of paraxial mesodermal genes Tbx6, Msgn1 and T and lower

levels of hematovascular mesoderm transcription factors ER71, SCL and Gata2 **(Figure 2.5, d)**.

As the Flk-1^{hi}/PdgfRa^{lo} cell population, that is normally enriched for hematovascular mesoderm was still present in Eomes-/- cultures at day 4, and by day 5 had increased in size **(Figure 2.5, c)**, we decided to culture the EBs further in pro-hematoendothelial conditions (VEGF and SCF) to examine Eomes requirements at later stages of YS-like hematovascular development (Irion et al., 2010; Nostro et al., 2008). Wild-type cultures robustly form hematopoietic progenitors that co-express c-Kit, and CD41/CD45, and upon re-plating generate primitive and definitive erythrocyte and myeloid/mixed hematopoietic colonies **(Figure 2.5, e,g)**. In striking contrast, Eomes-/- cultures generate very few if any CD41^{+}/CD45^{+} cells or primitive/definitive hematopoietic colonies **(Figure 2.5, e,g)**. Additionally, RT-qPCR analysis reveals a strong downregulation of SCL, Runx1, PU.1, Gata1 and Hbb-bh1 transcripts in day 6 Eomes-/- EBs, confirming the profound block in hematopoiesis **(Figure 2.5, f).** Day 6 Eomes-/- cultures, however, express normal levels of Cdh5, Flk-1, Flt-1 and Fli-1 transcripts and contain a small population of CD31^{+}/Cdh5^{+} cells **(Figure 2.5, f,h)**. Altogether these results suggest that endothelial specification still occurs in the absence of Eomes function, but Eomes activity is essential for the development of hematopoietic progenitors.

To further explore the impact of Eomes loss of function during YS-like hematoendothelial development we refined our differentiation system by isolating Flk-1^{+} cells from day 5 EBs (using magnetic activated cell sorting, MACS) and plating them on Matrigel in conditions known to promote the development of HE (Clarke et al., 2013) **(Figure 2.6, a,b)**. By day 8 wild-type Flk-1^{+} cells give rise to patches of adherent Cdh5^{+}/c-Kit^{+} HE cells that actively

undergo EHT, and generate semi-adherent and floating CD41^{+}/CD45^{+} hematopoietic cells **(Figure 2.6, c-e)**. Eomes-/- Flk-1^{hi} cells generate Cdh5^{+}/c-Kit^{+} endothelium, however, strikingly these cells fail to efficiently undergo EHT and as a result cultures lack CD41^{+}/CD45^{+} hematopoietic cells **(Figure 2.6, c-e)**. Altogether these results confirm that Flk-1^{+} cells that arise in Eomes-/- cultures are able to efficiently differentiate into endothelial cells, however, this endothelium cannot undergo EHT and generate hematopoietic progenitors.

2.2.6 Transcriptional characterization of Flk-1/PdgfRa mesodermal populations generated in Eomes loss-of-function cultures

To further characterize Eomes' role during mesoderm development, we performed RNA-seq on the various Flk-1/PdgfRa populations that form in wild-type and Eomes-/- EBs at day 4 as well as wild-type mES cells from day 0 **(Figure 2.7, a)**. Principal component analysis and hierarchical clustering were used to identify transcriptional similarities and differences between the various RNA-seq samples. The first three principal components captured the majority (>80%) of transcriptional variation between samples **(Figure 2.7, b)**. Biological replicates within groups clustered closely together when projected onto the first three principal components, demonstrating that the ES cell differentiation protocol we utilized is highly reproducible **(Figure 2.7, c,d)**. Principal component 1 accounts for 50% of the transcriptional variation between samples and separated day 0 mES cells from day 4 EB cell populations **(Figure 2.7, c)**. Principal component 1 was enriched for genes related to anterior/posterior pattern specification (T, Mesp1, Wnt5a and Msgn1) and vasculature development (Aplnr, Tal1 and Hand1) **(Figure 2.7, e)**. In contrast, principal component 2 separated the Flk-1^{hi}/PdgfRa^{-} sorted cell populations from the PdgfRa^{+} populations and was

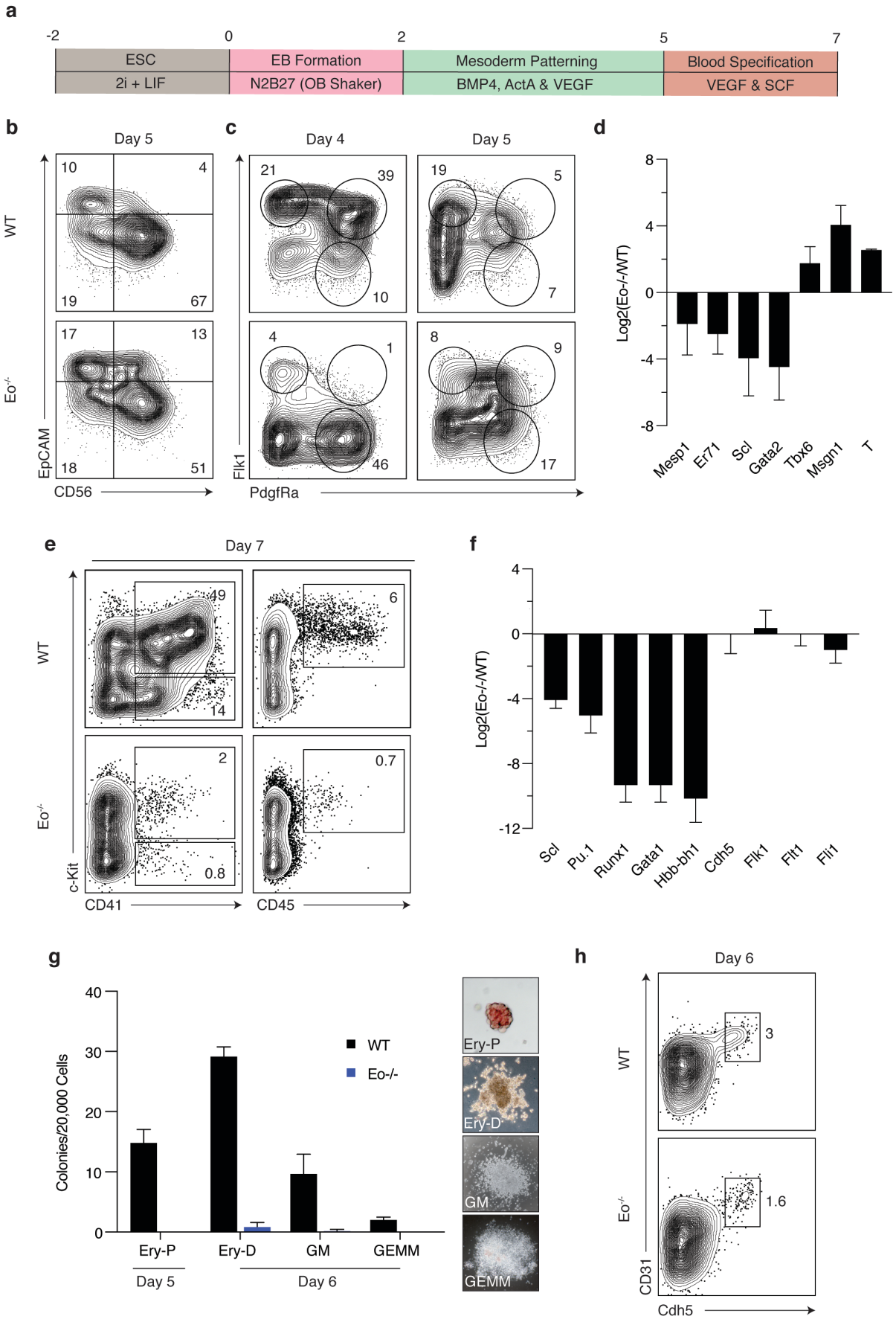


Figure 2.5 Eomes loss-of-function disrupts primitive and pro-definitive hematopoiesis

***Figure legend 2.5 continued*; (a)** The ESC differentiation protocol used for generation of hematopoietic and endothelial progenitors. **(b)** EpCAM and CD56 expression in wild-type (WT) (top) and Eomes$^{-/-}$ (bottom) EBs. (FACS plots from n=1 independent differentiation). **(c)** Flk-1 and PdgfRa expression in wild-type (WT) (top) and Eomes$^{-/-}$ (bottom) EBs at day 4 (left) and day 5 (right). (Representative FACS plots from n=3 independent differentiations). **(d)** Reverse transcription quantitative PCR (RT-qPCR) for hematopoietic, cardiovascular and paraxial mesoderm marker gene expression in day 4 EB cultures. (n=3 WT and n=3 Eomes$^{-/-}$ clones). **(e)** Day 7 Eomes$^{-/-}$ EB cultures lack hematopoietic progenitors marked by expression of CD41, CD45 and c-Kit. (Representative FACS plots from differentiations with n=3 WT and n=3 Eomes$^{-/-}$ clones.) **(f)** Reverse transcription quantitative PCR (RT-qPCR) of hematopoietic and endothelial marker gene expression in day 6 EB cultures. (n=3 WT and n=3 Eomes$^{-/-}$ clones). **(g)** Hematopoietic potential of cells isolated from WT and Eomes$^{-/-}$ EBs plated in hematopoietic colony assays to assess primitive erythrocyte and definitive erythro-myeloid colony potential, respectively. (Day 5, n=2 and Day 6, n=3) **(h)** Endothelial progenitors form in Eomes$^{-/-}$ and WT day 6 EBs. (Representative FACS plots from differentiations with n=3 WT and n=3 Eomes$^{-/-}$ clones.) [Error bars in bar charts represent the standard error of the mean]

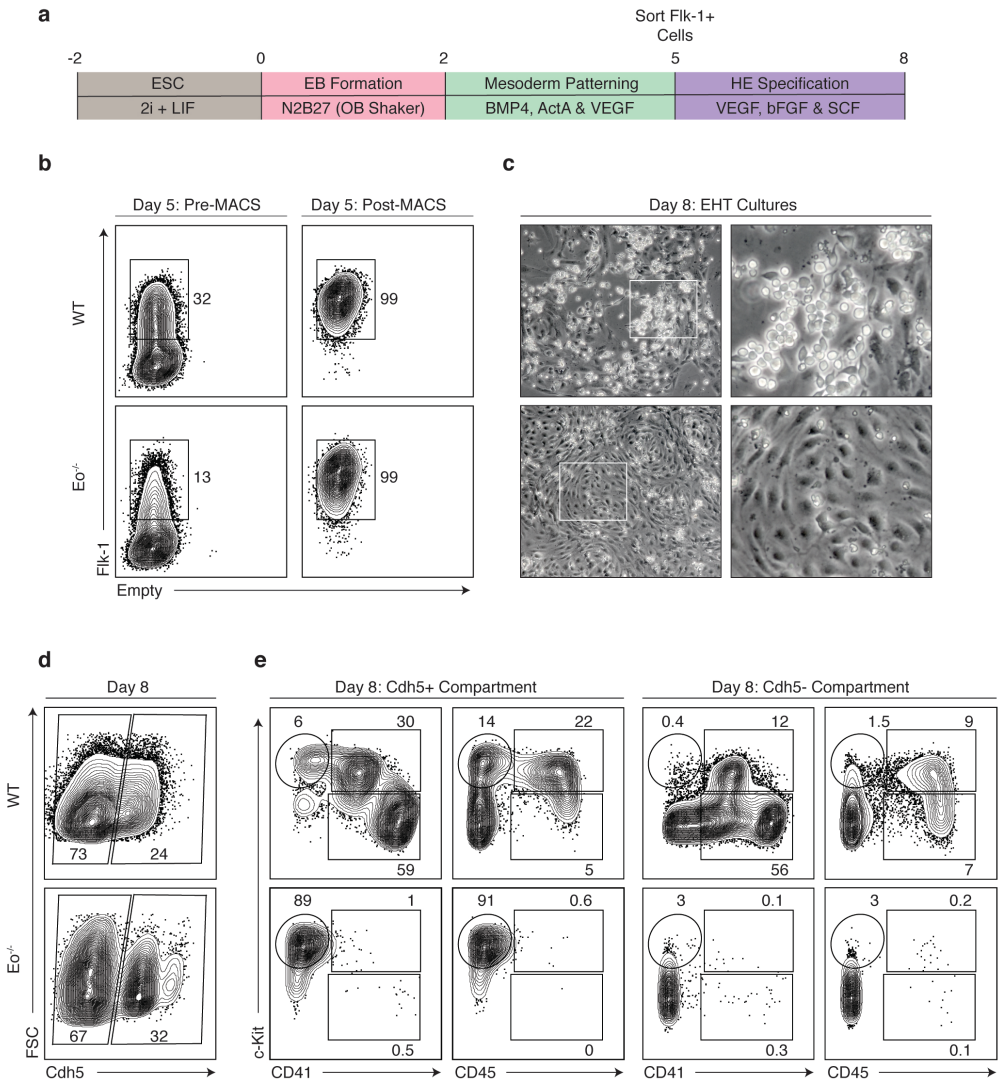


Figure 2.6 Eomes loss-of-function disrupts EHT

(a) Schematic of the endothelial-to-hematopoietic transition (EHT) differentiation protocol. At day 5 Flk-1+ cells are purified from EBs and plated on Matrigel in conditions that promote the generation of hemogenic endothelial cells and EHT. **(b)** Magnetic activated cell sorting strategy used to purify Flk-1+ cells from day 5 WT and Eomes$^{-/-}$ EBs. **(c)** Phase contrast images of WT (top) and Eomes$^{-/-}$ (bottom) EHT cultures at day 8. **(d)** Roughly similar proportions of endothelial cells (Cdh5^{+}, left) are generated in WT and Eomes$^{-/-}$ EHT cultures at day 8, however the Eomes$^{-/-}$ Cdh5^{+} and Cdh5- compartment lacks CD41^{+}/CD45^{+} hematopoietic progenitors. (Representative FACS plots from n=2 independent differentiations).

enriched for genes related to blood vessel morphogenesis (Tek, Tie1 and Cdh5) **(Figure 2.7, c-e)**. Finally, principal component 3 separated wildtype and Eomes-/- samples and was enriched for genes related to the interferon response (Gbp2, Ifit3) **(Figure 2.7, d,e)**.

To further explore the impact of Eomes loss of function on mesoderm development, I additionally evaluated the expression of published marker genes for various cell populations identified using scRNA-seq data from E6.5 to E8.5 mouse embryos (Pijuan-Sala et al., 2019) **(Figure 2.8)**. Interestingly, Eomes-/- Flk-1^{-}/PdgfRa^{+} cell populations express high levels of paraxial and somitic mesoderm markers including Tcf15, Meox1, Tbx6, Hoxa2, Aldh1a2 and Dll1 **(Figure 2.8)**. These results suggest that the PdgfRa+ cell population that forms in the absence of Eomes function is diverted towards a paraxial fate, even in cardiovascular inductive conditions. In contrast, Eomes-/- Flk-1^{hi}/PdgfRa^{-} cell populations correctly induce expression of marker genes for hematoendothelial progenitors (Etv2, Vgll4 and Mmp9) and endothelial cells (Esam, Cldn5 and Cdh5) **(Figure 2.8)**. Furthermore, Eomes-/- Flk-1^{hi}/PdgfRa^{-} cell populations express a subset of blood progenitor marker genes including transcriptional regulators that are essential for hematopoiesis including Lmo2, Gata2, and Myb **(Figure 2.8)**. Strikingly, EHT regulators, Runx1 and Gfi1/1b, and genes expressed in maturing erythroid cells, Gata1, Hbb-bh1 and Hbb-y are strongly downregulated in the Eomes-/- Flk-1^{hi}/PdgfRa^{-} cell population. Altogether, these results suggest that the Eomes-/- Flk-1^{hi}/PdgfRa^{-} cell population likely contains hematovascular mesoderm.

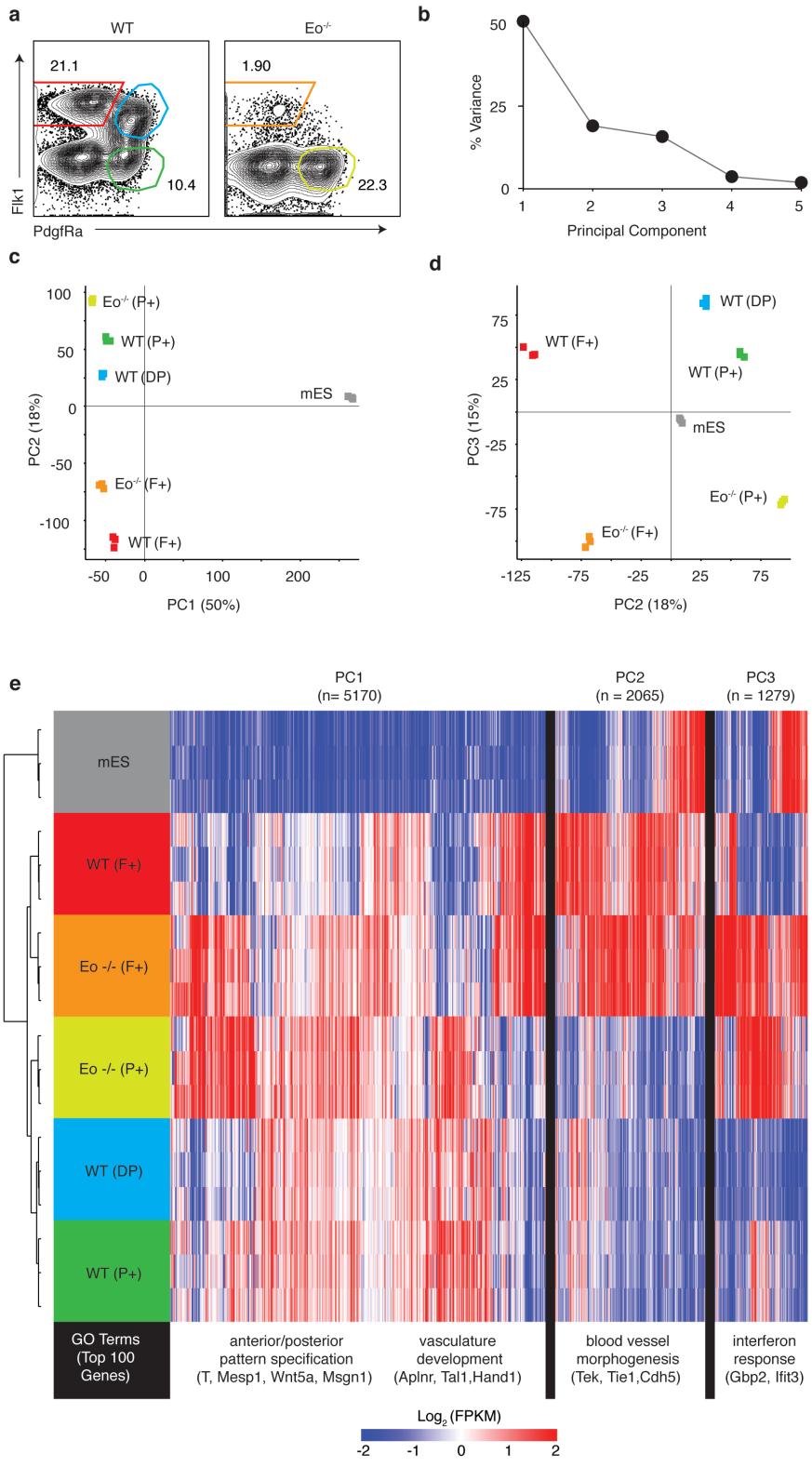


Figure 2.7 Comparing the transcriptional profiles of various Flk-1/PdgfRa mesodermal populations that form in wildtype and Eomes-loss-of-function EBs

Figure legend 2.7 continued; **(a)** Gating strategy used to sort Flk1^{hi}/PdgfRa^{-}, Flk1^{+}/PdgfRa^{+} and Flk1^{-}/PdgfRa^{+} cells for RNA-seq from day 4 wildtype and Eomes$^{-/-}$ EB cultures. (Representative FACS plots from n=3 independent differentiations). **(b)** The majority of the variation in gene expression amongst the various wildtype and Eomes$^{-/-}$ day 4 RNA-seq samples and day 0 wildtype mES cells is captured by the first three principal components. **(c, d)** Principal component plots for all RNA-seq samples showing PC1 vs. PC2 **(c)** and PC 2 vs. PC3 **(d)**. **(e)** Heatmap showing the Log_2FPKM expression of the genes that make up the first three principal components in the various RNA-seq samples. Hierarchical clustering using all genes (tree diagram, left side of panel) indicates that the transcriptomes of wildtype and Eomes$^{-/-}$ Flk1^{hi}/PdgfRa^{-} cells are more similar to each other than to the transcriptomes of the other wildtype and Eomes$^{-/-}$ Flk1^{+}/PdgfRa^{+} and Flk1^{-}/PdgfRa^{+} samples. Examples of GO Terms related to the top 100 genes that drive PC1, PC2 and PC3 are also shown below the heatmap. *RNA-seq analysis was done in collaboration with Anna Senft.*

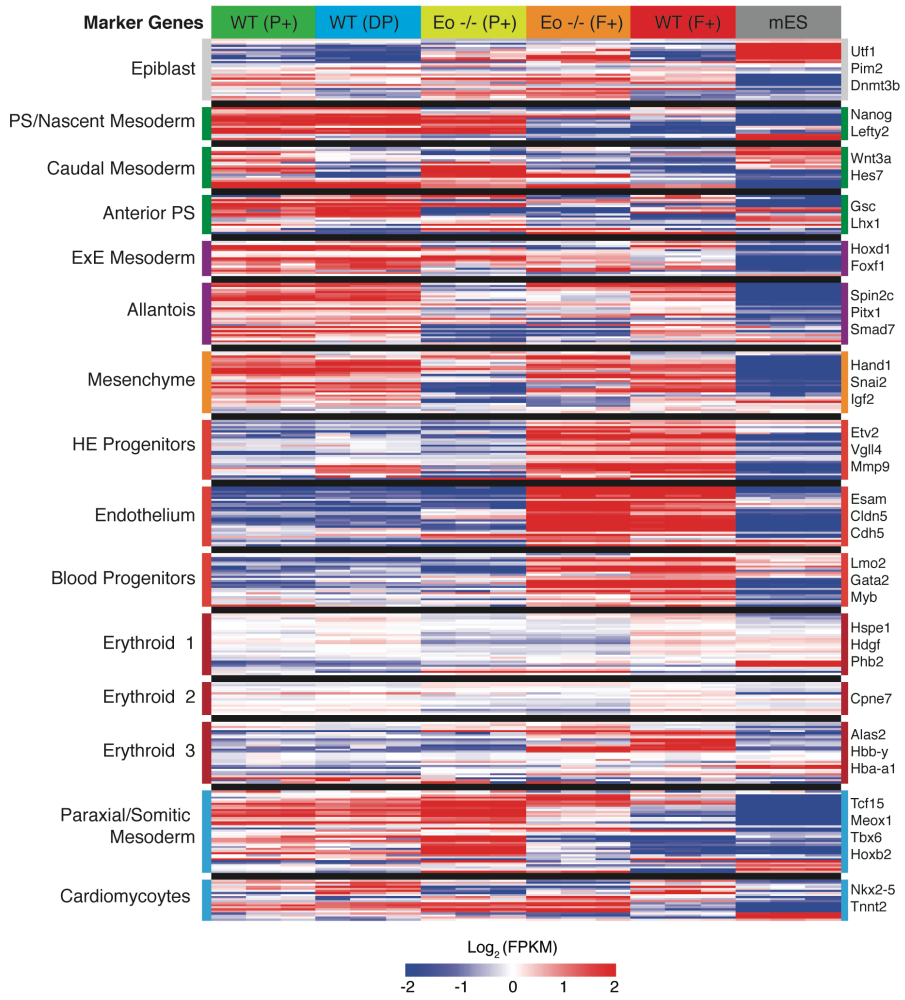


Figure 2.8 Expression of *in vivo* cell type markers in Eomes-/- and WT day 4 Flk1/PdgfRa EB populations

Marker genes are taken from the mouse gastrulation atlas. (Pijuan-Sala et al., 2019)

2.2.7 scRNA-seq analysis of Eomes mutant Flk-1^{hi}/PdgfRa^{-} cells

As Eomes-/- ES cells are able to differentiate into endothelium but not hematopoietic progenitors, we reasoned that the profound block in hematopoietic development may result because a subset of hematopoietic mesoderm, normally present in the Flk-1^{hi}/PdgfRa^{-} mesoderm population, is not generated in the absence of Eomes function. To assess whether a subset of hematopoietic mesoderm is lost, in collaboration with Professor Marella de Bruijn, I performed single-cell RNA-seq (scRNA-seq) at day 4 and day 5 on the Flk-1^{hi}/PdgfRa^{-} populations that form in Eomes-/- and wild-type EBs. Eomes-/- and wild-type Flk-1^{hi}/PdgfRa^{-} cells were sorted using FACS **(Figure 2.9, a)** and put through the 10X genomics platform to generate single cell transcriptional profiles. After quality control and pre-processing an integrated analysis of 7,610 wild-type and 7,610 Eomes-/- cells (3805 cells per day/per genotype) was performed using Seurat v3 (Butler et al., 2018) that allowed the identification of 13 cellular sub-populations **(Figure 2.9, c)**. Cell types were assigned to these 13 clusters by comparing conserved marker genes across genotypes for each cluster to markers previously used to document discrete cell populations present in E6.5 to E8.5 embryos (Pijuan-Sala et al., 2019) **(Table 4)**.

Cells that constitute clusters 1-6 express mesodermal (T, Mixl1, Mesp1) and hematoendothelial progenitor marker genes (SCL, Etv2 and Lmo2) and are predominantly made up of day 4 cells **(Figure 2.9, b-d and f)**. By contrast, clusters 7-13 are predominantly made up of day 5 cells that lack expression of mesodermal markers and instead express endothelial (Cdh5, Pecam1, Tek, Esam, Sox17), allantoic (Spin2c, Twist1, Pitx1), EHT (Runx1/Gfi1b) and hematopoietic (Gata1, Hbb-bh1) genes **(Figure 2.9, b-d and f)**. Comparison of the relative contributions of Eomes-/- and wild-type cells to the 13 clusters **(Figure 2.9, e)** demonstrates that Eomes-/- and wild-type cells contribute a relatively equal

number of cells to mesodermal/hematoendothelial progenitor clusters 2-6 at day 4. Cluster 1, however, is predominantly made up of Eomes-/- cells. A day later Eomes-/- Flk-1^{hi}/PdgfRa^{-} cells mainly contribute to hematoendothelial progenitor, endothelial and allantoic clusters 9-13 at the expense of contributing to hematopoietic clusters 7 and 8 **(Figure 2.9, e)**.

Additionally, this analysis allowed us to identify genes that are differentially expressed in wildtype versus Eomes-/- cells in each of the 13 sub-clusters identified **(Table 5)**. Interestingly, the known downstream Eomes target, Mixl1 (Izumi et al., 2007a; Tosic et al., 2019), was significantly downregulated in mesoderm clusters 1 and 2 **(Figure 2.9, f)**. Furthermore, Mesp1 was significantly downregulated and the epithelial marker EpCAM was significantly upregulated in Eomes-/- cells in cluster 1. Strikingly, the most highly down-regulated gene in the small number of Eomes-/- cells that contribute to hematopoietic clusters 7/8 was Runx1, the master regulator of definitive hematopoiesis(de Bruijn and Dzierzak, 2017) **(Table 5 and Figure 2.9, f)**. ER71 and Scl, genes known to sit atop the transcriptional hierarchy and direct hematopoietic specification from mesoderm (Koyano-Nakagawa and Garry, 2017; Porcher et al., 2017), however, were expressed at similar levels in the various clusters **(Figure 9, f)**.

In collaboration with Ivan Imaz-Rosshandler, Dr. John Marioni and Professor Bertie Gottgens we compared our *in vitro* scRNA-seq dataset to a recently published scRNA-seq dataset generated from E6.5 to E8.5 embryos (Pijuan-Sala et al., 2019), hereafter referred to as the mouse atlas. This allowed us to assess how well our wildtype and Eomes$^{-/-}$ Flk-1^{hi}/PdgfRa^{-} *in vitro* populations mimic normal murine embryonic development.

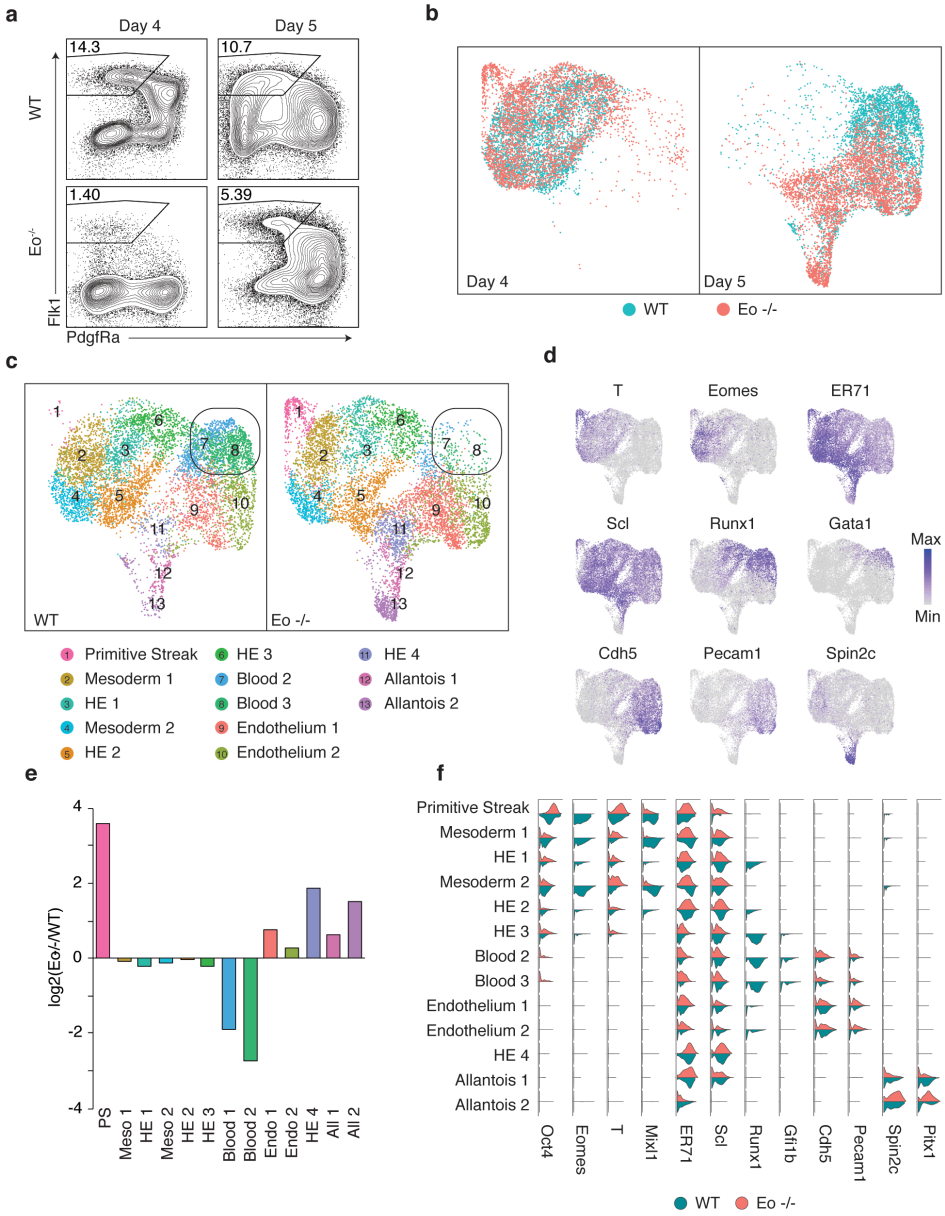


Figure 2.9 scRNA-seq suggests that hematoendothelial progenitors are still specified in the absence of Eomes function but blood progenitors are lost

(a) Gating strategy used to sort Flk1^{hi}/PdgfRa^{-} cells from day 4 and day 5 wildtype and Eomes$^{-/-}$ EBs for 10X scRNA-seq. **(b, c)** Uniform manifold approximation and projection (UMAP) plots. WT (blue) and Eomes$^{-/-}$ (red) Flk-1^{hi}/PdgfRa^{-} cells from day 4 (left) and day 5 (right) EBs (3805 cells/genotype/day) **(c)** WT (left) and Eomes$^{-/-}$ (right) cells coloured by their Seurat cluster/cell type annotation denoted in the legend below. The black box highlights clusters 7 and 8 that are diminished in the Eomes$^{-/-}$cultures. **(d)** Normalized expression levels of the indicated genes overlaid on UMAPs for all cells. **(e)** Log2 fold change in the abundance of Eomes$^{-/-}$ cells with respect to WT cells in each Seurat cluster. **(f)** Violin plots showing mesodermal, hematovascular and allantoic gene expression levels in the WT (blue) and Eomes$^{-/-}$ (red) cells within the various Seurat clusters. sc*RNA-seq experiments/analyses were done in*

Figure legend 2.9 continued; *collaboration with Marella de Bruijn, Neil Ashley, Guanlin Lang and Supat Thongjuea.*

A mutual-nearest-neighbor algorithm was used to identify the most similar cells present in the mouse atlas to our 7,610 wild-type and 7,610 Eomes-/- cells generated *in vitro*. Using this approach, cell type identities and embryonic stages from the mouse atlas were assigned to each of the cells in our scRNA-seq dataset **(Figure 2.10, a-c)**. The majority of day 4 wildtype cells are most similar to hematoendotheilal progenitors (grey) from E7.0 to E7.5 mouse embryos **(Figure 2.10, a-c)**. In contrast, day 5 wildtype cells contain hematoendothelial progenitors (grey), endothelial cells (green) and blood progenitors 1/2 (orange/red) from later embryonic stages (E7.5-E8.5) **(Figure 2.10, a-c)**. Similarly, the majority of day 4 Eomes$^{-/-}$ cells map back to hematoendothelial progenitors (grey) from E7.0 – E8.0 mouse embryos **(Figure 2.10, a-c)**. The day 5 Eomes-/- Flk-1^{hi}/PdgfRa^{-} cell population contains hematoendothelial progenitors (grey), endothelial cells (green), allantois (purple) and extraembryonic mesodermal cells (pink) from later stage (E8.0-E8.5) embryos **(Figure 2.10, a-c)**. In accordance with our previous analysis, the cellular subpopulations missing in day 5 Eomes-/- Flk-1^{hi}/PdgfRa^{-} cells (black box) are most similar to blood progenitor populations in the embryo (orange/red) **(Figure 2.10, a)**. A mapping probability score was also assigned to each cell indicating the extent of similarity between its transcriptome and the transcriptome of its most similar cell in the mouse atlas **(Figure 2.10, d)**. The vast majority of both wildtype and Eomes-/- cells have mapping probability scores >0.5, which suggests that the majority of our *in vitro* cells are highly similar to their matching *in vivo* counterparts.

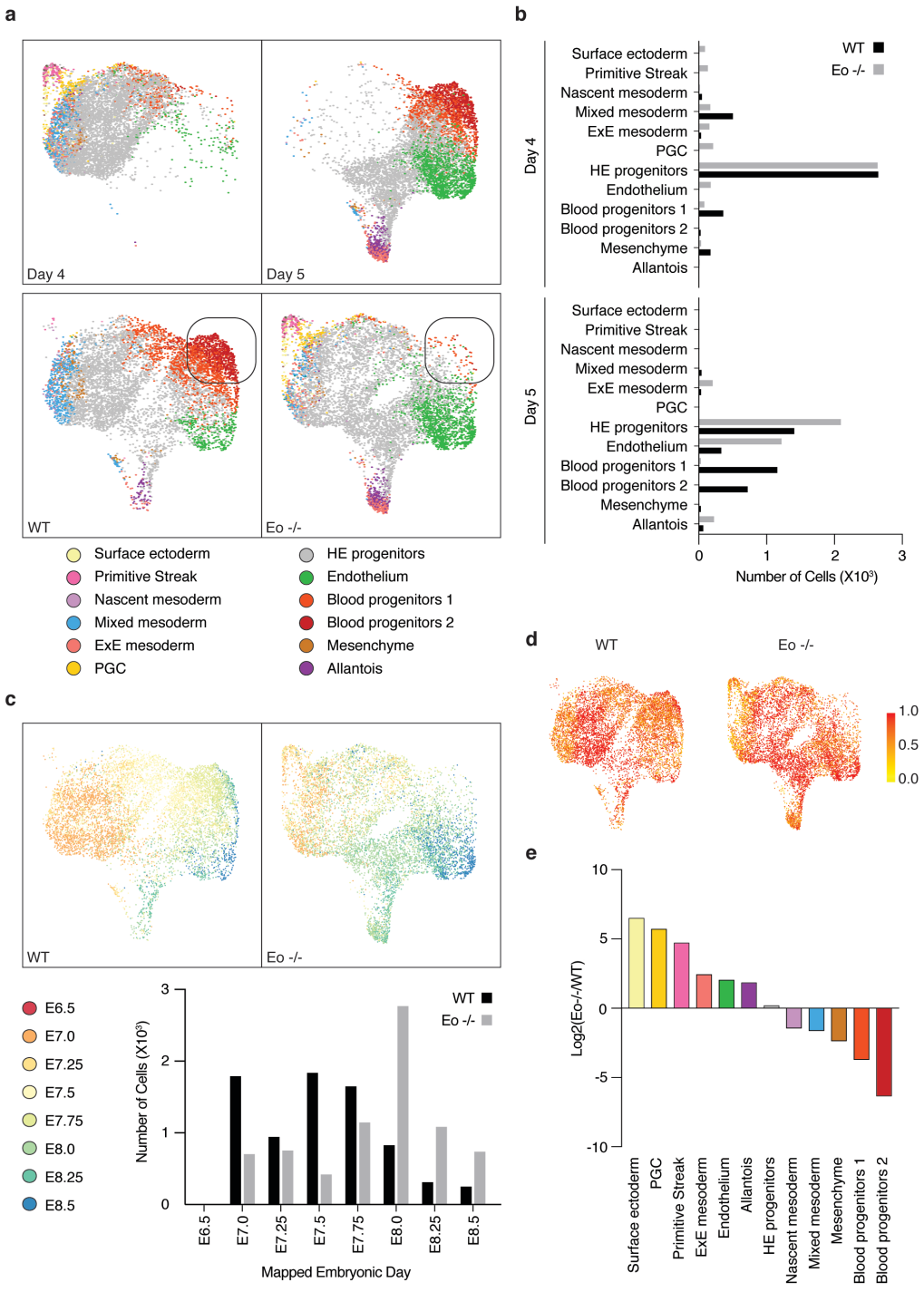


Figure 2.10 Mapping WT and Eomes-/- Flk1^{hi}/Pdgfra^{-} cells generated *in vitro* onto the *in vivo* mouse gastrulation atlas

Figure legend 2.10 continued; **(a)** Mapped cell types in UMAP embeddings. Cells are coloured by the nearest mapped cell type from the mouse atlas generated from scRNA-seq data of E6.5 to E8.5 mouse embryos, as indicated in the legend at the bottom of the panel. (HE = hematoendothelial) **(b)** Bar chart showing the abundance of different mapped cells types in day 4 (upper panel) and day 5 (lower panel) Flk-1^{hi}/PdgfRa^{-} wildtype (black) or Eomes-/- (grey) cell populations. **(c)** Mapped embryo stages in UMAP embeddings. Cells are coloured by the nearest mapped embryo stage in the mouse atlas as indicated in the legend in the bottom left hand side of the panel. Bar chart shows the number of wildtype (black) or Eomes-/- (grey) cells from each embryo stage. **(d)** Mapped mapping scores in UMAP embeddings. **(e)** Log2 fold change in the abundance of Eomes-/- cells with respect to WT cells for various mapped cell types. sc*RNA-seq analyses were done in collaboration with Ivan Imaz-Rosshandler, John Marioni and Bertie Gottgens.*

Comparing the relative contributions of Eomes-/- and wild-type cells to the various cell types present in the mouse atlas reinforces that Eomes-/- cells contribute to endothelial and allantois clusters at the expense of contributing to hematopoietic clusters **(Figure 2.10, e)**. Interestingly, Eomes-/- Flk-1^{hi}/PdgfRa^{-} cells do not become stuck in a primitive developmental fate as they generate endothelial and HE progenitors similar to those from E8.0-E8.5 embryos **(Figure 2.10, c)**. Finally, mapping wildtype and Eomes-/- Flk-1^{hi}/PdgfRa^{-} cells back onto the differentiation trajectory for hematoendothelial cells **(Figure 2.11)**, reinforces that the block in hematopoietc development occurs in Eomes-/- EB cultures after specification of HE progenitors.

2.2.8 Eomes is non-essential for the expression of SCL during hematovascular development in vitro

Our *in vitro* differentiation experiments demonstrate that Eomes loss-of-function results in a similar phenotype to published SCL loss-of-function mutants that lack primitive and definitive hematopoietic progenitors (Porcher et al., 2017). Our bulk-RNA-seq and scRNA-seq data, however, suggests that SCL transcription is unperturbed at day 4 and 5 in the Flk-1^{hi}/PdgfRa^{-} cell populations generated in the absence of Eomes function **(Figure 2.12, a,b)**.

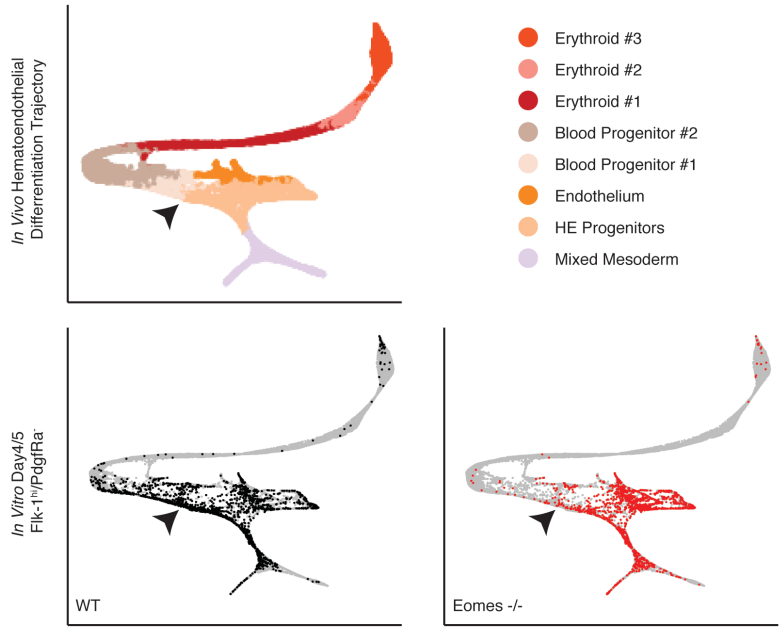


Figure 2.11 Eomes-/- cells do not transition from hematoendothelial progenitors into blood progenitors
Wildtype and Eomes-/- Flk-1^{hi}/PdgfRa^{-} cells generated *in vitro* were mapped back onto the hematoendothelial differentiation trajectory generated from hematoendothelial cells present in the mouse atlas (Pijuan-Sala et al., 2019).

To more thoroughly assess the impact of Eomes loss-of-function on SCL expression during hematopoiesis we re-generated the Eomes-/- allele in ESCs that contain an SCL-mCherry reporter allele (Chagraoui et al., 2018) using CRISPR-Cas9 **(Figure 2.12, c-e)**. In this cell line mCherry fluorescent protein is linked to the C-terminus of SCL downstream of a self-cleaving 2A peptide sequence. In accordance with our RNA-seq results, a high proportion of Eomes-/- Flk-1^{hi}/PdgfRa^{-} cells at day 5 express wild-type levels of SCL-mCherry (**Figure 2.12, f)**. A day later the vast majority (>85%) of cells in WT cultures express SCL-mCherry and the majority of these SCL+ cells express the hematopoietic marker CD41**(Figure 2.12, g)**. In equivalent stage Eomes-/- SCL-mCherry cultures a small population of cells (<5%)

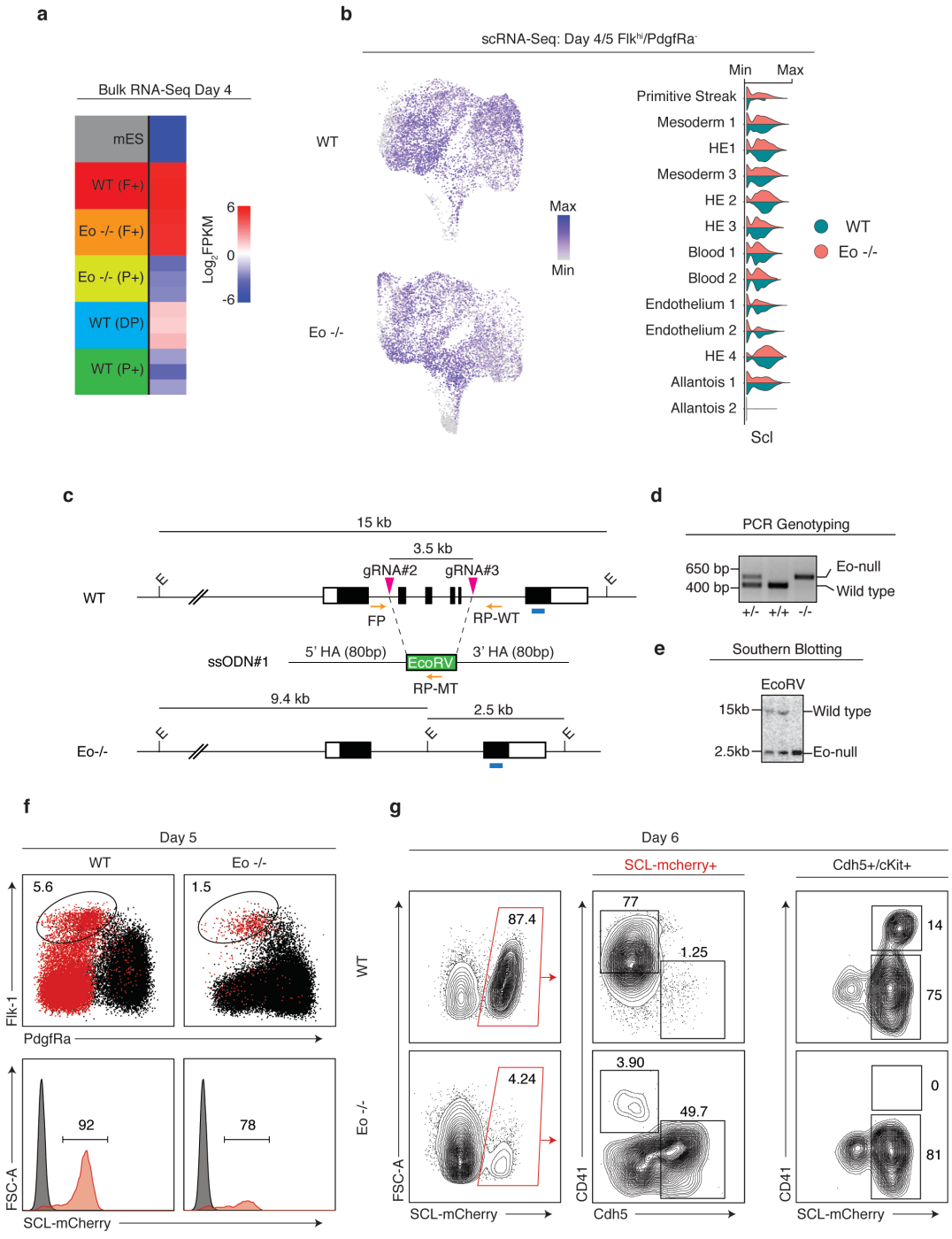


Figure 2.12 Eomes is not required for SCL expression

(a) Normalized SCL expression in various bulk RNA-seq samples from day 4 EBs (N=3 independent differentiations) **(b)** Normalized expression of SCL overlaid on UMAPs for all single cells collected from day 4/5 $Flk^{hi}/PdgfRa^{-}$ wildtype (top) or $Eomes^{-/-}$ (bottom) EBs (3805 cells/day/genotype, left side of panel). Violin plots showing SCL expression levels in the WT (blue) and $Eomes^{-/-}$ (red) cells within the various Seurat clusters (right side of panel) **(c)** The targeting strategy used to re-generate the Eomes-loss of function allele. An ssODN was used to patch an EcoRV site in between introns 1 and 5 subsequent to deletion of a 3.5 kb region,

Figure legend 2.12 continued; including exons 2-5 at the Eomes locus. Pink arrows indicate the locations of Cas9-gRNA induced DNA double strand breaks in intron 1 and intron 5. Blue lines (exon 6) indicate the location of a 3' external Southern blotting probe. Orange arrows indicate the location of primers used for PCR genotyping. E = EcoRV. **(d)** PCR genotyping of Eomes-/- ESCs; WT band size is 401bp, Eomes-/- band size is 535 bp. **(e)** Southern blots showing wild type (15kb) and targeted (2.5kb) alleles in and SCL-mCherry ESC lines. **(f)** Flk-1, PdgfRa and SCL-mCherry expression in day 5 WT (left) or $Eomes^{-/-}$ (right) EBs. Coloured dots indicate cells positive for the expression of SCL-mCherry. Histograms depict SCL-mCherry expression levels in the Flk-1^{hi}/$PdgfRa^{-}$ compartment (grey peaks depict expression in a control cell line). (Representative FACS plots from differentiations with N=1 Reporter $Eomes^{+/+}$ and N=1 Reporter $Eomes^{-/-}$ clone.) **(g)** Day 6 $Eomes^{-/-}$ EB cultures contain an SCL-mCherry population that predominantly expresses Cdh5 (left side of panel). Day 6 EB cultures of $Eomes^{-/-}$ $Cdh5^{+}$/c-Kit^{+} endothelial cells express wild-type levels of SCL-mCherry but lack a $CD41^{hi}$ population. (right side of panel) (Representative FACS plots from differentiations with N=1 SCL-mCherry $Eomes^{+/+}$ and N=1 SCL-mCherry $Eomes^{-/-}$ clone.)

express wildtype levels of SCL-mCherry **(Figure 2.12, g)**. Very few of these Eomes-/- SCL-mCherry+ cells express CD41 and instead approximately half of these cells express the endothelial marker Cdh5 **(Figure 2.12, g)**. Additionally, the c-Kit+/Cdh5+ HE cell population present in Eomes-/- cultures expresses wild-type SCL-mCherry expression levels, but does not undergo EHT and express high levels of CD41**(Figure 2.12, g)**. These results demonstrate that the block in hematopoiesis observed in Eomes-/- cultures cannot simply be explained due to a loss of SCL expression in mesoderm/endothelial cell populations.

2.2.9 Eomes is essential for the development of Runx1+ HE

In contrast to SCL, our bulk RNA-seq data revealed that Runx1 expression is perturbed in the Flk-1^{hi}/$PdgfRa^{-}$ cells that form at day 4 in Eomes-/- EB cultures **(Figure 2.13, a)**. Additionally, our scRNA-seq data shows that Runx1 transcript expression is lost in the Flk-1^{hi}/$PdgfRa^{-}$ population due to the absence of developing blood progenitor populations (**Figure 2.13, b)**. Previous studies have shown that Runx1 is expressed in ExM, primitive

erythrocytes and during the formation of HE (de Bruijn and Dzierzak, 2017). Runx1 is required for EHT and the generation of all definitive hematopoietic cells, however, its loss of function does not perturb the specification of primitive erythrocytes (de Bruijn and Dzierzak, 2017; Lancrin et al., 2009). We therefore became interested in assessing whether the block in definitive hematopoiesis in Eomes-/- cultures occurs because Runx1+ HE is not formed.

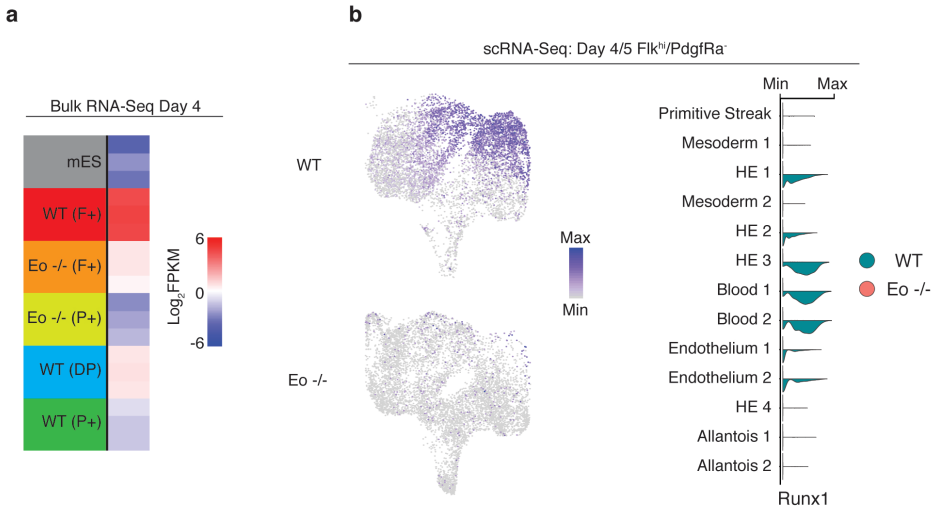


Figure 2.13 Eomes is required for the expression of Runx1

(a) Normalized Runx1 expression in various bulk RNA-seq samples from day 4 EBs (N=3 independent differentiations) **(b)** Normalized expression of Runx1 overlaid on UMAPs for all single cells collected from day 4/5 Flk^{hi}/PdgfRa^{-} wildtype (top) or Eomes$^{-/-}$ (bottom) EBs (3805 cells/day/genotype, left side of panel). Violin plots showing Runx1 expression levels in the WT (blue) and Eomes$^{-/-}$ (red) cells within the various Seurat clusters (right side of panel).

To answer this question, we re-generated the Eomes-/- allele in Runx1-Venus reporter ESCs using the same CRISPR-Cas9 strategy previously outlined **(Figure 2.12, c)**. In line with our RNA-seq results, day 4 and 5 Eomes-/- EBs, including the Flk-1^{hi}/PdgfRa^{-} population, lack Runx1-Venus expression **(Figure 2.14, a)**. Flk-1+ cells generated in Runx1-Venus Eomes$^{+/+}$ and Runx1-Venus Eomes$^{-/-}$ EBs were MACS sorted at day 5 and plated in EHT culture conditions **(Figure 2.14, b)**. At day 8 of EHT culture Runx1-Venus Eomes$^{+/+}$ cultures are filled with budding hematopoietic cells **(Figure 2.14, c, upper panel)**. By

contrast, equivalent stage Runx1-Venus Eomes$^{-/-}$ cultures contain swirling endothelial cells but lack budding hematopoietic cells **(Figure 2.14, c, lower panel)**. In line with our previous results Eomes$^{-/-}$Runx1-Venus day 5 EBs and day 8 EHT cultures lack clonogenic progenitors for primitive erythrocyte and pro-definitive erythro-myeloid lineages, respectively **(Figure 2.14, d)**. Strikingly, Runx1-Venus expression normally marks a CD41-/lo HE subset within the c-Kit+/Cdh5+ compartment **(Figure 2.14, e, purple gate)**. Upon EHT, this Runx1+ HE upregulates CD41 and/or CD45, generating Runx1-Venus+/CD41+ and Runx1-Venus+/CD45+ hematopoietic cells in day 8 cultures **(Figure 2.14, e)**. Strikingly, Eomes-/- EHT cultures lack a Runx1-Venus+ c-Kit+/Cdh5+ HE subpopulation **(Figure 2.14, e, purple gate)**. Additionally, the Cdh5- compartment in Eomes-/- cultures lack Runx1-Venus+ CD41+/CD45+ hematopoietic cells **(Figure 2.14, f)**. Therefore, the block in definitive hematopoiesis in Eomes-/- EHT cultures is associated with the loss of a population of Runx1+ HE and definitive hematopoietic progenitors.

To test whether Eomes regulates Runx1 expression in a cell autonomous fashion, we performed co-culture experiments **(Figure 2.15)**. Wild-type ESCs were mixed with Runx1-Venus or Eomes-/- Runx1-Venus ESCs at day 0 of differentiation. Wild-type co-cultures at day 6 contain CD41+ hematopoietic cells that are Runx1-Venus^{lo} and Runx1-Venus^{hi} **(Figure 2.15, top panel)**. In contrast, Runx1-Venus expression is barely detectable in CD41+ cells generated in equivalent stage Eomes-/- cultures **(Figure 2.15, bottom panel)**. These results demonstrate that Eomes promotes robust induction of Runx1 expression in a cell autonomous fashion during hematopoiesis.

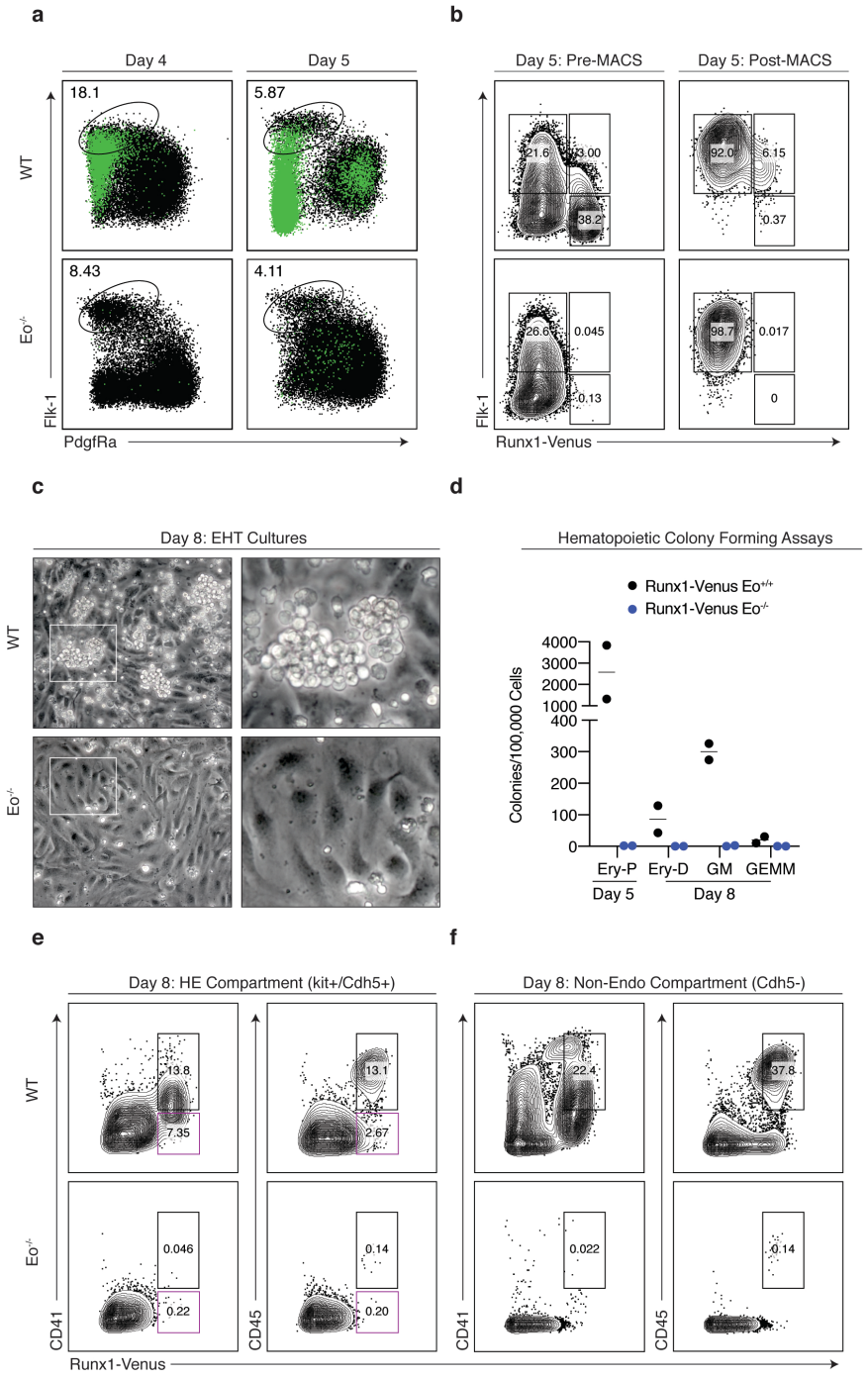


Figure 2.14 Eomes is essential for the generation of Runx1+ HE

(a) Flk-1, PdgfRa and Runx1-Venus expression in day 5 WT (top) or Eomes-/- (bottom) EBs. Coloured dots indicate cells positive for the expression of Runx1-Venus. **(b)** Magnetic activated cell sorting strategy used to purify Flk-1+ cells from day 5 Eomes$^{+/+}$ Runx1^{Venus} and Eomes$^{-/-}$ Runx1^{Venus} EBs. **(c)** Phase contrast images of day 8 Eomes$^{+/+}$ Runx1^{Venus} (top) and Eomes$^{-/-}$ Runx1^{Venus} (bottom) EHT cultures. **(d)** Hematopoietic potential of cells isolated from day 5/8 Eomes$^{+/+}$ Runx1^{Venus} (black) and Eomes$^{-/-}$ Runx1^{Venus} (blue) cultures, plated in hematopoietic colony assays to assess primitive erythrocyte and definitive erythro-myeloid

Figure legend 2.14 continued; colony potential, respectively. (N = 2 independent differentiations). **(e,f)** Day 8 Eomes$^{-/-}$ Runx1^{Venus} hemogenic endothelial cells (kit+/Cdh5+) and non-endothelial cells (Cdh5-) lack expression of Runx1-Venus and hematopoietic markers CD41/CD45. (Representative FACS plots from N=2 independent differentiations).

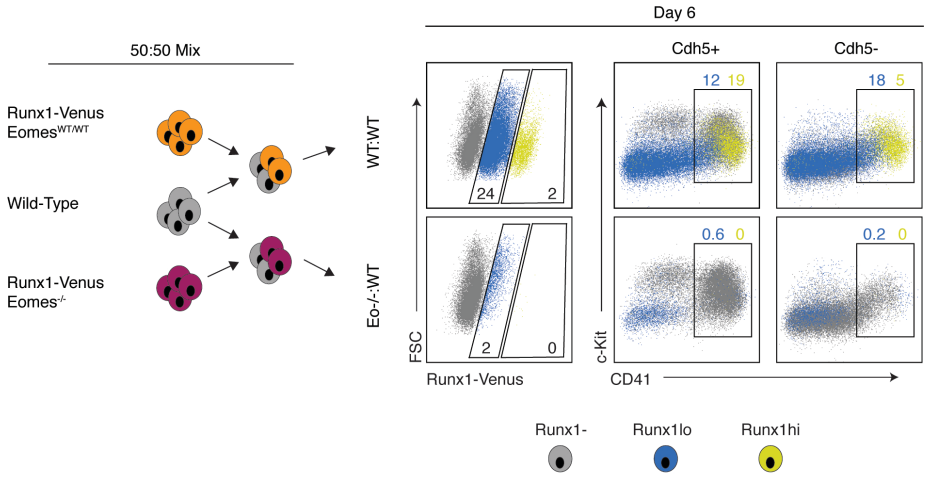


Figure 2.15 Eomes is required cell autonomously for Runx1 expression.

At day 0 WT (grey) ESCs were mixed in equal proportions with either Eo+/+ Runx1-Venus ESCs (orange, WT:WT) or Eomes-/- Runx1-Venus ESCs (purple, Eomes-/-:WT). Day 6 bulk EHT WT:WT (top FACS panel) co-cultures contain populations of cells that express different levels of Runx1-Venus (Runx1-negative = grey dots, Runx1-lo = blue dots, Runx1+ = yellow dots). Eomes-/-:WT (bottom FACS panel) co-cultures contain a CD41+ (gate) cell population in Cdh5+ (middle FACS panel) and Cdh5- (right FACS panel) populations that lacks Runx1lo/+ cells. The percentages of Runx1-Venuslo/+ cells within the CD41+ cell population are indicated by the coloured numbers in the middle and right FACS panels. (Representative FACS plots from co-culture differentiations with n=1 Runx-1 Venus Eomes+/+ and n=2 Runx1-Venus Eomes-/- clones.)

2.2.10 Runx1 re-expression in Eomes-/- EHT cultures rescues EHT and the production of pro-definitive blood cells

SCL is required for the production of CD41+ hematopoietic cells (Mikkola et al., 2003) and previous studies suggest that SCL-null ESCs fail to generate HE that expresses Tie2/cKit (Lancrin et al., 2009). In contrast, Runx1 is essential for EHT but is dispensable for the formation of HE (de Bruijn and Dzierzak, 2017). Runx1-null endothelial cells appear to

initiate EHT but undergo apoptosis as they try and release from the endothelial layer (Lancrin et al., 2009). To further define Eomes requirements during HE development we compared Eomes-/- (Arnold and Robertson, 2009), SCL-null (Shivdasani et al., 1995) and Runx1-null (Wang et al., 1996) ESC differentiation cultures. Interestingly, while SCL-null, Runx1-null and Eomes-/- cells generate Cdh5+/c-Kit+ endothelial cells in our differentiation systems **(Figure 2.16, a,b)**, only Runx1-null and Eomes-/- ESCs give rise to a small endothelial population that expresses low levels of CD41 **(Figure 2.16, a,b (red gate))**, which has been previously associated with HE (Eilken et al., 2009). These results suggest that HE is at least partially specified in Eomes-/- cultures.

To further clarify whether or not the endothelium present in Eomes-/- cultures is hemogenic we re-expressed Runx1 in Eomes-/- EHT cultures using a previously described Runx1 inducible mES cell line (iRunx1) (Lancrin et al., 2009; Lie et al., 2018). iRunx1 cells are Runx1-/- and have a Runx1b construct inserted into the ROSA26 locus that can be induced via the addition of doxycycline. Day 5 iRunx1 Eomes$^{+/+}$ EBs contain primitive erythrocyte progenitors that are not present in equivalent stage iRunx1 Eomes$^{-/-}$ EBs **(Figure 2.17, b)**. To see if re-expression of Runx1 in Eomes-/- EHT cultures can rescue definitive hematopoiesis, doxycycline was added to iRunx1 Eomes$^{+/+}$ and iRunx1 Eomes$^{-/-}$ EHT cultures from day 7 to day 9 **(Figure 2.17, a)**. Day 8 iRunx1 Eomes$^{-/-}$ EHT cultures contain definitive erythroid and myeloid clonogenic progenitors that are not present in non-dox induced cultures **(Figure 2.17, c)**. Additionally, the induction of Runx1 from day 7-9 in both iRunx1 Eomes$^{+/+}$ and iRunx1 Eomes$^{-/-}$ EHT cultures rescues the generation of budding Cdh5+/CD41+/CD45+ hematopoietic progenitors **(Figure 2.17, d)**. Altogether these results demonstrate that the primary role for Eomes during definitive hematopoiesis is to endow HE

with the capacity to express Runx1 such that EHT and definitive hematopoiesis can occur.

Additionally, these results suggest that HE is specified in Eomes-/- cultures.

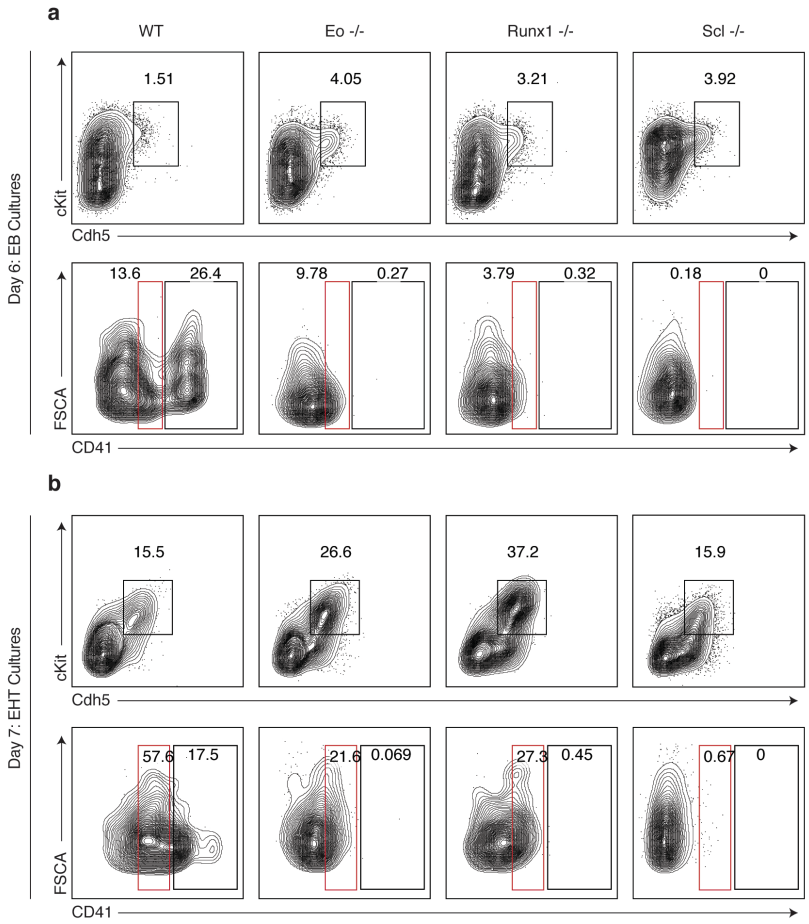


Figure 2.16 Eomes-/- endothelium immunophenocopies Runx1-null endothelium

(a,b) Flow cytometry of day 6 EB **(a)** and day 7 EHT **(b)** cultures reveals the presence of a c-Kit+/Cdh5+/CD41lo (red gate) subset present in Eomes-/- and Runx1-null cultures that is not present in SCL-null cultures. (FACS plots from n=1 independent differentiation).

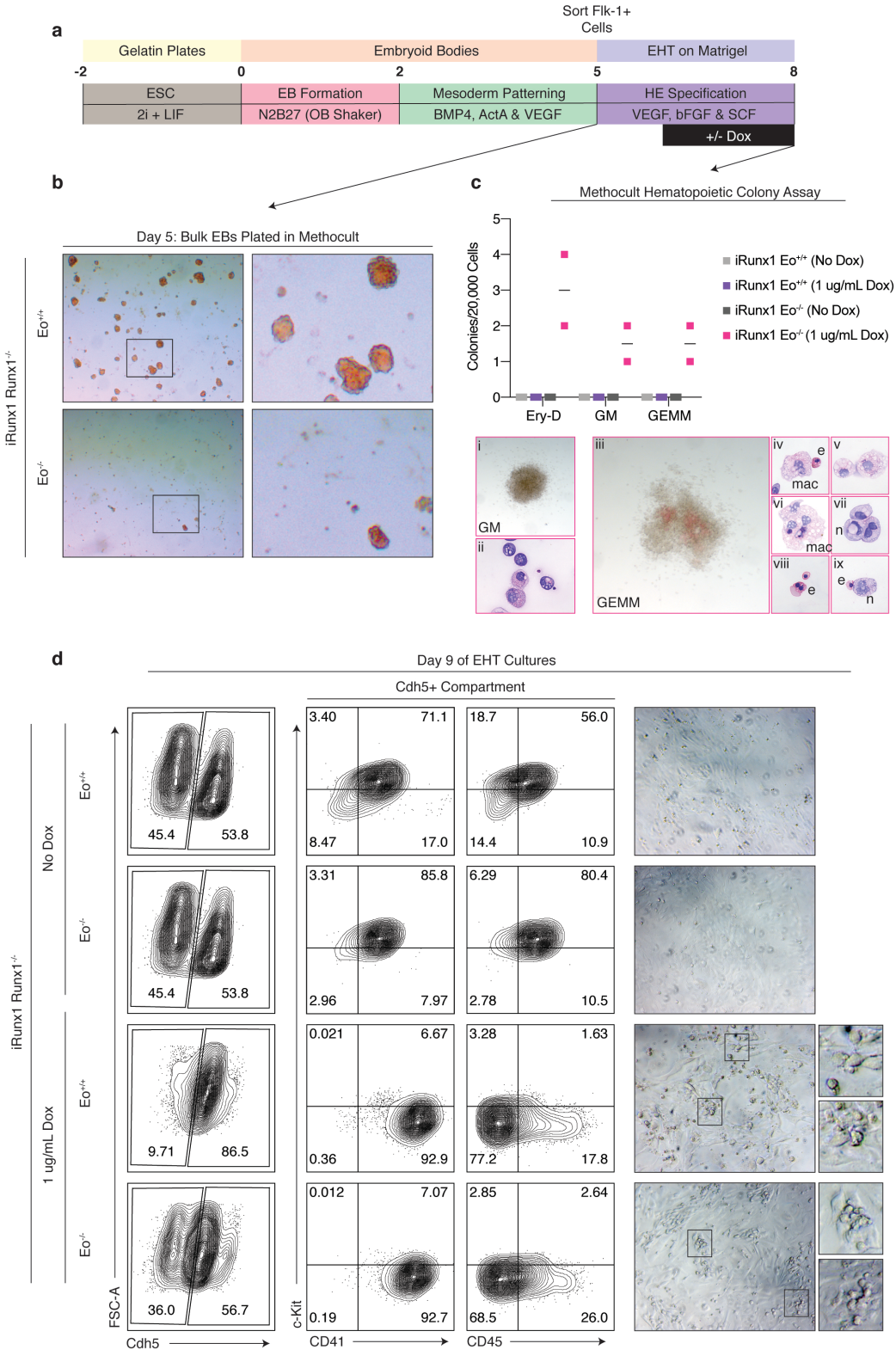


Figure 2.17 Re-expression of Runx1 in Eomes loss-of-function EHT cultures rescues pro-definitive hematopoiesis

(a) Schematic of the endothelial to hematopoietic transition (EHT) differentiation protocol. From day 6 to day 8 doxycycline was added to EHT cultures to induce the expression of

Figure legend 2.17 continued; Runx1. **(b)** Representative photomicrographs of Methocult M3434 plates containing primitive erythrocyte colonies generated from day 5 bulk iRunx1 Runx1$^{-/-}$ Eomes$^{+/+}$ (top) versus iRunx1 Runx1$^{-/-}$ Eomes$^{-/-}$ EBs. **(c)** Hematopoietic potential of cells isolated from day 8 iRunx1 Runx1$^{-/-}$ Eomes$^{+/+}$ (grey/purple) and iRunx1 Runx1$^{-/-}$ Eomes$^{-/-}$ (dark grey/pink) EHT cultures. Dox was either added or not added from day 6-8 and individual cells were plated in hematopoietic colony assays to assess definitive erythro-myeloid colony potential (top panel). Photomicrographs of representative GM (i) and GEMM (iii) colonies generated from iRunx1 Runx1$^{-/-}$ Eomes$^{-/-}$ day 8 EHT cultures in which Dox was added from day 6-8. (ii, iv-ix) H&E stains of cytospun hematopoietic cells from the respective colonies (bottom panel). **(d)** Flow cytometry and photomicrographs of day 9 iRunx1 Runx1$^{-/-}$ Eomes$^{+/+}$ and iRunx1 Runx1$^{-/-}$ Eomes$^{-/-}$ EHT cultures in which dox was either added or not added from day 7-9. (FACS plots from n=1 independent differentiation).

2.2.11 Eomes influences chromatin accessibility at SCL bound enhancers in hematovascular mesoderm

To assess the effect of Eomes function on chromatin accessibility, in collaboration with Anna Senft, I performed ATAC-seq (Buenrostro et al., 2013) on day 4 wild-type and Eomes-/- Flk-1^{hi}/PdgfRa^{-} hematovascular mesoderm populations **(Figure 2.18, a)**. These were equivalent FACS populations to those taken for bulk RNA-seq analysis **(Figure. 2.7, a)**. 7% (4180/59582) of the total ATAC-seq peaks were differentially accessible in wildtype versus Eomes-/- hematovascular mesoderm **(Figure 2.18, b)**. The majority of these differentially accessible sites have reduced levels of chromatin accessibility (87% = 3629) in Eomes-/- cells and are located in distal intergenic regions >5 kb from nearby transcriptional start sites **(Figure 2.18, b,c)**. The few sites with increased chromatin accessibility (13% = 551) in the Eomes-/- cells are also located in distal intergenic regions **(Figure 2.18, c)**. Sites with reduced chromatin accessibility are enriched for binding motifs for hematopoietic regulators such as Gata1/2, SCL:Gata1, Erg, Ets1, Fli1 and Spi1 **(Figure 2.18, d, bottom panel)**. In contrast, sites with increased ATAC-seq signal in Eomes-/- hematovascular mesoderm are

enriched for binding motifs related to the AP1 transcription factor family **(Figure 2.18, d, top panel)**.

GREAT analysis (McLean et al., 2010) identified 843 and 3639 genes associated with the sites of increased and reduced chromatin accessibility in Eomes-/- hematovascular mesoderm, respectively. Of the 843 genes located nearby sites of increased accessibility, 249 were upregulated and 43 were downregulated **(Figure 2.18, e, top panel)**. Hierarchical clustering reveals a subset of upregulated genes located nearby sites of increased chromatin accessibility are related to endothelial/epithelial migration, endothelial cell differentiation and blood vessel morphogenesis **(Figure 2.18, f, top panel)**. Of the 3639 genes located nearby sites of decreased accessibility, 523 were upregulated and 629 were downregulated **(Figure 2.18, e, top panel)**. Hierarchical clustering reveals a subset of downregulated genes located nearby sites of decreased chromatin accessibility are related to blood vessel development, cardiac muscle tissue morphogenesis, digestive tract development and hemopoiesis **(Figure 2.18, f, bottom panel)**.

Strikingly, when we compared our differentially accessible ATAC-seq peaks to published ChIP-seq datasets (Org et al., 2015) from day 4 Flk-1^{+} cells generated using a EB hematopoietic differentiation protocol, we found that the majority of Eomes-dependent sites with reduced accessibility were enriched for enhancer marks (H3K4Me1 and H3K27Ac) and SCL occupancy **(Figure 2.19, a)**. GREAT analysis of the 949 overlapping sites of reduced accessibility that correlate with SCL occupancy reveals these are enriched for genes related to hematopoietic development **(Figure 2.19, b)**. Of these Eomes-dependent, SCL occupied sites, 231 are associated with genes that are also significantly downregulated in Eomes-/- Flk-1^{hi}/PdgfRa^{-} cells. This list includes genes critical for primitive erythrocyte development,

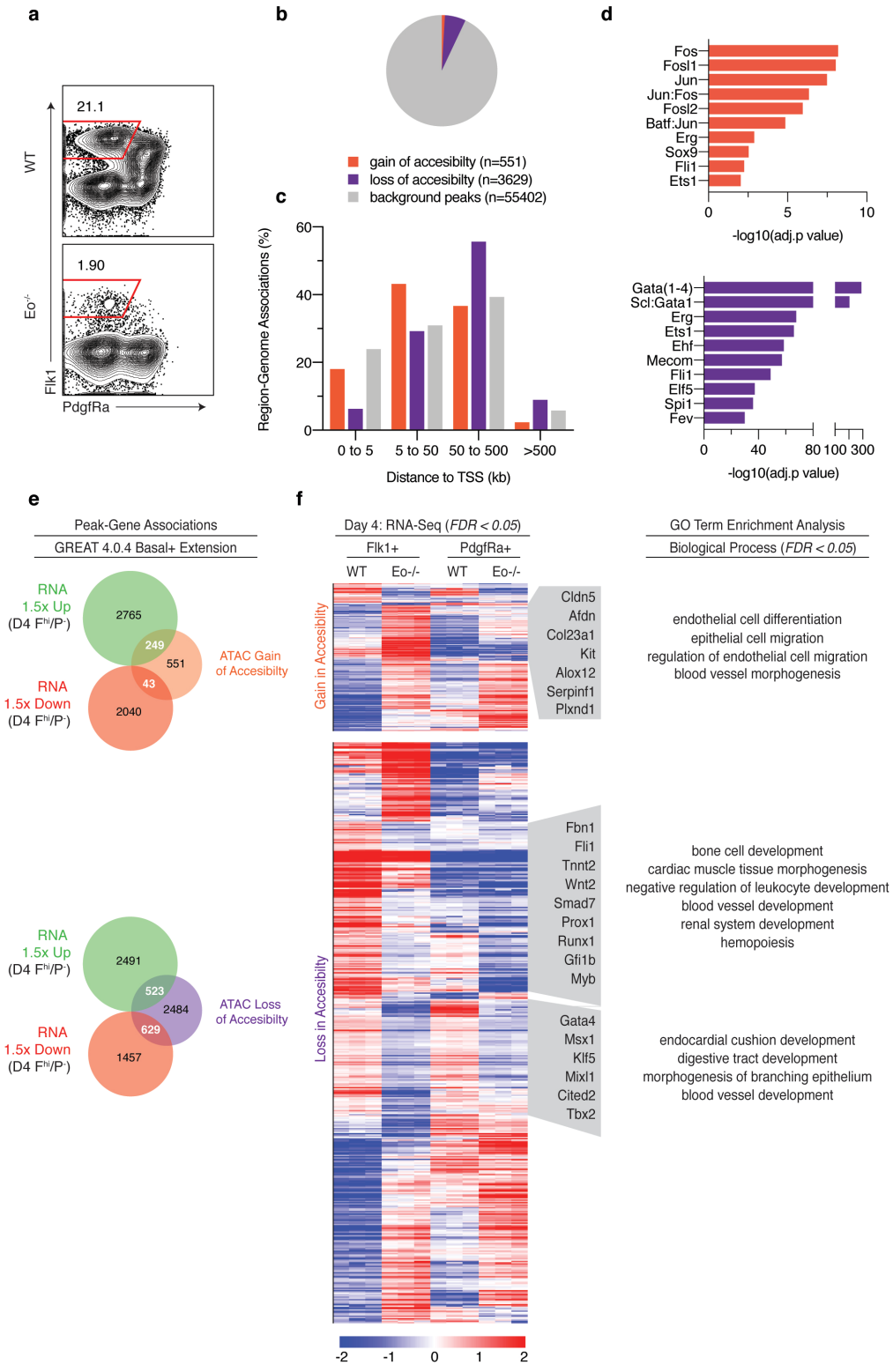


Figure 2.18 Assessing changes in chromatin accessibility in the Flk-1^{hi}/PdgfRa^{-} hematovascular mesoderm population generated in Eomes loss of function cultures

(a) Gating strategy used to sort Flk1^{hi}/PdgfRa^{-} cells for ATAC-seq from day 4 wildtype and Eomes$^{-/-}$ EB cultures. (Representative FACS plots from n=3 independent differentiations).

Figure legend 2.18 continued; **(b)** Pie chart depicting the proportion of ATAC peaks that lose (purple) or gain (orange) chromatin accessibility in Eomes-/- day 4 Flk-1hi/PdgfRa- cells. **(c)** Bar graph depicting the distribution of ATAC peaks located near transcriptional start sites (TSS) with unchanged (grey), reduced (purple) or increased (orange) chromatin accessibility. **(d)** Analysis of motif enrichment under sites of increased (top panel, orange) or reduced (bottom panel, purple) chromatin accessibility. **(e)** Venn diagrams depicting the overlap of sites of increased (top panel) and decreased (bottom panel) chromatin accessibility with genes that are differentially expressed in day 4 WT vs. Eomes$^{-/-}$ Flk1^{hi}/PdgfRa^{-} cells. **(f)** Hierarchically clustered heatmap of gene expression for the overlapping genes that are differentially expressed and linked to nearby sites of increased (top panel) or decreased (bottom panel) chromatin accessibly. GO terms for the subset of genes highlighted in grey are listed on the right-hand side of the panel. *ATAC-seq experiments/analyses were done in collaboration with Anna Senft.*

including Gata1 and Nfe2, and those governing EHT and definitive hematopoiesis, namely Runx1, Gfi1/1b, Ikzf1 and Myb. Many of the observed changes in chromatin accessibility map to previously identified enhancer regions at these loci **(Figure 2.19, c)** (Onodera et al., 1997; Schutte et al., 2016). Consistent with the finding that Eomes is non-essential for SCL expression levels, there was no noticeable impact on chromatin accessibility at the SCL locus **(Figure 2.19, c)**. These results demonstrate that Eomes regulates the accessibility of SCL bound *cis*-regulatory elements that normally coordinate hematopoietic development.

2.2.12 Inspecting changes in chromatin accessibility in the Eomes-/- PdgfRa+ paraxial mesoderm population

Additionally, ATAC-seq was performed on the Flk-1^{-}/PdgfRa^{+} populations that forms at day 4 in wildtype and Eomes-/- EB cultures **(Figure 2.20, a)**. 4% (1966/44950) of the total ATAC-seq peaks were differentially accessible in wildtype versus Eomes-/- paraxial mesoderm **(Figure 2.20, b)**. Three quarters of these differentially accessible sites have reduced levels of chromatin accessibility (75% = 1477) in Eomes-/- cells and are predominantly located in

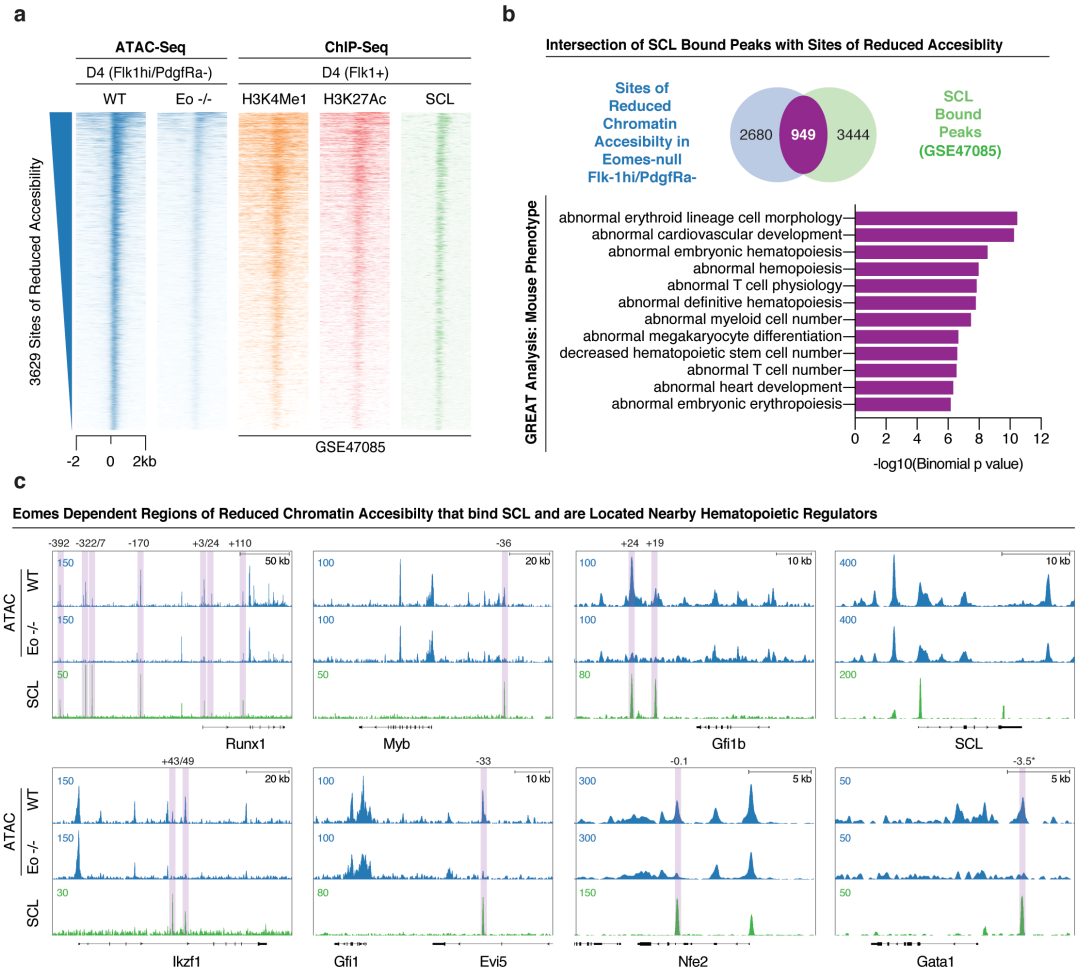


Figure 2.19 Eomes regulates chromatin accessibility at SCL bound regulatory regions nearby hematopoietic regulators

(a) Heatmaps showing ATAC signals from WT (blue, left) or Eomes-/- (blue, right) day 4 Flk-1^{hi}/PdgfRa^{-} cells and ChIP signal for H3K4Me1 (orange), H3K27Ac (red) and SCL (green) occupancy from day 4 WT Flk-1+ cells. Heatmaps show a 4kb flanking region surrounding sites of reduced chromatin accessibility in day 4 Eomes-/- Flk-1hi /PdgfRa- cells. **(b)** Venn diagram depicting the overlap of SCL bound regions and sites of reduced chromatin accessibility. GREAT analysis of significantly enriched GO Terms in the Mouse Phenotype category for the 949 shared genomic regions (purple) shows enrichment of hematopoietic related terms. **(c)** IGV snapshots of ATAC-seq (blue) and ChIPSeq (green) tracks highlighting hematopoietic regulators that have nearby genomic regions with reduced chromatin accessibility in Eomes-/- Flk-1hi /PdgfRa- cells that are also bound by SCL in WT Flk-1+ mesoderm are highlighted by purple bars. Numbers above the purple bars indicate the relative location of these sites in kilobases to the TSS of the indicated genes. (*the -3.5 enhancer at the Gata1 locus was called as a peak by MACS2 ($p<0.05$) in only the WT Flk-1hi /PdgfRa- samples

distal intergenic regions, >5 kb from nearby transcriptional start sites **(Figure 2.20, b,c)**. Sites with increased chromatin accessibility (25% = 551) in Eomes-/- Flk-1^{-}/PdgfRa^{+} cells are also located in distal intergenic regions **(Figure 2.20, c)**. Sites with reduced chromatin accessibility are enriched for binding motifs for hematopoietic/cardiovascular regulators such as Gata1/2/3/4, SCL:Gata1, Nkx2-5 and Runx1 **(Figure 2.20, d, bottom panel)**. In contrast, sites with increased ATAC-seq signal in Eomes-/- paraxial mesoderm are enriched for binding motifs such as Hoxa9, Hoxc9, T, Meis1 and Myb **(Figure 2.20, d, top panel)**.

GREAT analysis identified 496 and 1170 genes associated with the sites of increased and reduced chromatin accessibility in Eomes-/- paraxial mesoderm, respectively. Of the 496 genes located nearby sites of increased accessibility, 217 were upregulated and 46 were downregulated **(Figure 2.20, e, top panel)**. Hierarchical clustering reveals a subset of upregulated genes located nearby sites of increased chromatin accessibility related to rhombomere development, somitogenesis and striated muscle tissue development **(Figure 2.20, f, top panel)**. Of the 1170 genes located nearby sites of decreased accessibility, 175 were upregulated and 363 were downregulated **(Figure 2.20, e, bottom panel)**. Hierarchical clustering reveals a subset of downregulated genes located nearby sites of decreased chromatin accessibility related to endocardial cushion formation and heart/mesoderm morphogenesis **(Figure 2.20, f, bottom panel)**.

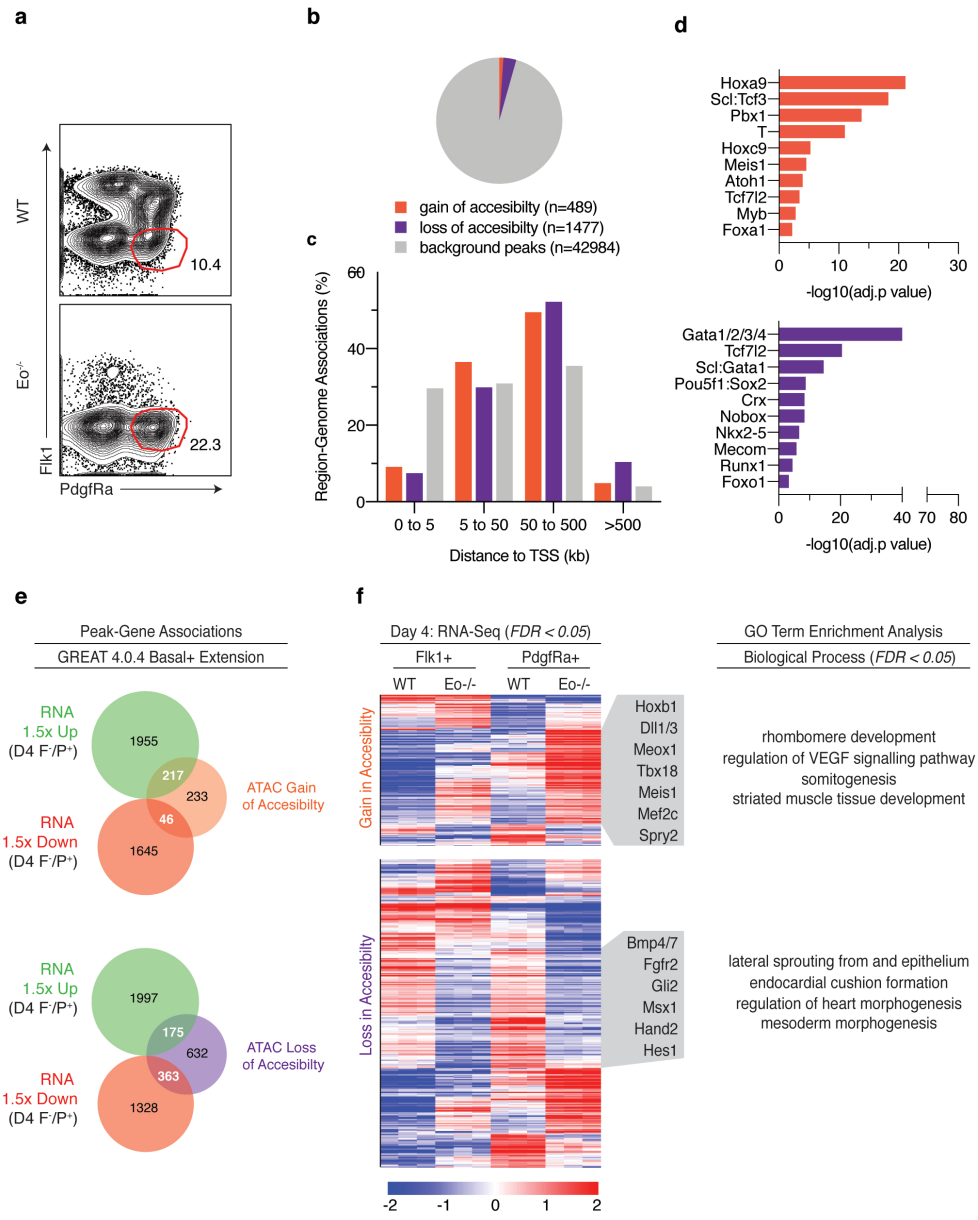


Figure 2.20 Assessing changes in chromatin accessibility in the Flk-1-/PdgfRa+ paraxial mesoderm population generated in Eomes loss of function cultures

(a) Gating strategy used to sort Flk1^{-}/PdgfRa^{+} cells for ATAC-seq from day 4 wildtype and Eomes$^{-/-}$ EB cultures. (Representative FACS plots from n=3 independent differentiations). **(b)** Pie chart depicting the proportion of ATAC peaks that lose (purple) or gain (orange) chromatin accessibility in Eomes-/- day 4 Flk-1hi/PdgfRa- cells. **(c)** Bar graph depicting the distribution of ATAC peaks located near transcriptional start sites (TSS) with unchanged (grey), reduced (purple) or increased (orange) chromatin accessibility. **(d)** Analysis of motif enrichment under sites of increased (top panel, orange) or reduced (bottom panel, purple) chromatin accessibility. **(e)** Venn diagrams depicting the overlap of sites of increased (top panel) and

Figure legend 2.20 continued; decreased (bottom panel) chromatin accessibility with genes that are differentially expressed in day 4 WT vs. Eomes$^{-/-}$ Flk1^{-}/PdgfRa^{+} cells. **(f)** Hierarchically clustered heatmap of gene expression for the overlapping genes that are differentially expressed and linked to nearby sites of increased (top panel) or decreased (bottom panel) chromatin accessibly. GO terms for the subset of genes highlighted in grey are listed on the right-hand side of the panel.

2.2.13 Generating Eomes-V5 ESCs to identify Eomes genomic targets using ChIP-seq

To identify Eomes target genes during hematoendothelial development I generated ESC lines expressing either N- or C-terminally V5-tagged Eomes. I designed a strategy to insert a V5 epitope tag at the N-terminus of Eomes using CRISPR-Cas9 and an ssODN repair template **(Figure 2.21, a)**. Eo$^{GFP/+}$ ESCs (Arnold et al., 2009) were electroporated and an initial round of PCR screens was used to identify putatively targeted clones **(Figure 2.21, b)**. Eo$^{GFP/N\text{-}V5}$ clones were grown up and differentiated into hematovascular mesoderm and flow cytometry analysis and protein extraction was performed at day 4. Western blotting revealed that only one of the three Eomes isoforms was successfully V5 tagged; additionally, Eomes expression was dysregulated in Eo$^{GFP/N\text{-}V5}$ cells **(Figure 2.21, c)**. Furthermore, cardiac mesoderm (Flk-1^{+}/PdgfRa^{+}) production was compromised in these cultures suggesting that the insertion of the V5 tag to the N-terminus of Eomes disrupts Eomes function **(Figure 2.21, d, red gate)**.

To circumvent these issues, a CRISPR-Cas9 strategy was used to insert a V5 tag into the C-terminus of Eomes in WT CCEs **(Figure 2.22, a)**. PCR screens were used to identify putatively homozygously targeted clones (Eo$^{V5/V5}$) **(Figure 2.22, b)**. Eo$^{V5/V5}$ clones were differentiated into hematovacular mesoderm and flow cytometry, immunostaining and protein extraction was performed at day 4. Western blotting revealed that all three Eomes isoforms

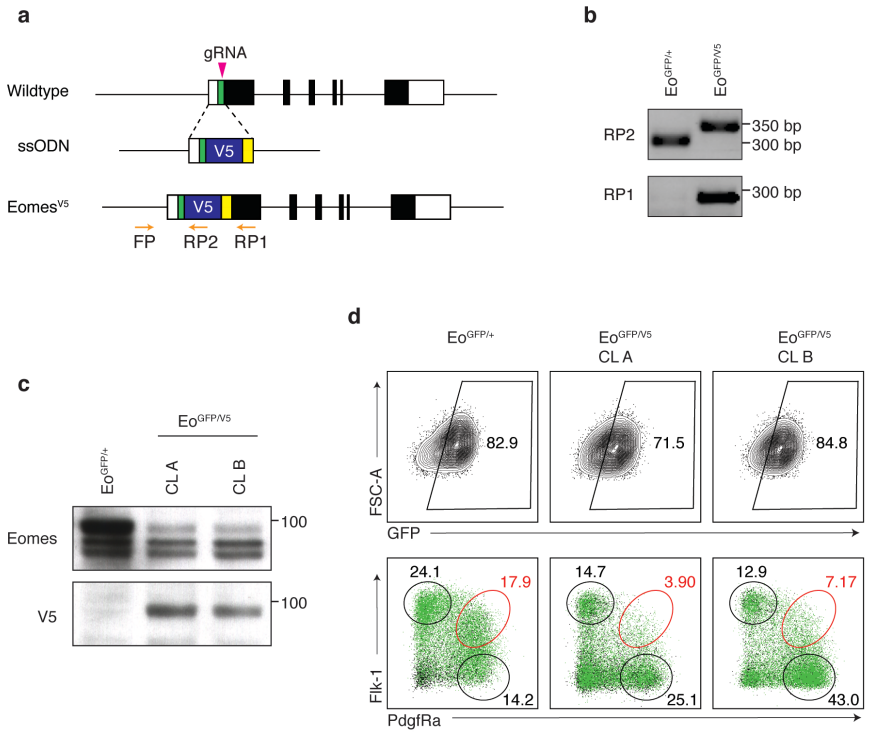


Figure 2.21 Generation of an ES cell line expressing N-terminally V5-tagged Eomes

(a) The targeting strategy used to insert a 3XGly-V5 tag directly downstream of the ATG translational start codon (exon 1) at the N-terminus of the Eomes locus using CRISPR-Cas9 and an ssODN repair template. The pink arrow indicates the location of the Cas9-gRNA induced DNA double strand break. Orange arrows indicate the location of primers used for PCR genotyping. **(b)** PCR genotyping of an V5-Eomes targeted clone; WT band size is 250bp, V5-Eomes band size is 301 bp. **(c)** Western blotting of whole cell protein lysates from $Eo^{V5/V5}$ and $Eomes^{GFP/+}$ day 4 EBs shows that only a single Eomes protein isoform (upper panel) is V5 tagged (lower panel) in both $Eomes^{V5/V5}$ clones. **(d)** Flk-1/PdgfRa expression in $Eomes^{GFP/+}$ (left) and $Eomes^{V5/V5}$ (middle/right) day 4 EBs. Green dots are EoGFP+ cells.

were successfully tagged with the V5 epitope tag **(Figure 2.22, c)**. Immunostaining experiments demonstrate that day 4 $Eo^{V5/V5}$ EBs have similar nuclear staining patterns for Eomes and V5 expression **(Figure 2.22, d)**. Finally, $Eo^{V5/V5}$ EB differentiation cultures robustly generate cardiac mesoderm (Flk-1$^+$/PdgfRa$^+$) and c-Kit$^+$/CD41$^+$ hematopoietic progenitors **(Figure 2.22, e)**, cell populations absent in Eomes-/- cultures, demonstrating that C-terminally V5 tagged Eomes functions normally in this context. Expression of Eo-V5 in the various cell populations labelled by Flk-1/PdgfRa at day 3-5 was evaluated using

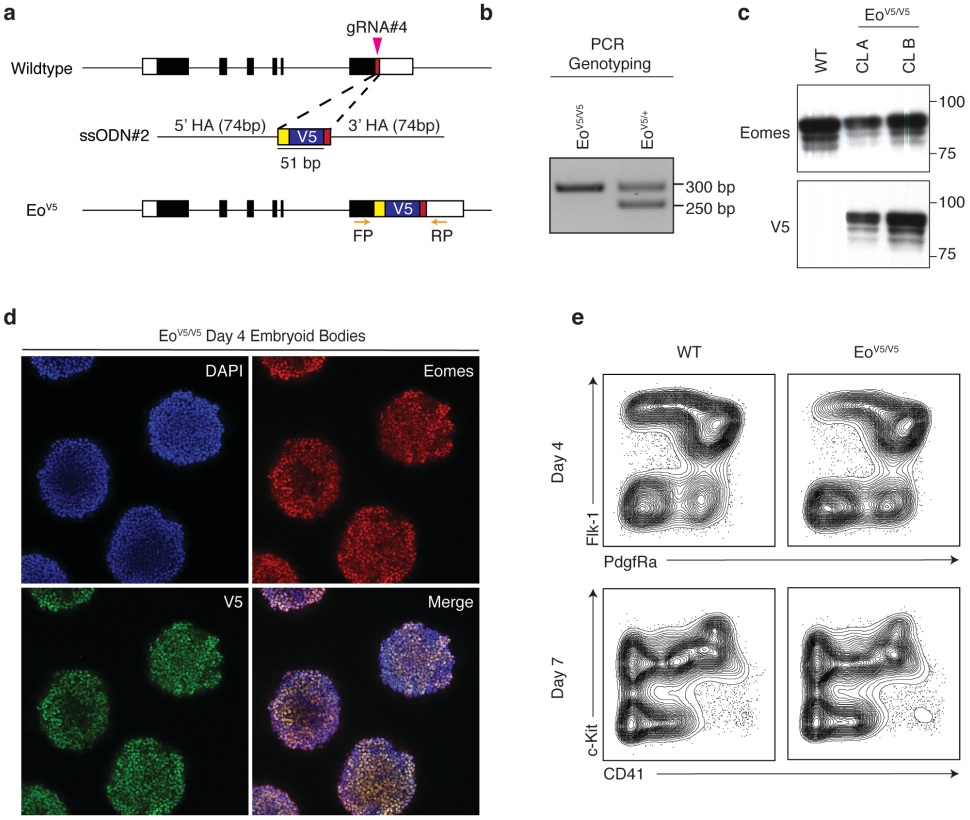


Figure 2.22 Generation of an ES cell line expressing C-terminally V5-tagged Eomes

(a) The targeting strategy used to insert a 3XGly-V5 tag directly upstream of the UAG translational stop codon (exon 6) at the C-terminus of the Eomes locus using an ssODN. The pink arrow indicates the location of the Cas9-gRNA induced DNA double strand break. Orange arrows indicate the location of primers used for PCR genotyping. **(b)** PCR genotyping of Eomes-V5 targeted clones; WT band size is 250bp, Eo-V5 band size is 301 bp. **(c)** Western blotting of whole cell protein lysates from Eomes$^{V5/V5}$ and WT day 4 EBs shows that all three isoforms of Eomes protein (upper panel) are V5 tagged (lower panel) in both Eo$^{V5/V5}$ clones. **(d)** Immunofluorescence staining of Eo$^{V5/V5}$ day 4 EBs for Eomes (red) and V5 (green). Nuclei are counter stained with DAPI (blue). **(e)** Flk-1/PdgfRa (top) and CD41/c-Kit (bottom) expression in WT (left) and EoV5/V5 (right) day 4 and day 7 EBs, respectively. (Representative FACS plots from differentiations with n=1 WT and n=2 EoV5/V5 clones.)

intracellular flow cytometry with an anti-V5 antibody conjugated to FITC. The V5+ gate was delineated using equivalent stage wildtype EBs as a control **(Figure 2.23, a)**. Eo-V5 expression peaked at day 4 of differentiation **(Figure 2.23, a,b)**. At day 4, Eo-V5 was

expressed in approximately 20% of the Flk-1^{hi}/PdgfRa^{-} hematovascular and Flk-1^{-}/PdgfRa^{+} paraxial mesodermal cells **(Figure 2.23, b)**.

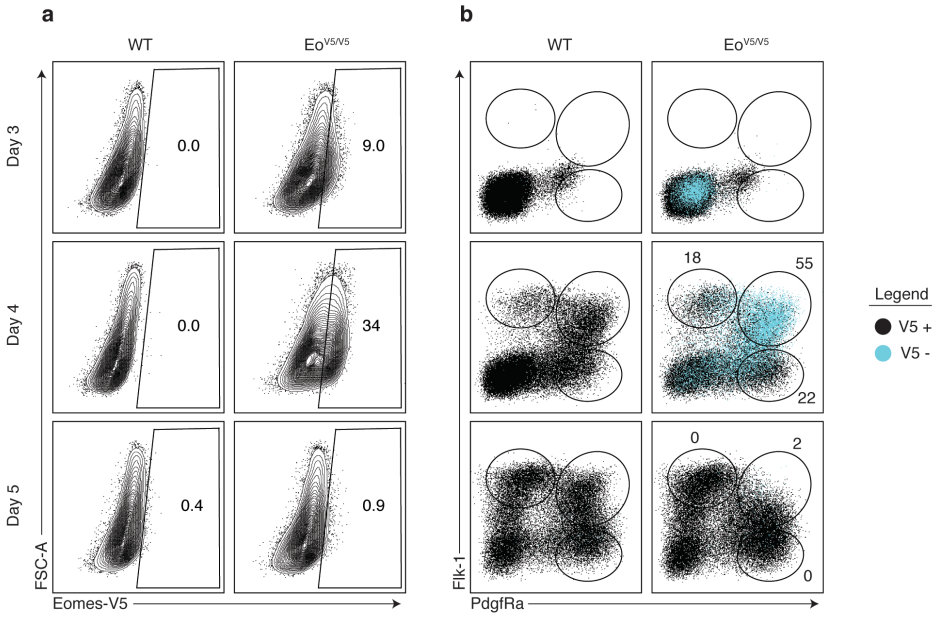


Figure 2.23 Expression pattern of Eomes-V5 during hematovascular differentiation
(a) V5 protein expression was evaluated in day 3-5 Eomes$^{V5/V5}$ EBs using intracellular flow cytometry; equivalent stage WT EBs were used as a gating control **(a)**. Additionally, EBs were also stained for Flk-1 and PdgfRa expression **(b)**; blue dots indicate cells that are V5+ and numbers indicate the proportion of cells in the respective gate that are V5+.

ChIP-Western experiments confirmed that crosslinked Eo-V5 chromatin complexes can be successfully immunoprecipitated using ChIP-grade V5 antibodies **(Figure 2.24)**. Therefore, I used two independent Eo$^{V5/V5}$ ESC clones (CL A and CL B) to perform ChIP-seq on bulk day 4 EBs **(Figure 2.25, a)**. As a control for non-specific V5 antibody binding day 4 wildtype EBs were used **(Figure 2.25, a)**. V5-Eomes bound genomic regions common to both clones were highly enriched for T-box binding motifs, including a previously published Eomes binding motif (Teo et al., 2011) **(Figure 2.25, b**). Eomes bound genomic regions were predominantly located >5 kb from transcriptional start sites and were linked to genes related to biological

processes such as abnormal germ layer morphology, abnormal mesoderm morphology, abnormal gastrulation and abnormal developmental patterning **(Figure 2.25, b,c)**.

To identify direct Eomes targets in hematovascular (Flk-1^{hi}/PdgfRa^{-}) and paraxial (Flk-1^{-}/PdgfRa^{+}) mesoderm compartments we identified Eomes ChIP peak associated genes that were differentially expressed in these populations. 35% of genes (189/541) linked to Eomes ChIP peaks were found to be mis-regulated in day 4 Flk-1^{hi}/PdgfRa^{-} Eomes-/- cells **(Figure 2.25, d, top panel)** including transcriptional regulators (Runx1, Mixl1, Klf5, Pbx1, Tbx3, Foxf1, Meis2) and signaling molecules (Dkk1, Gli2, Fzd7, Lefty2) with known roles during hematovascular development. In day 4 Flk-1^{-}/PdgfRa^{+} cells 30% of genes (166/541) linked to Eomes ChIP peaks were mis-regulated including signaling molecules (Lefty2 and Fgf8) and transcriptional regulators (Klf5, Gata4, Meis2).

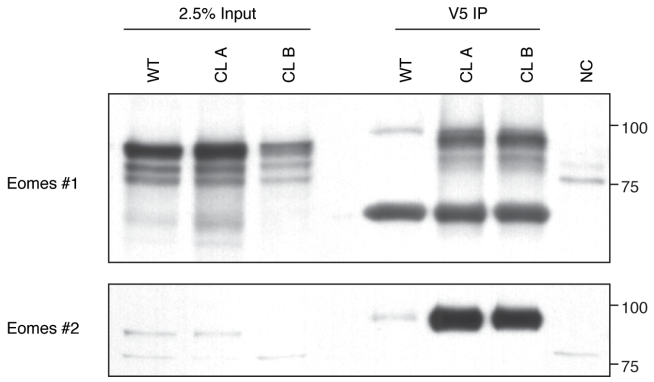


Figure 2.24 ChIP-Western demonstrates that crosslinked Eomes-V5 complexes can be immunoprecipitated
Immunoprecipiation of Eomes-V5 complexes was performed using a ChIP Grade anti-V5 antibody. Western blots were performed using either a rabbit polyclonal (Eomes #1) or a rat monoclonal (Eomes #2) antibody. (IP = immunoprecipitated)

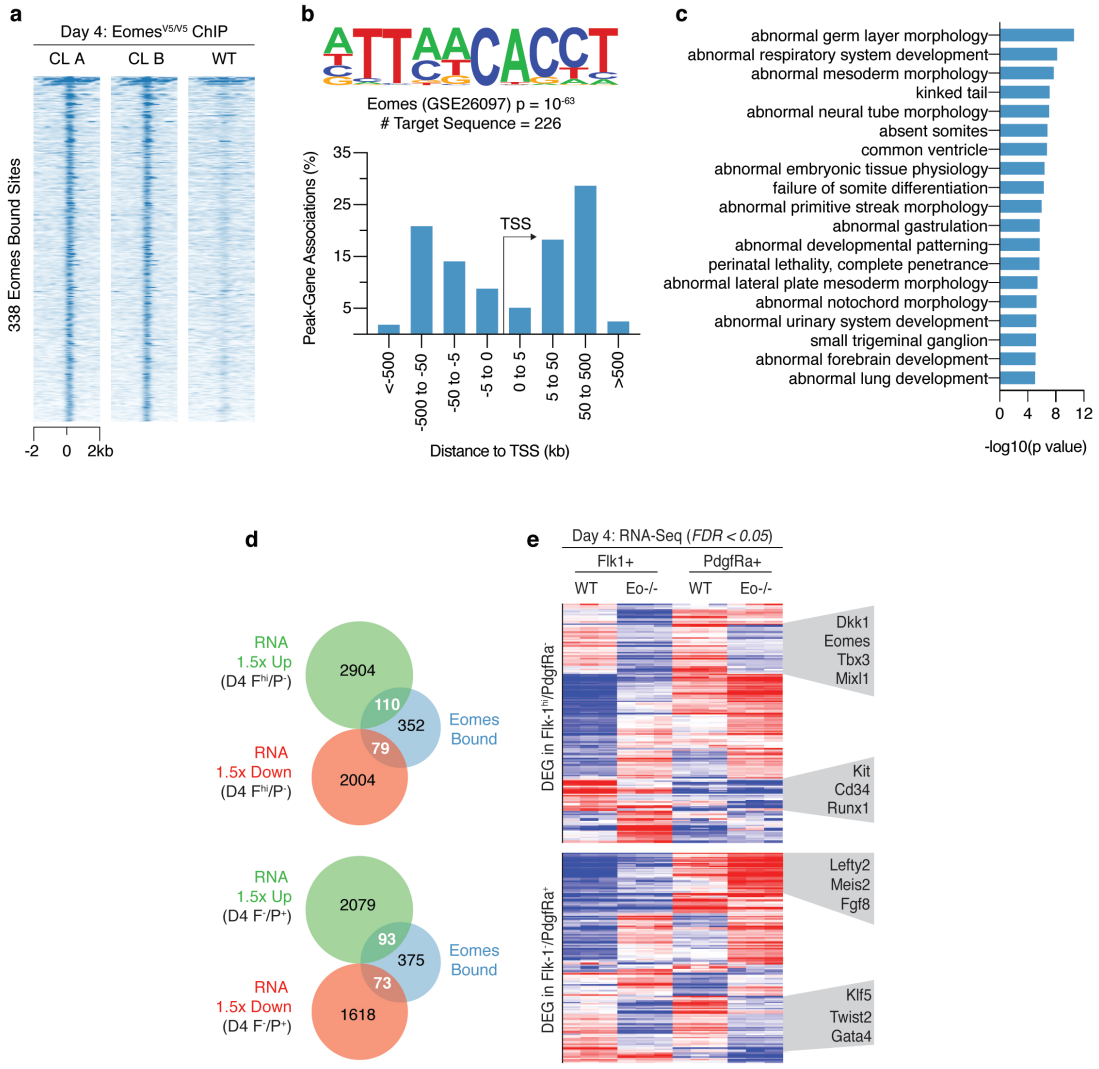


Figure 2.25 Assessing Eomes' genomic targets in day 4 bulk EB cultures

(a) Heatmaps of ChIP peaks in a 4kb region from day 4 EBs from two independent Eomes$^{V5/V5}$ clones. **(b)** An Eomes consensus binding motif identified using HOMER is enriched under ChIP-seq peaks (top). Bar graph (below) depicts the distribution of ChIP-seq peaks relative to nearby transcriptional start sites. **(c)** GO terms (mouse phenotype) for the 541 genes associated with the 338 Eomes-V5 ChIP-seq peaks. **(d)** Venn diagrams depicting the overlap of Eomes-V5 ChIP peak associated genes with genes that are differentially expressed in day 4 WT vs. Eomes$^{-/-}$ Flk1^{hi}/PdgfRa^{-} (top panel) or day 4 WT vs. Eomes$^{-/-}$ Flk1^{-}/PdgfRa^{+} (bottom pannel) cells. **(e)** Hierarchically clustered heatmap of gene expression for the overlapping genes that are linked to Eomes-V5 ChIP peaks and differentially expressed in day 4 WT vs. Eomes$^{-/-}$ Flk1^{hi}/PdgfRa^{-} (top panel) or day 4 WT vs. Eomes$^{-/-}$ Flk1^{-}/PdgfRa^{+} (bottom pannel) cells.

2.2.14 Eomes, Tead4 and Smad2/3 bind regions transiently marked by H3K27Ac during early stages of hematopoieitc development

Next, I examined published ChIP-seq datasets (Goode et al., 2016; Wang et al., 2017) to evaluate co-occupancy by other transcriptional regulators, as well as DNase1 hypersensitivity sites and histone marks located near our identified Eomes bound regions during hematopoietic differentiation **(Figure 2.26)**. Interestingly, the majority of Eomes occupied sites were found to be marked by H3K27Ac and display DNase hypersensitivity in hemangioblasts (T^+/Flk-1^+) but not HE (kit+/Tie2+) or hematopoietic progenitors ($CD41^+$) **(Figure 2.26, a and Figure 2.28, b)**. Strikingly, many Eomes occupied sites are also bound by Smad2/3, intracellular effectors of the Activin/Nodal signaling pathway, as well as the TEA domain TF Tead4 **(Figure 2.26, a)**. Overlapping Eomes, Smad2/3 and Tead4 peaks identified 72 sites corresponding to genes strongly associated with hematopoiesis and mesoderm development **(Figure 2.26, b)**. We observe co-occupancy at genes down-regulated in day 4 Flk-1^{hi}/PdgfRa$^-$ Eomes-/- EBs **(Figure 2.26, b)** including at the promoter region of Mixl1, a previously described Eomes regulated gene as well as putative *cis*-regulatory elements controlling Dkk1 and Tbx3 expression **(Figure 2.26, c)**. Interestingly, Eomes binds a possible enhancer located 181kb upstream of the Runx1 TSS (-181), that is marked transiently by H3K27Ac and also bound by Tead4 and Smad2/3 **(Figure 2.26, c)**.

Utilizing CRISPR-Cas9, the putative Runx1 enhancer (-181) that we identified was homozygously deleted in the Runx1-Venus cell line (Runx1-Venus -181Runx1$^{\Delta/\Delta}$) **(Figure 2.27, a)**. At day 5 Runx1-Venus expression was not perturbed in Runx1-Venus -181Runx1$^{\Delta/\Delta}$ EBs, nor was hematopoietic development disrupted **(Figure 2.27, b)**. These results demonstrate that the -181 Runx1 genomic region is non-essential for the expression of Runx1. A recent ChIP-seq study performed by the Arnold group (Tosic et al., 2019),

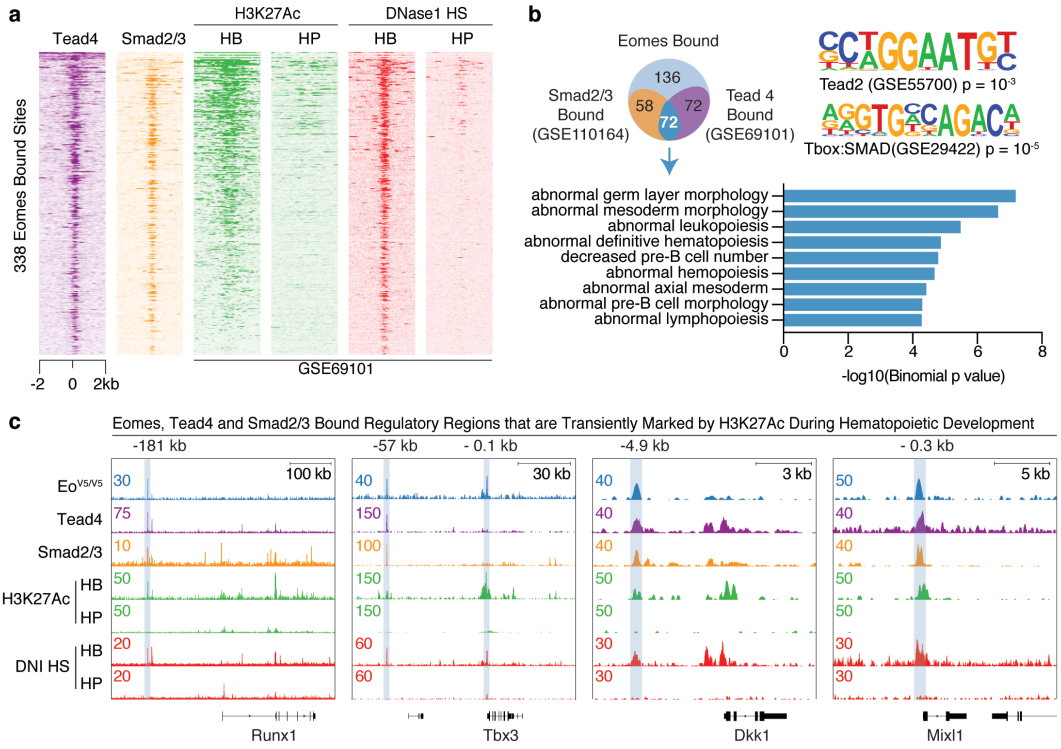


Figure 2.26 Genomic regions marked transiently by H3K27Ac are bound by Eomes, Tead4 and Smad2/3 during early stages of hematopoietic mesoderm development

(a) Heatmaps showing ChIP-seq signal for Tead4 (purple) and Smad2/3 (orange) occupancy in day 3 or day 4 Flk-1+ EB cultures, respectively. Heatmaps showing ChIP-seq signal for H3K27Ac (green) histone modifications in hemangioblast (HB) and hematopoietic (HP) cells. Heatmaps showing DNAseI hypersensitivity signal in hemangioblast (HB) and hematopoietic (HP) cells. All heatmaps show a 4kb region flanking peak centres of the 338 Eomes bound sites. **(b)** Venn diagram depicting the overlap of the Eomes, Smad2/3 and Tead4 bound regions. GREAT analysis reveals significantly enriched hematopoietic related GO Terms in the Mouse Phenotype category for the 72 Eomes, Smad2/3 and Tead4 overlapping genomic regions (blue). Tead2 and Tbox:Smad motifs identified using HOMER that are significantly enriched under the Eomes bound ChIP-seq peaks. (right side of panel) **(c)** IGV snapshots of Eomes, Tead4, Smad2/3 and H3K27Ac ChIP-seq peaks overlapping with DNase1 hypersensitivity (DN1 HS). Blue bars highlight Eomes bound sites and the numbers above indicate the relative location of these sites in kilobases to the TSS of the gene indicated. (HB = hemangioblast (T_+ /Flk-1_+); HP =hematopoietic progenitor ($CD41_+$))

however, shows binding of Eomes-GFP to many more sites at the Runx1 locus **(Figure 2.27, c, blue, yellow and orange columns)**. Interestingly, Eomes binds near both Runx1 promoters **(P1 and P2, yellow bars)** and to a 171 kb region upstream of P1 **(-171, orange bar)** that depends upon Eomes function for its accessibility in the Flk-1^{hi}/PdgfRa^{-} population. Additionally, the -171 genomic region is marked transiently by H3K27Ac during hematopoietic differentiation and is also bound by Tead4, Smad2/3 and Scl in similar stage EBs. Eomes-GFP also binds to the previously described Runx1 +110 enhancer that depends on Eomes activity for its accessibility in the Flk-1^{hi}/PdgfRa^{-} population (Schutte et al., 2016). Altogether, these results suggest that Eomes regulates Runx1 expression through binding a number of genomic regions at the Runx1 locus. Further deletion studies should be performed to ascertain the precise roles of the various Eomes bound sites for the regulation of Runx1 expression during EHT and hematopoietic development.

2.2.15 Comparing Eomes ChIP peaks with Eomes-dependent SCL bound cis-regulatory regions

Finally, we overlaid our day 4 Eomes ChIP-seq peaks with the ATAC-seq peaks with reduced accessibility in day 4 Flk-1^{hi}/PdgfRa^{-} Eomes-/- mesoderm as well as the SCL ChIP-seq peaks from day 4 wild-type Flk-1^{+} EBs (Van Handel et al., 2012) **(Figure 2.28, a).** Very few of the ATAC peaks (33/3629) or SCL ChIP Peaks (19/4393) are bound by Eomes at day 4 **(Figure 2.28, a)**. Interestingly, many of the Eomes ChIP peaks are normally accessible at early mesodermal (T^{+}/Flk-1^{-}) stages of development and become marked by H3K27Ac after the onset of Flk-1 expression (Goode et al., 2016) **(Figure 2.28, b)**. By contrast, Eomes-dependent ATAC peaks normally bound by SCL only become accessible in the hemangioblast (T^{+}/Flk-1^{+}) population **(Figure 2.28, b)**. These results suggest that Eomes-

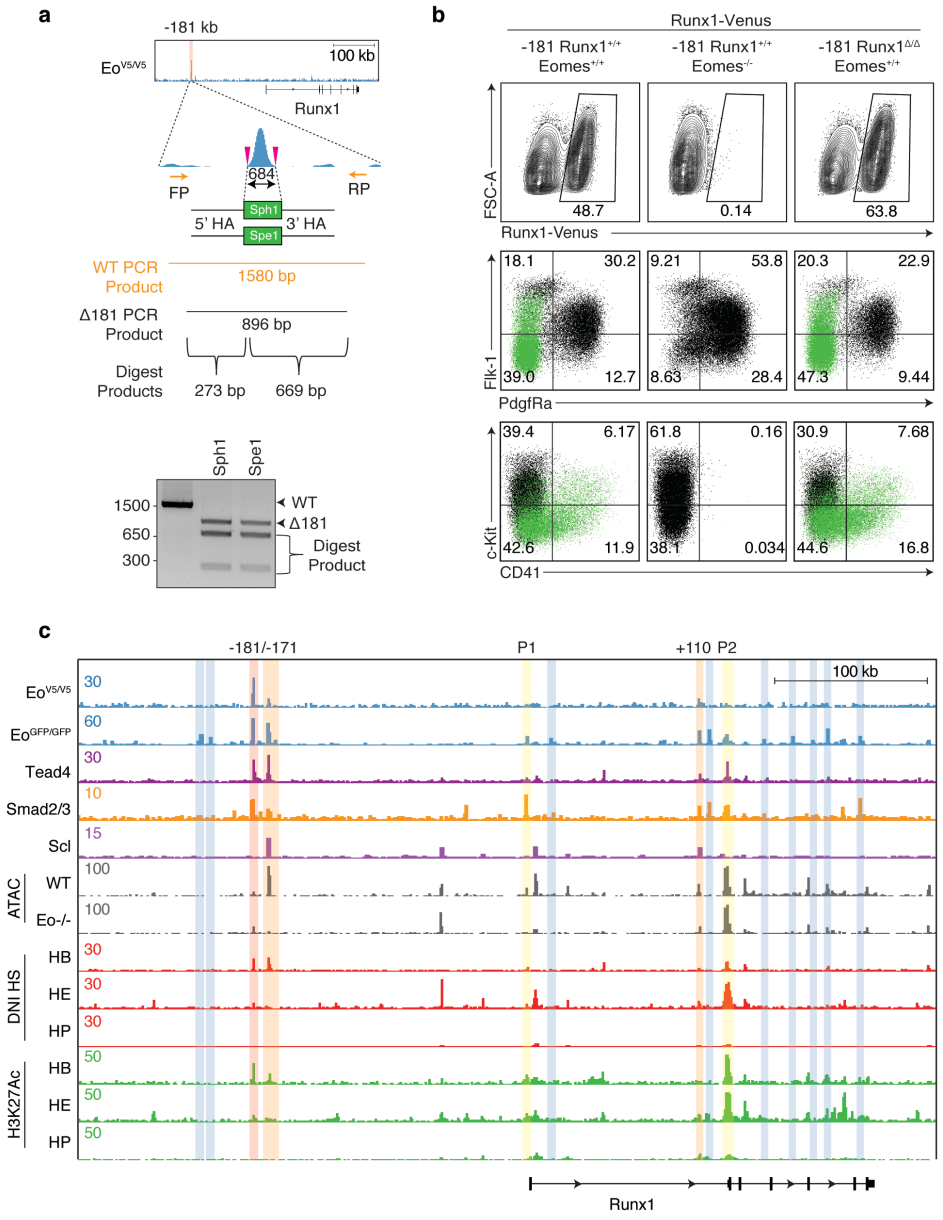


Figure 2.27 Eomes binds numerous genomic regions surrounding the Runx1 locus

(a) A targeting strategy used to remove the Eomes bound genomic region 181 kb upstream of Runx1 P1. Two ssODNs were used to patch in either a Sph1 or Spe1 restriction site subsequent to removal of a 684 bp region surrounding the Eomes bound site. Pink arrows indicate the locations of Cas9-gRNA induced DNA double strand breaks flanking either side of the -181 Runx1 region. Orange arrows indicate the location of primers used for PCR genotyping. Successful homozygous deletion of the -181 kb Eomes bound region in ES clones was confirmed by successful digestion of an 896 bp PCR product into 273 bp and 669 bp products using both Sph1 and Spe1. WT band size is 1580bp. **(b)** Runx1-Venus, Flk-1/PdgfRa and CD41/cKit expression in day 5 Runx1-Venus Eomes$^{+/+}$ -181 Runx1$^{+/+}$ (left panel), Runx1-

Figure legend 2.27 continued; Venus Eomes$^{-/-}$ -181 Runx1$^{+/+}$ (middle panel) and Runx1-Venus Eomes$^{+/+}$ -181 Runx1$^{\Delta/\Delta}$ (right panel) EBs. Green dots indicate cells positive for the expression of Runx1-Venus based on the gating strategy shown in the upper panel. **(c)** IGV snapshots of Eomes$^{V5/V5}$, Eomes$^{GFP/GFP}$, Tead4, Smad2/3 and Scl ChIP-seq peaks. H3K27Ac ChIP-seq peaks and DNase1 hypersensitivity (DN1 HS) at different stages of hematopoietic development in vitro (HB = hemangioblast (T_+ /Flk-1_+); HE = hemogenic endothelium (Tie2+/Kit+); HP =hematopoietic progenitor (CD41_+)). Coloured bars highlight Eomes bound sites identified in the Eomes$^{GFP/GFP}$ dataset. The numbers above the coloured columns indicate the relative location of these sites in kilobases to the TSS at P1 of the Runx1 locus. P1 = promoter 1; P2 = promoter 2.

dependent SCL bound *cis*-regulatory regions become accessible only subsequent to Eomes functional activity at earlier stages in the hematopoietic differentiation pathway.

2.2.16 The Generation of an Eomes$^{iCre\text{-}nLacZ}$ Reporter Allele

To perform additional retrospective fate mapping studies I generated another mouse strain in which an iCre.IRES.nLacZ.pA (Eomes$^{iCre\text{-}nLacZ}$) cassette is introduced into the first exon of the Eomes coding region followed by a removable, LoxP-flanked neomycin selection cassette **(Figure 2.29, a)**. A southern blotting strategy was utilized to identify 4 successfully targeted mESCs **(Figure 2.29, a,b)**. X-gal staining of E6.5 and E7.5 Eomes$^{iCre\text{-}nLacZ}$ mouse embryos confirmed that LacZ expression patterns mimic the known expression patterns for Eomes at equivalent developmental stages **(Figure 2.29, c)**.

To assess the contribution of Eomes expressing cells to sites of definitive haematopoiesis Eomes$^{iCre\text{-}nLacZ}$ male mice were crossed with female ROSA26^{LacZ} mice and the resulting embryos were stained for LacZ activity **(Figure 2.30, a)**. At E9.5/E10.5 there were two classes of embryos: approximately half of the LacZ+ embryos were virtually completely blue whilst the other half were only partially blue. This discrepancy may be due to stochastic early

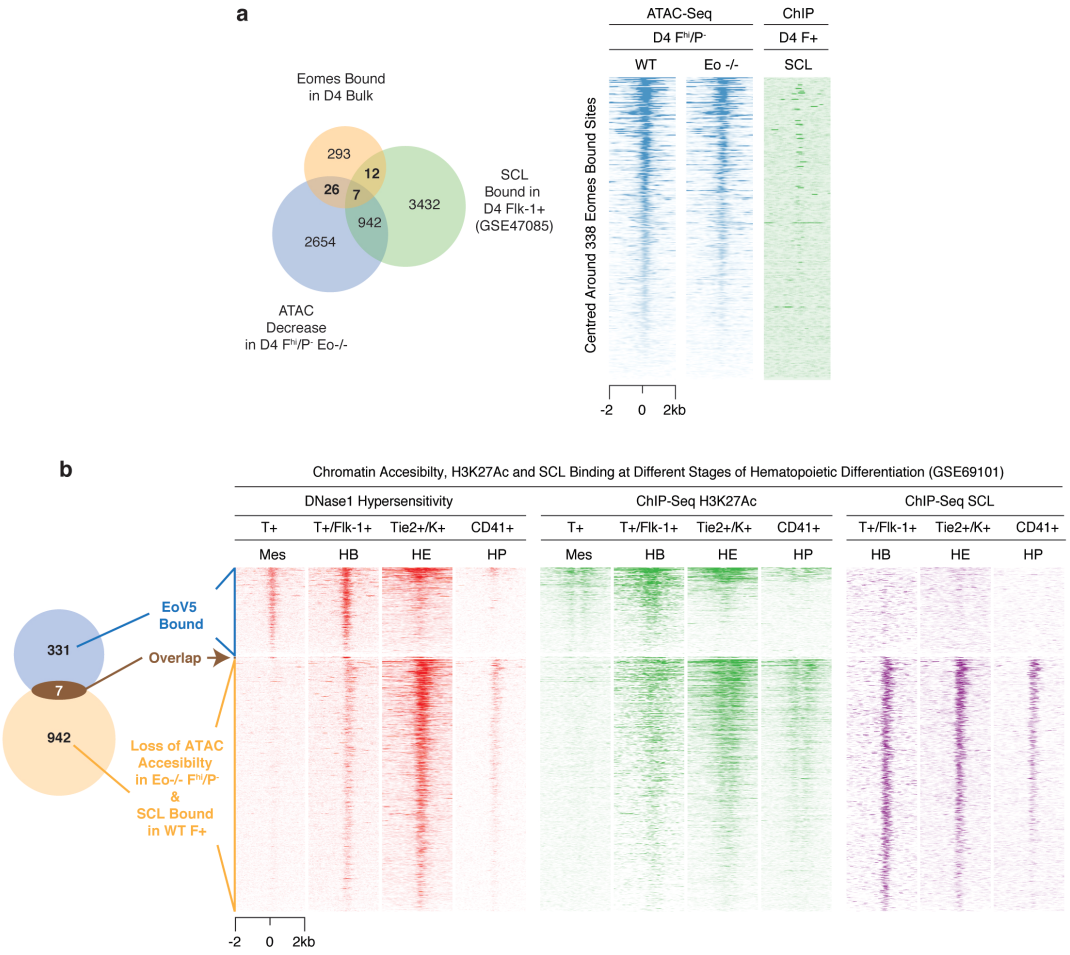


Figure 2.28 Comparing Eomes bound ChIP-seq peaks with the subset of ATAC-seq peaks that are Eomes-dependent and normally bound by SCL at various stages of hematopoietic differentiation

(a) Venn diagram depicting the overlap of Eo-V5 ChIP-seq peaks in D4 EBs, SCL ChIP-seq peaks in D4 Flk-1+ EBs and sites of reduced chromatin accessibility in day 4 Eomes-/- Flk-1+/PdgfRa- cells. (b)Heatmaps showing ATAC signals from WT (blue, left) or Eomes-/- (blue, right) day 4 Flk-1^{hi}/PdgfRa^{-} cells and SCL ChIP-seq signal (green) from day 4 WT Flk-1+ cells. All heatmaps show a 4kb region flanking peak centres of the 338 Eomes bound sites. **(b)** Venn diagram depicting the overlap of Eo-V5 ChIP-seq peaks in D4 EBs with sites of reduced chromatin accessibility in day 4 Eomes-/- Flk-1hi /PdgfRa cells that are normally bound by SCL in WT day 4 Flk-1+ cells. Heatmaps show DNaseIhypersensitivity signal, ChIP-seq signal for H3K27Ac (green) histone modifications and SCL occupancy in different cell populations that develop during hematopoietic differentiation (Mes = mesoderm, HB = hemangioblast, HE = hemogenic endothelium, HP = hematopoietic progenitor. All heatmaps show 4kb regions flanking peak the peak regions indicated in the Venn diagram.

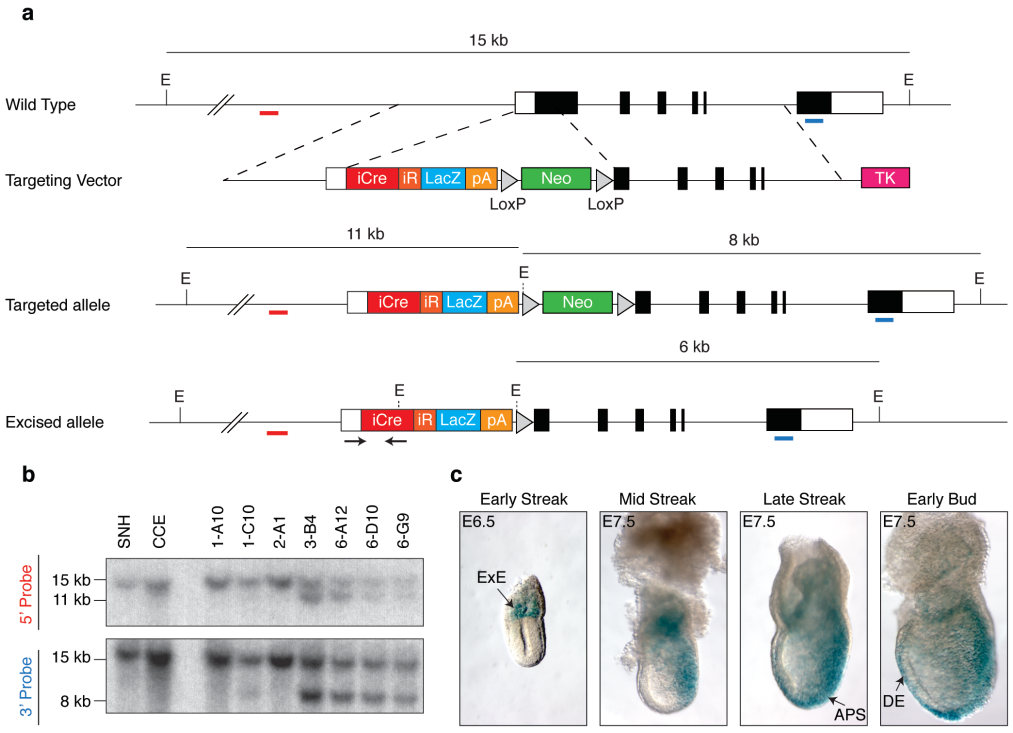


Figure 2.29 Generation of an Eomes.iCre-LacZ allele for fate mapping

(a) Targeting strategy used to generate Eomes$^{iCre\text{-}LacZ/+}$ mice. An iCre.IRES.nLacZ.pA cassette was introduced into the first exon of the Eomes coding region followed by a removable, LoxP-flanked (grey arrows) neomycin selection cassette. EcoRV restriction sites are indicated by vertical black lines (E). Probe 1 (red horizontal bar) and Probe 2 (blue horizontal bar) are external to the 5' and 3' homology arms of the targeting vector. TK, thymidine kinase. N, Neo. iCre, improved Cre-recombinase. E, EcoRV **(b)** Southern blotting reveals four mESC lines successfully targeted at one allele with the Eomes$^{iCre\text{-}LacZ}$ targeting vector. **(c)** X-Gal staining of E6.5 and E7.5 Eomes$^{iCre\text{-}LacZ}$ embryos reveals LacZ expression in the known regions of Eomes expression. ExE, extra-embryonic ectoderm. APS, anterior primitive streak. DE, definitive endoderm.

expression patterns of Eomes-iCre in the epiblast. We decided to further analyse the embryos that were partially blue, as these embryos looked more similar to previous LacZ fate mapping studies using other Eomes^{Cre} mouse strains. At E9.5/E10.5 a subset of mesoderm derived cells of the visceral yolk-sac, including hematopoietic and endothelial cells, are LacZ+ in these embryos **(Figure 2.30, b,c)**. Interestingly, at day E10.5 round budding hematopoietic cells and a subset of endothelial cells are LacZ+ **(Figure 2.30, c)**.

These results suggest that endothelial cells of the dorsal aorta, where the HSC is first generated, may be derived from Eomes expressing mesodermal precursors.

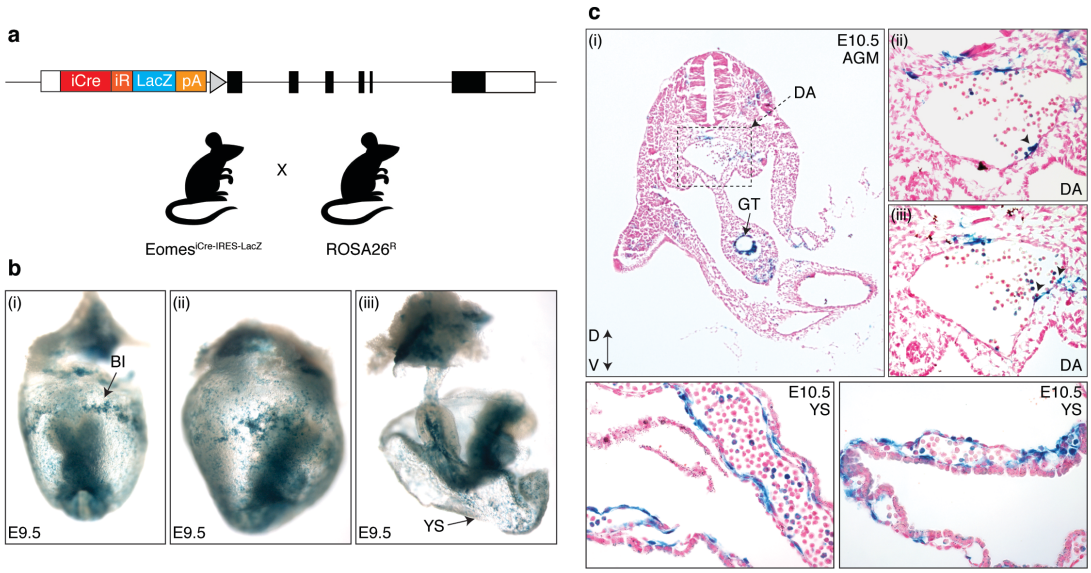


Figure 2.30 Eomes.iCre-LacZ expressing cells give rise to hematopoietic and endothelial cells at sites of definitive hematopoiesis

(a) Mice carrying an improved Cre recombinase (iCre) inserted into the ATG start site at the Eomes locus were crossed to ROSA26^{R} reporter mice that express LacZ upon Cre induced recombination. **(b,c)** Descendants of Eomes$^{iCre\text{-}LacZ}$ expressing cells give rise to hematopoietic and endothelial cells of the YS BIs. Wholemount X-gal staining was performed on E9.5 **(b)** and E10.5 **(c)** embryos and sections were counterstained with nuclear fast-red to highlight non-labelled cells. (AGM = aorta, gonad and mesonephros, DA = dorsal aorta, GT = gut tube, BI = blood islands, YS = yolk-sac, D = dorsal, V = ventral)

2.2.17 An Experimental System to Address the Timing of Eomes Activity During the Primitive and Definitive Waves of Hematopoiesis

Eomes is expressed dynamically at the outset of gastrulation and is clearly required for both primitive and definitive YS-like hematopoiesis *in vitro*. It remains to be determined whether or not Eomes plays a common role or two separate roles in different progenitor pools during the development of these different hematopoietic progenitors. To try and resolve this question I will make use of a cell line from the NIA in which Eomes expression is dox

regulatable (Nishiyama et al., 2009). In the Eomes-NIA cell line the long form of Eomes cDNA, followed by an IRES-VENUS cassette, is inserted into the ROSA26 locus (Nishiyama et al., 2009). The removal of dox from culture media induces the expression of Eomes-IRES-Venus in this ES cell line.

Eomes-NIA cells were put through the hematovascular EB differentiation protocol and dox was removed from day 2-4, day 2-5 or from day 4-5 **(Figure 2.31, a)**. At day 4 and 5 the expression of mesodermal markers Flk-1 and PdgfRa were analyzed alongside the expression of Eomes-Venus **(Figure 2.31, b)**. The continuous addition of dox to EBs efficiently suppresses the induction of Eomes-Venus **(Figure 2.31, b,d)**. Interestingly, induction of Eomes from day 2-4 increases the proportion of Flk-1^{hi}/PdgfRa^{-} cells **(Figure 2.31, b)**. Furthermore, when Eomes is continuously induced from day 2-5 Flk-1^{hi}/PdgfRa^{-} cells predominate at day 5 **(Figure 2.31, c)** and far fewer hemoglobinized cells are generated compared to the other minus dox conditions **(Figure 2.31, d)**. A day later hematopoietic (CD41+/c-Kit+) and endothelial cells (Cdh5+/CD31+) are efficiently generated in the various culture conditions in which Eomes expression is induced via dox removal **(Figure 2.31, d)**. These results demonstrate that temporal regulation of Eomes can be accomplished in Eomes-NIA cells during hematendothelial development *in vitro*. Finally, homozygous deletion of exons 2-5 of Eomes (Eomes$^{-/-}$) in the Eomes-NIA ES cells was successfully performed using my previously described CRISPR strategy (data not shown). Future work will utilize these Eomes$^{-/-}$ Eomes-NIA cells to address when during differentiation Eomes re-expression is able to rescue primitive and definitive hematopoiesis.

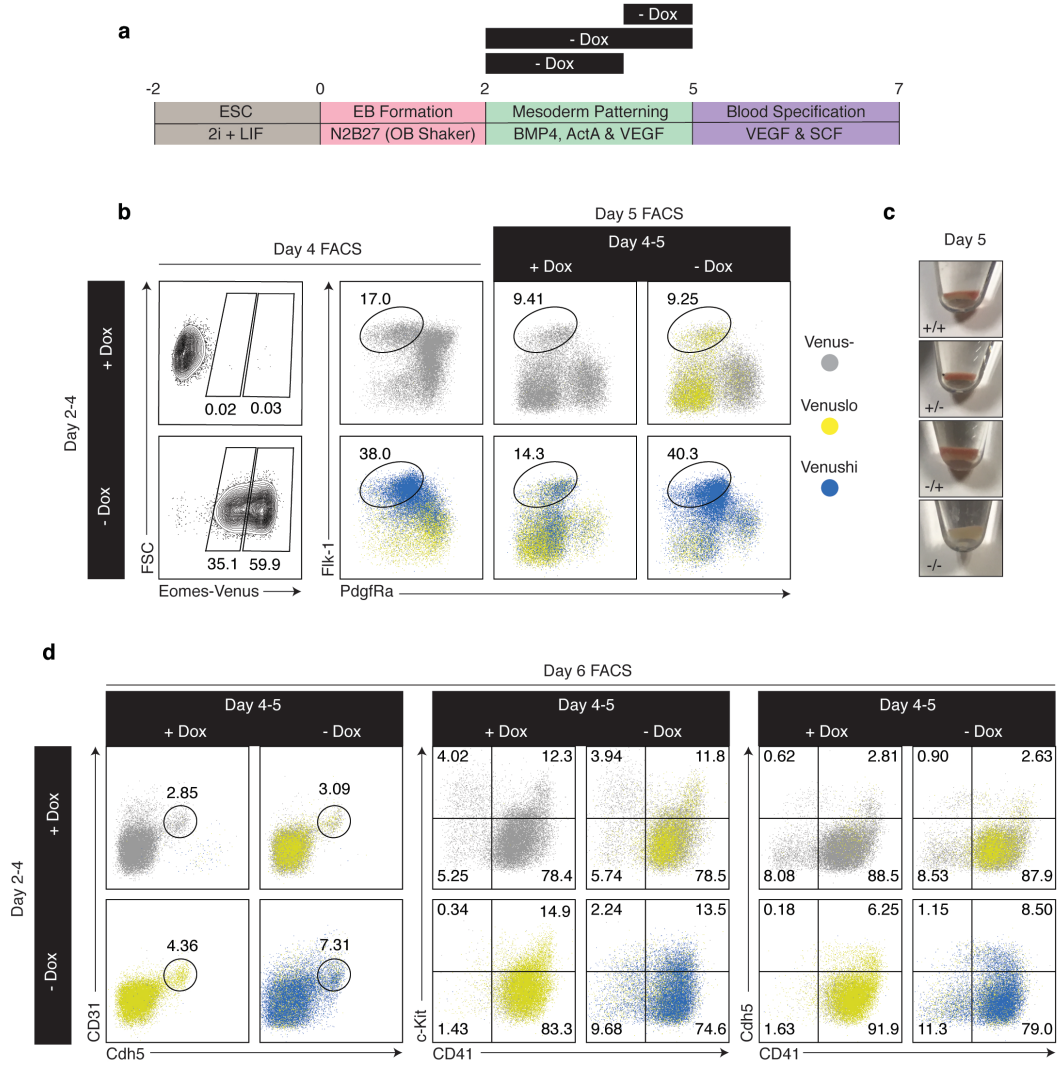


Figure 2.31 Regulating Eomes expression during hematovascular differentiation

(a) Eomes was induced via the removal of dox at different stages of the differentiation protocol depicted. 0.4 ug/mL dox was removed from cultures to induce the expression of Eomes from day 2-4, day 2-5 or day 4-5. As a control, 0.4 ug/mL of dox was kept in culture for the entire differentiation protocol. **(b)** Flk-1, PdgfRa and Eomes-Venus expression was evaluated in day 4 (left panel) and day 5 EBs (right panel) in which dox was either removed or added from day 2-4 and from day 4-5. These EBs contain populations of cells that express different levels of Eomes-Venus (Venus-negative = grey dots, Venus-lo = yellow dots, Venus-hi = blue dots). **(c)** Images of cell pellets from dissociated EBs at day 5. (+/+, +/-, -/+ and -/- indicates whether or not dox was added to culture from day 2-4/2-5). **(d)** Hematopoietic (CD41/cKit) and endothelial (Cdh5/CD31) marker expression in day 6 EBs. (FACS plots from n = 1 differentiation)

2.3 SUMMARY OF FINDINGS

Here we demonstrate that Eomes is transiently expressed in Flk1+ mesodermal progenitors that generate virtually all YS hematopoietic and endothelial cells *in vivo*. When Eomes is conditionally deleted from the epiblast, ExM markers, Flk-1 and ER71, are no longer expressed in late streak stage embryos. Utilizing an *in vitro* model of YS hematopoiesis, we find that Eomes-/- ES cells are able to generate, albeit at a reduced level, a population of Flk-1^{hi}/PdgfRa^{-} cells. Additionally, the Eomes-/- cultures are enriched for Flk-1^{-}/PdgfRa^{+} cells that express high levels of paraxial mesodermal genes.

Bulk and scRNA-seq experiments suggest that the Eomes$^{-/-}$ Flk-1^{hi}/PdgfRa^{-} cell populations contain developing hematoendothelial progenitors and endothelial cell populations similar to those found in the *in vitro* WT Flk-1^{hi}/PdgfRa^{-} cell populations and E7.5-E8.5 mouse embryos. Strikingly, the Eomes$^{-/-}$ Flk-1^{hi}/PdgfRa^{-} compartment lacks developing Runx1+ blood progenitor cells. Flow cytometry, colony forming assays and RT-PCR performed at later stages of YS-like hematovascular differentiation reveals that Eomes function is essential for the production of primitive erythrocytes and pro-definitive hematopoietic progenitors but non-essential for the generation of endothelial cells.

Utilizing ESC reporter lines, we find that Eomes is expressed prior to both SCL and Runx1 during mesoderm patterning. Eomes activity, however, is only essential for the expression of Runx1, not SCL, within the developing hematovascular lineage. Strikingly, Runx1+ hemogenic endothelium is not generated in the absence of Eomes function. Re-expression of Runx1 in Eomes$^{-/-}$ endothelial cultures, however, is sufficient to rescue definitive

hematopoiesis. These results demonstrate that Eomes sits upstream of Runx1 expression in the HE lineage.

ATAC-seq profiling of Eomes$^{-/-}$ and wildtype Flk-1^{hi}/PdgfRa^{-} hematoendothelial progenitors reveals that Eomes governs the accessibility of numerous hematopoietic enhancers that SCL normally utilizes to specify the blood cell fate, including previously described Runx1 enhancers. Interestingly, ChIP-seq experiments performed using Eomes$^{V5/V5}$ EBs suggests that Eomes coordinates the development of hemogenic competent mesoderm in the context of Activin/Nodal and Tead-Yap signaling. Additionally, ChIP-seq experiments performed by another group demonstrate that Eomes binds to numerous genomic regions at the Runx1 locus. Collectively, these experiments demonstrate that Eomes sits at the top of a transcriptional hierarchy, functioning upstream of Runx1 expression and SCL functional activity, to promote hemogenic competence of the entire YS mesodermal lineage **(Figure 2.32)**.

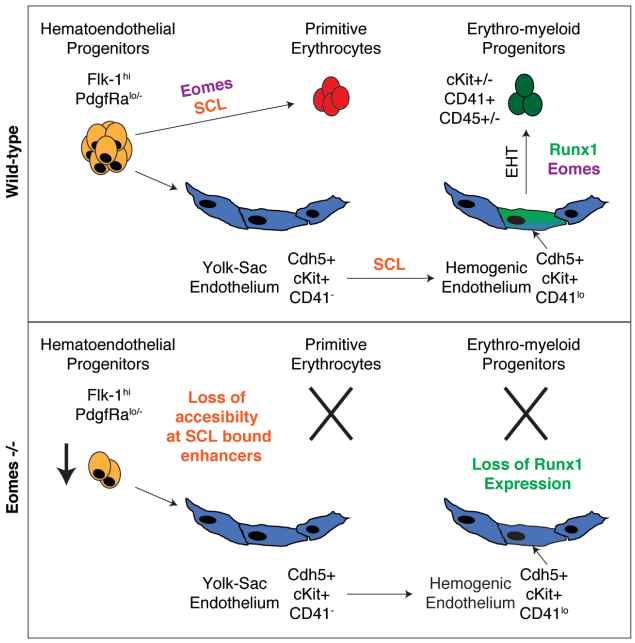


Figure 2.32 Eomes regulates the generation of primitive erythrocytes upstream of SCL functional activity and EHT upstream of Runx1 expression in the HE lineage

Model summarizing the effects of Eomes-loss-of-function on the first two waves of hematopoiesis that occur in the YS. Hematoendothelial progenitors are still generated in the absence of Eomes-function, albeit at lower levels than in wildtype cultures. Eomes-/- hematoendothelial progenitors lack chromatin accessibility at numerous hematopoietic enhancers that are normally bound by SCL and are thus unable to transition into primitive erythrocyte progenitors. Eomes-/- hematoendothelial progenitors can generate HE, however, this HE does not upregulate Runx1 expression and is therefore incapable of undergoing EHT and producing definitive hematopoietic cells.

CHAPTER 3 : TRANSCRIPTIONAL DIVERSITY AND POTENCY OF EOMES EXPRESSING CELLS DURING GASTRULATION

3.1 INTRODUCTION

The mouse body plan is laid down during a dynamic morphogenetic process called gastrulation that begins 6.0 days post-fertilization (Arnold and Robertson, 2009). At the outset of gastrulation, formation of the primitive streak (PS) demarcates the posterior side of the embryo. Within the PS epiblast cells undergo an epithelial to mesenchymal transition (EMT) and give rise to mesodermal and definitive endodermal (DE) cells. Cells egressing the developing PS at different times and sites along the anterior-posterior axis give rise to distinct mesodermal and DE subtypes (Kinder et al., 1999; Tam et al., 1997). The first wave of cells to traverse the posterior aspect of the PS predominantly generate yolk-sac mesoderm. In contrast, later waves that migrate through more anterior portions of the PS give rise to cardiac mesoderm and definitive endoderm.

Fate mapping studies by the Robertson lab have demonstrated that Eomes expressing cells give rise to specific mesodermal subsets (yolk-sac, cardiac and lateral plate), the entire definitive endoderm lineage and derivatives of the node(Arnold et al., 2008; Costello et al., 2011). These fate mapping studies exploited genetically modified mice with Cre recombinase knocked into the translational start site of Eomes. Population level studies of this kind, however, are inadequate to determine the heterogeneity of Eomes+ progenitors. Questions regarding the individual fates of single Eomes expressing progenitors/progeny and the timing of their lineage bifurcations, therefore, remain unanswered. The overarching

second aim of my thesis project is to uncover the potency of Eomes+ cells egressing the PS during mouse gastrulation. To accomplish this, clonal lineage tracing experiments will be performed in real-time utilizing light sheet imaging and *ex vivo* embryo culture techniques. Additionally, scRNA-seq experiments of Eomes+ progenitors from mouse gastrulas will complement these clonal lineage tracing studies. This experimental system will allow us to unambiguously assign potencies to Eomes expressing progenitors and ascertain the timing of lineage bifurcations during early stages of YS, cardiac and definitive endoderm development. Furthermore, these experiments will provide information about the transcriptional heterogeneity of these early progenitor populations.

3.2 RESULTS

3.2.1 Production of targeted ESCs for clonal lineage tracing of Eomes progenitors

To resolve the potencies of Eomes expressing progenitors we produced two genetically modified mouse lines, $Eomes^{CreER}$ and $Eomes^{CreER\text{-}nLacZ}$, to enable us to perform clonal lineage tracing experiments. Single cell tracking experiments will be performed using E6.5 embryos generated from crosses of $Eomes^{CreER}$/$Eomes^{CreER\text{-}nLacZ}$ with $ROSA^{YFP}$ females(Srinivas et al., 2001). Tamoxifen addition will induce pulsed labelling of Eomes expressing progenitors in *ex vivo* cultures that will then be followed in real time for 24-48 hours using fluorescent light sheet microscopy.

Two targeting vectors were produced **(Figure 3.1, a & Figure 3.2, a)** which contained tamoxifen inducible Cre recombinase knocked into the translational start site at the Eomes locus, causing deletion of the first 500 bp of Eomes' first exon. In the first targeting vector ($Eomes^{CreER}$) CreERT2 cDNA was followed by a β-globin polyA signal **(Figure 3.1, a)**. In the

second targeting vector (Eomes$^{CreER\text{-}nLacZ}$) CreERT2 cDNA was followed by an internal ribosomal entry site, nuclear LacZ cDNA and an SV40 polyA signal **(Figure 3.2, a)**. Both targeting vectors contained loxP flanked neomycin resistance cassettes for positive selection and a thymidine kinase cassette, downstream of the 3' end of the targeting vector, for negative selection against random integration of the targeting vector. Both targeting vectors contained a 5' homology arm made up of 2.6 kb upstream of the Eomes start codon and a 3' homology arm containing 5.2 kb of genomic sequence downstream of Exon 1 **(Figure 3.1, a & Figure 3.2, a)**.

Southern blotting was utilized to identify successfully targeted ESCs **(Figure 3.2, b & Figure 3.3, b)**. In total, 7 correctly targeted clones were identified for the first targeting vector, Eomes^{CreER} **(Figure 3.2, b)** and 4 correctly targeted clones were identified from the second targeting vector, Eomes$^{CreER\text{-}nLacZ}$ **(Figure 3.3, b)**. Genetically modified mouse strains were produced via blastocyst injection of Eomes^{CreER} and Eomes$^{CreER\text{-}nLacZ}$ ES cells. Finally, X-gal staining of E6.5 and E7.5 Eomes$^{CreER\text{-}nLacZ}$ mouse embryos confirmed LacZ expression patterns mimic the known expression patterns for Eomes at equivalent developmental stages **(Figure 3.3, c)**.

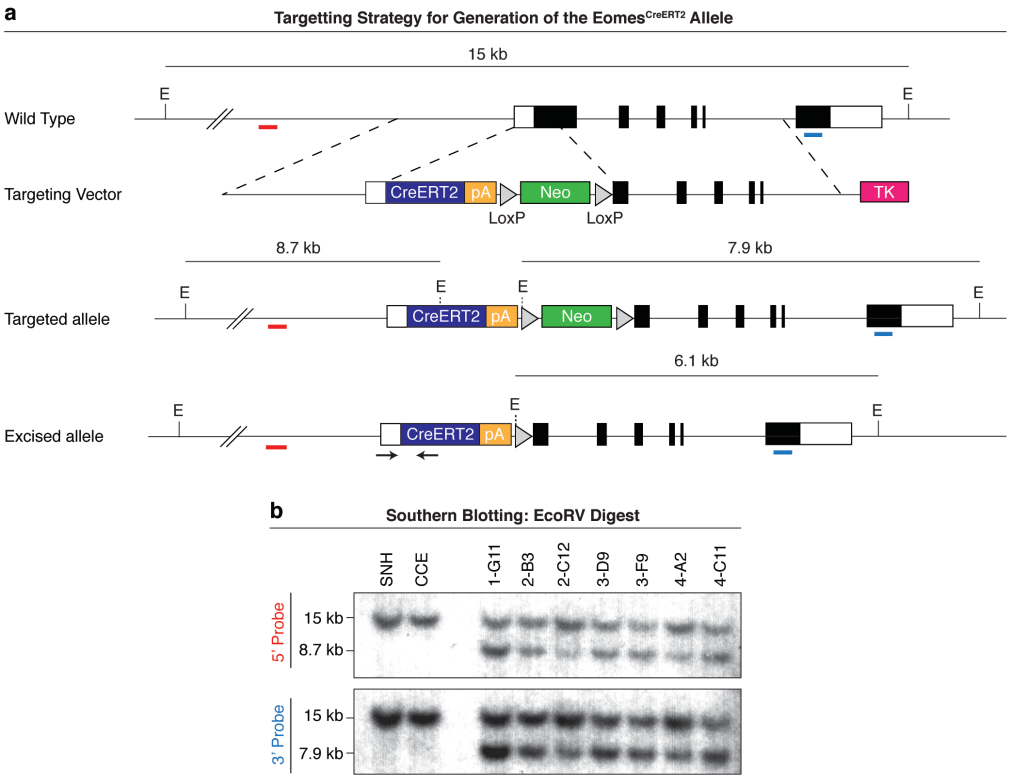


Figure 3.1 Generation of an Eomes.CreERT2 mouse strain for lineage tracing

(a) Targeting strategy used to generate Eomes$^{CreER/+}$ mice. A CreERT2.pA cassette was introduced into the first exon of the Eomes coding region followed by a removable, LoxP-flanked (grey arrows) neomycin selection cassette. EcoRV restriction sites are indicated by vertical black lines (E). Probe 1 (red horizontal bar) and Probe 2 (blue horizontal bar) are external to the 5' and 3' homology arms of the targeting vector. TK, thymidine kinase. N, Neo. Cre, CreERT2. E, EcoRV **(b)** Southern blotting reveals seven mESC lines successfully targeted at one allele with the Eo^{CreER} targeting vector.

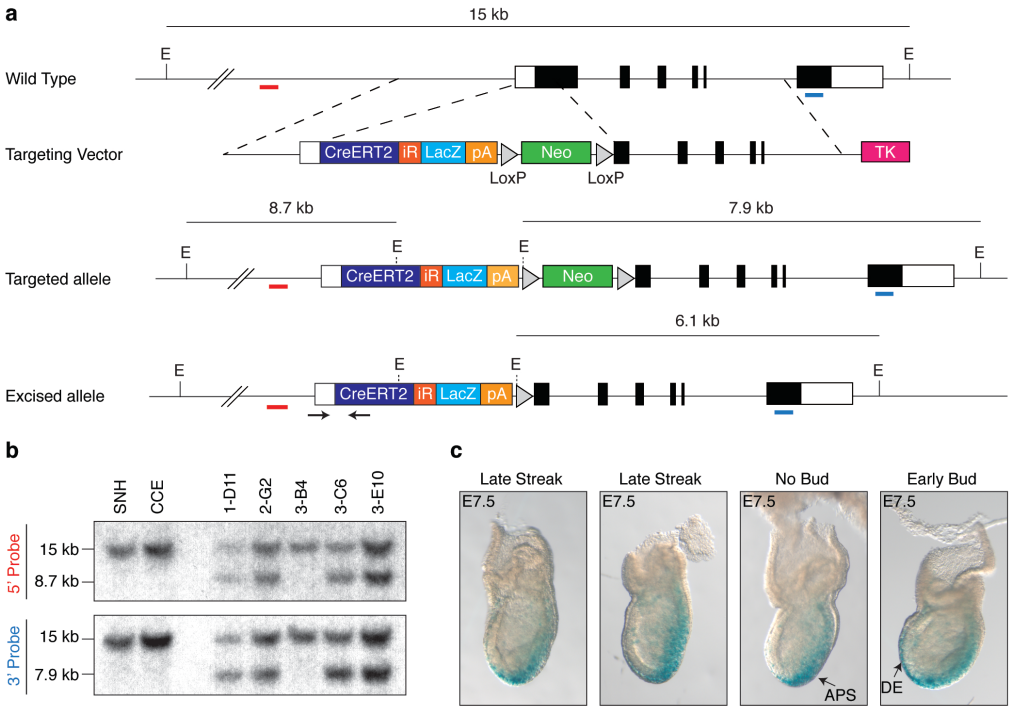


Figure 3.2 Generation of an Eomes.CreERT2-LacZ mouse strain for lineage tracing

(a) Targeting strategy used to generate Eomes$^{CreER\text{-}LacZ/+}$ mice. A CreERT2.IRES.nLacZ.pA cassette was introduced into the first exon of the Eomes coding region followed by a removable, LoxP-flanked (grey arrows) neomycin selection cassette. EcoRV restriction sites are indicated by vertical black lines. Probe 1 (red horizontal bar) and Probe 2 (blue horizontal bar) are external to the 5' and 3' homology arms of the targeting vector. TK, thymidine kinase. N, Neo. Cre, CreERT2. E, EcoRV. iR, IRES. **(b)** Southern blotting reveals four mESC lines successfully targeted at one allele with the Eomes$^{CreER\text{-}LacZ}$ targeting vector. **(c)** X-Gal staining of E7.5 Eomes$^{CreER\text{-}LacZ/+}$ embryos reveals LacZ expression in known regions of Eomes expression. APS, anterior primitive streak. DE, definitive endoderm.

3.2.2 Isolation of Eomes.GFP+ progenitors from mouse embryos

To resolve the transcriptional heterogeneity within the mouse gastrula research groups have used unbiased scRNA-seq/RNA-seq approaches (Peng et al., 2019; Pijuan-Sala et al., 2019). To specifically probe the transcriptional heterogeneity of early Eomes+ progenitors in the mouse gastrula we will combine FACS and scRNA-seq technology. To test whether or

not it is possible to isolate individual Eomes.GFP+ cells we set up timed mating's between $Eo^{GFP/+}$ C57/Bl6 (Arnold et al., 2009) male mice and CD1 females. At E6.5, embryos were dissected and pooled based on GFP expression using a fluorescent microscope. From 3 litters, 25 GFP positive embryos were recovered, staged and dissociated. After dissociation, the cells were run through a flow cytometer and analyzed for GFP expression (Fig. 4). This trial suggests that it is feasible to isolate individual Eomes.GFP+ cells from early stage mouse gastrulas.

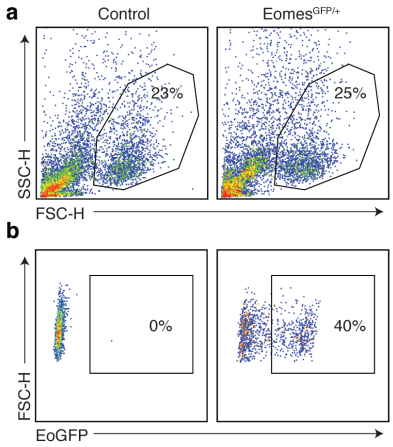


Figure 3.3 Isolation of Eomes.GFP+ progenitors from early PS stage mouse embryos
$Eo^{GFP/+}$ C57/Bl6 males were crossed with CD1 females, embryos were dissected at E6.5, pooled as wild type or Eo.GFP+ utilizing a fluorescent microscope and then dissociated and evaluated via flow cytometry. **(a)** Cells were gated based on forward scatter (FSC) and side scatter (SSC). **(b)** The GFP+ gate was set based on the wild-type control pool (left side).

3.3 SUMMARY OF FINDINGS

I have produced two genetically modified mouse strains, Eomes.CreERT2 and Eomes.CreERT2-LacZ, to use for clonal lineage tracing experiments. Additionally, I have demonstrated that it is possible to isolate Eomes.GFP+ cells from E6.5 $Eomes^{GFP/+}$ embryos. In the future, I will utilize this FACS strategy to perform scRNA-seq of Eomes.GFP+ cells from E6.0-E7.5 mouse embryos. Furthermore, I will use the two CreERT2 mouse lines to determine the potencies of Eomes+ progenitors that generate the definitive endoderm and multiple mesodermal subtypes (extraembryonic, cardiac/cranial, lateral-plate) by following them in real time using light sheet imaging. These experiments will refine our understanding of the lineage hierarchy that exists during mouse gastrulation.

CHAPTER 4 : GENERAL DISCUSSION

4.1 DISCUSSION AND FUTURE WORK

4.1.1 Reconciling the differences between in vitro and in vivo Eomes loss-of-function experiments

Here we uncover a novel role for Eomes during the development of the hematopoietic lineages of the murine YS. Our *in vivo* fate mapping and immunostaining studies, as well as analysis of another group's scRNA-seq hematoendothelial differentiation trajectories (Pijuan-Sala et al., 2019), reveals that Eomes is transiently expressed in nascent Flk-1+ ExM that gives rise to virtually all YS hematopoietic and endothelial cells. We find that conditional deletion of Eomes in the epiblast impairs the induction of Flk-1 and ER71, genes normally expressed in the developing ExM, essential for YS vasculogenesis and hematopoiesis (Koyano-Nakagawa and Garry, 2017; Lee et al., 2008; Liu et al., 2012; Shalaby et al., 1995). These results suggest that Eomes activity is required for the generation of ExM *in vivo*. In contrast, utilizing an in vitro model of YS-hematopoiesis we demonstrate that Eomes$^{-/-}$ ES cells have the capacity to generate, albeit at a reduced level, Flk-1^{hi}/PdgfRa^{-} hematoendothelial progenitors that express ER71. scRNA-seq comparisons demonstrate that these Eomes-/- Flk-1^{hi}/PdgfRa^{-} cells are very similar transcriptionally to hematoendothelial progenitors that arise in E7.5-E8.5 mouse embryos (Pijuan-Sala et al., 2019).

Why are Flk-1+/ER71+ hematoendothelial progenitors generated *in vitro* but not *in vivo* when Eomes function is disrupted? Previous *in vivo* studies have shown that Eomes deletion from the epiblast impairs the induction of Mesp1 and consequently the delamination and migration of nascent mesodermal cells from the PS (Arnold et al., 2008; Costello et al., 2011). This migratory block disrupts the normal development and patterning of the mouse

gastrula. PS outgrowths grown in serum-conditions from Eomes$^{\Delta epi}$ embryos, however, downregulate E-cadherin and undergo migration (Arnold et al., 2008). Similarly, Eomes-/- ES cells undergo CAM switching and an EMT like process in our EB cultures. Therefore, Eomes-/- hematoendothelial progenitors likely arise *in vitro* because in this context they receive the correct inductive signals, that are not available to them in Eomes$^{\Delta epi}$ embryos.

Why is there a reduction in the frequency of Flk-1^{hi}/PdgfRa^{-} hematoendothelial progenitors in Eomes-/- cultures? A previous study demonstrates a reduction in the generation of Flk-1+ mesoderm and hematopoietic progenitors in Mixl1-null ES differentiation cultures (Ng et al., 2005). Further studies by the same group suggest that this block occurs in part because Flk-1 is a direct target of Mixl1(Pereira et al., 2012). Eomes sits upstream of Mixl1 during mesendoderm differentiation (Izumi et al., 2007a) and Eomes directly binds the Mixl1 protomer in this context (Tosic et al., 2019). Furthermore, re-expression of Eomes in T-null/Eomes-/- ES cells rescues the expression of Flk-1, however, Eomes does not directly bind the Flk-1 promoter (Tosic et al., 2019). Interestingly, we find here that Eomes binds the Mixl1 promoter in bulk day 4 EBs during hematovascular differentiation. Additionally, Mixl1 is downregulated in Eomes$^{-/-}$ mesodermal populations 1 and 2, cellular subsets of the Flk-1^{hi}/PdgfRa^{-} cell population that arise at day 4 in culture. The efficient induction of Flk-1 expression during hematoendothelial development, therefore, likely depends on Eomes-dependent induction of Mixl1 in this lineage at the outset of gastrulation.

4.1.2 Eomes sits upstream of SCL functional activity

We reasoned that the profound block in primitive and definitive hematopoietic development that occurs in Eomes-/- cultures may result because Eomes regulates SCL expression.

RNA-seq and SCL-mCherry reporter line experiments, however, demonstrate that SCL expression is unperturbed in Eomes-/- hematoendothelial progenitors. Interestingly, ATAC-seq analysis reveals that a suite of enhancers that SCL normally binds (Org et al., 2015) are inaccessible in day 4 Eomes-/- Flk-1^{hi}/PdgfRa^{-} cells. These Eomes-dependent SCL enhancers may be inaccessible due to the loss of a hematopoietic mesodermal subset in the Eomes-/- Flk-1^{hi}/PdgfRa^{-} population. Our scRNA-seq analysis, however, suggests this is unlikely as both day 4 Eomes-/- and WT Flk-1^{hi}/PdgfRa^{-} cell populations contain similar HE progenitor subsets. To further refine our understanding of the cell populations in which Eomes regulates chromatin accessibility, scRNA-seq/scATAC-seq experiments should be performed in the future.

Interestingly, it has been shown previously that the accessibility of SCL bound enhancers in Flk-1+ hematopoietic mesoderm does not rely on SCL function (Org et al., 2015). These finding suggests that SCL does not function as a pioneer factor in the context of hematopoietic specification of mesoderm. Interestingly, our analysis of another group's dataset (Goode et al., 2016) suggests that SCL bound Eomes-dependent enhancers only become accessible during normal hematopoietic differentiation after the onset of Flk-1 expression. As Eomes is expressed prior to Flk-1 and SCL during hematoendothelial development we reasoned that Eomes may directly regulate the accessibility of these Eomes-dependent SCL enhancers. Our ChIP-seq results, however, do not suggest this is the case as the vast majority of Eomes-dependent SCL bound enhancer regions are not occupied by Eomes. Instead, Eomes binds genomic regions that are accessible at earlier mesodermal stages of development that are marked transiently by H3K27Ac in mesoderm and hemangioblast populations. It therefore seems likely that intermediary proteins, activated by an Eomes-dependent transcriptional network during mesoderm development, are responsible for opening up SCL enhancers. In this case, the functional ability of SCL to

drive hematopoietic specification relies on an Eomes coordinated epigenetic landscape. In accordance with this notion a recent study by the Arnold group also finds that Eomes regulates enhancer accessibility during mesoderm development *in vitro (Tosic et al., 2019)*. Future studies will need to clarify precisely how Eomes functions upstream of SCL to prepare the chromatin landscape for hematopoiesis.

4.1.3 Eomes regulates Runx1 expression in the HE lineage

Eomes-/- and Runx1-/- EB/EHT cultures contain a CD41lo/Cdh5+/cKit+ endothelial subset that is not produced in equivalent stage SCL-/- cultures. This is in line with a previous study that reveals an absence of these markers in presumptive SCL-/- HE cells that arise in chimeric E8.5 embryos (Pijuan-Sala et al., 2019). Previous studies have suggested that while Runx1 activity is dispensable for HE development, SCL function is absolutely required for the specification of HE (Lancrin et al., 2009; Liakhovitskaia et al., 2014). As mentioned previously, SCL expression is unperturbed in Eomes-/- cultures in both hematoendothelial progenitors and endothelial cell populations. Strikingly though, Eomes-/- EHT cultures lack a Runx1+ CD41lo/Cdh5+/cKit+ HE population.

What role then does Eomes play in the specification of HE? Are Eomes-dependent SCL enhancers (approx. 900) essential for the transition of hematoendothelial progenitors into HE or is SCL still able to specify HE in the absence of Eomes function? We show here that re-expression of Runx1 in Eomes-/- EHT cultures is sufficient to rescue EHT and the formation of pro-definitive hematopoietic colonies. These results strongly suggest that the CD41lo/Cdh5+/cKit+ endothelial subset present in Eomes-/- cultures is HE. Furthermore, these results confirm our scRNA-seq results which suggested that a

hematoendothelial/endothelial progenitor subset in the Flk-1hi/PdgfRa- population that normally generates HE is not lost in the absence of Eomes function. Therefore, the primary role for Eomes during YS-like pro-definitive hematopoiesis is to endow the HE lineage with the capacity to express Runx1.

Recent experiments in the mouse suggest that hemogenic competency of YS endothelial progenitors is actively restrained via BMI1-dependent silencing of Runx1 expression (Eliades et al., 2016). Additionally, re-expression of Runx1 in non-HE cells is sufficient to convert them into HE during a narrow developmental time window within the mouse YS (Yzaguirre et al., 2018). Considering the entire endothelial lineage is derived from Eomes expressing precursors, it is tantalizing to speculate that Eomes endows every YS endothelial cell with the capacity to express Runx1. If this is the case, then HE versus non-HE specification likely relies upon BMI1 dependent silencing of Runx1 within the YS endothelium.

4.1.4 Eomes is essential for the generation of primitive erythrocytes

In addition to Eomes requirements for the generation of definitive hematopoietic progenitors, we also show that Eomes is essential for the development of primitive erythrocytes. It has been well established that Runx1 loss-of-function does not disrupt the specification of primitive erythrocytes (de Bruijn and Dzierzak, 2017). In line with this we find that Runx1-/- ES cells are able to generate EryP colonies in our differentiation protocol. Therefore, Eomes must play a separate role, beyond activation of Runx1, during the development of the primitive hematopoietic lineage. As primitive erythrocyte specification absolutely requires SCL functional activity (Porcher et al., 1996; Shivdasani et al., 1995) it seems likely that

Eomes-/- hematoendothelial progenitors do not transition into primitive erythrocytes because the SCL enhancer landscape is inaccessible. In line with this notion a number of SCL bound enhancers known to drive genes essential for primitive erythrocyte development, Nfe2 and Gata1, are inaccessible in Eomes-/- HE progenitors.

4.1.5 Eomes binds cis-regulatory regions at the Runx1 locus and regulates the accessibility of Runx1 enhancers

By what mechanism does Eomes coordinate the development of HE cells capable of inducing Runx1 expression and undergoing EHT? Our *in vivo* and *in vitro* experiments suggest that Eomes is only expressed transiently in Flk1+ mesodermal progenitors at the outset of gastrulation (E6.5), a few days prior to the development of Runx1+ HE in the yolk-sac (E8.25). Interestingly, our ATAC-seq demonstrates that Flk-1^{hi}/PdgfRa^{-} hematoendothelial progenitors that form in the absence of Eomes function lack chromatin accessibility at previously described (+3, +24, +110, -322, -327) (Schutte et al., 2016) and potentially novel (+140, -171, -392) Runx1 enhancers. Additionally, our ChIP-seq experiments suggest that Eomes/Tead4/Smad2/3 co-occupy a novel *cis*-regulatory region located 181 kb upstream of the Runx1 TSS at mesodermal stages of development.

While deletion of the putative -181 Runx1 enhancer does not disrupt Runx1 expression, recent experiments by the Arnold group (Tosic et al., 2019) demonstrate that Eomes binds a number of additional regions that surround the Runx1 locus. Additionally, Eomes re-expression rescues Runx1 expression in their EB culture system (Tosic et al., 2019). Altogether these results, alongside the results presented in chapter 2 of this thesis, strongly suggest that Eomes governs the emergence of a complex *cis*-regulatory landscape at the Runx1 locus that primes EHT. Eomes likely primes the Runx1 chromatin landscape in

nascent mesoderm for Runx1 induction at later developmental stages. Future experiments that delete individual Eomes bound genomic regions at the Runx1 locus, alongside chromatin conformation capture experiments, will further refine our understanding of how Eomes coordinates Runx1 expression in the HE lineage.

4.1.6 A hemogenic signaling niche during gastrulation

How does a single transcription factor, Eomes, coordinate the development of cardiac, hematopoietic and definitive endoderm lineages? It seems likely that different PS signaling contexts endow Eomes with alternate functional activities and this allows Eomes to initiate different developmental trajectories. We find here that the majority of Eomes ChIP-seq peaks are located at *cis*-regulatory regions active transiently during mesodermal stages of hematopoietic development (Goode et al., 2016). Strikingly, many of these Eomes bound sites are co-occupied in similar stage EBs by Tead4 (Goode et al., 2016) and Smad2/3 (Wang et al., 2017), TFs that act downstream of Hippo/YAP and Activin/Nodal signalling, respectively. Furthermore, computational analysis shows that sites co-bound by this triad of TFs are associated with genes regulating both mesoderm and blood cell development.

Interestingly, a previous study demonstrates that disruption of Tead-YAP complex formation profoundly disrupts EHT and the generation of $CD41^{+}$ cells (Goode et al., 2016). Furthermore, Tead signalling is specifically required during mesodermal stages of development *in vitro*, coincident with the onset of Eomes functional activity. Activin/Nodal signalling is also essential for hematopoietic development *in vitro* (Nostro et al., 2008). It therefore seems likely that Eomes guides hematopoietic mesoderm development in the context of active Activin/Nodal and Tead/YAP signalling. Consistent with this, recent studies

suggest that Activin/Nodal and Tead4-Yap signalling pathways are active in the proximal epiblast/PS/ExM, cell populations that express Eomes and generate the YS BIs (Peng et al., 2019).

4.1.7 A strategy to uncouple primitive and pro-definitive hematopoietic progenitors

What remains to be determined is precisely when and in what cell population/populations Eomes acts to endow hematopoietic competence. Does Eomes act early, in a broad posterior epiblast population? Or does Eomes play different roles in YS primitive hematopoietic and definitive hematopoietic progenitor populations that traverse the PS at different times and in different signaling contexts? A previous study shows that conditional inactivation of Eomes in the PS using a T.Cre deleter strain has no noticeable impact on embryonic development (Arnold et al., 2008). Additionally, we have performed preliminary experiments which suggest that Eomes conditional deletion with a Mesp1.Cre deleter strain has no detrimental effects during embryogenesis. As both Mesp1 and T are expressed broadly within migratory YS mesodermal precursors, shortly after their ingression through the PS, Eomes is likely only required for YS hematopoiesis within a narrow developmental time window in the proximal epiblast/PS. Future rescue experiments using the Eomes-/-Eomes-NIA cell line will allow me to refine our understanding of the timing of Eomes functional requirements during both primitive and definitive YS-like hematopoiesis.

4.1.8 Does Eomes regulate Runx1 expression in the HSC lineage?

Fate mapping studies, using the new Eomes$^{iCre\text{-}LacZ}$ allele that I generated, demonstrate that intra-aortic clusters and a subset of endothelial cells that line the ventral side of the dorsal aorta at E10.5 are derived from Eomes expressing precursors. This region of the embryo is the most well characterized site of HSC production (Ditadi et al., 2017; Dzierzak and Speck, 2008). It is therefore tantalizing to speculate that Eomes also endows the HE lineage that generates the HSC with the capacity to induce Runx1 expression. At the moment, however, it is very difficult to study this as we do not have a robust *in vitro* model of HSC development and there is no obvious way to conditionally delete Eomes in the HE lineage that generates the HSC *in vivo* without disrupting mouse gastrulation.

4.1.9 Resolving the potencies of Eomes+ progenitors during gastrulation

I am hopeful that the Eomes^{CreERT2} and Eomes$^{CreERT2\text{-}LacZ}$ mouse lines that I have generated will prove useful tools to reveal the potencies of Eomes+ progenitors that arise during gastrulation. It will be particularly interesting to determine whether or not Eomes expression marks discrete progenitors that generate HE of the YS and AGM as well as the elusive hemangioblast? More broadly, what are the potencies of Eomes+ progenitors that generate hematopoietic, vascular, cardiac and definitive endoderm lineages? Finally, how variable are the transcriptomes of these emerging Eomes+ progenitor populations? Answers to these questions will further refine our understanding of the lineage hierarchy and relate this hierarchy to gene expression patterns. These findings will ultimately provide stem cell scientists with information about the progenitor populations they must first generate if they

hope to efficiently produce cell derivatives from the various Eomes-dependent lineages *in vitro*.

4.1.10 Eomes and the development of paraxial meosderm

Paraxial mesoderm gives rise to somites that produce striated muscle and cartilage. Day 4 Eomes loss-of-function EB cultures generate Flk-1^{-}/PdgfRa^{+} cells at the expense of generating Flk-1+ mesodermal populations. This Eomes-/- Flk-1^{-}/PdgfRa^{+} population has increased chromatin accessibility nearby genes related to somitogenesis and rhombomere development and expresses high levels of paraxial mesodermal markers such as Tcf15, Meox1 and Msgn1. Chimera experiments demonstrate that Eomes-/- ES cells can give rise to paraxial/somitic mesoderm *in vivo* (Costello et al., 2011). Additionally, our day 4 ChIP-seq experiments suggest that Eomes binds *cis*-regulatory regions nearby genes related to absent somite formation and failure of somite differentiation. Future experiments should evaluate whether ectopic Eomes induction, using our Eomes-NIA line, suppresses paraxial mesoderm development in low BMP signaling conditions that promote paraxial mesoderm development (Craft et al., 2013). If Eomes overexpression does suppress paraxial mesoderm development this suggests that Eomes aids the specification of hematopoietic and cardiac mesoderm during gastrulation via suppressing the acquisition of alternate mesodermal fates.

4.2 CONCLUDING REMARKS

Eomes is clearly very important for the development of a diverse set of mesodermal lineages that arise during mouse gastrulation from the epiblast. In chapter 3, I develop tools and an experimental strategy to resolve the number and diversity of Eomes expressing progenitors that arise during gastrulation. In chapter 2, I uncover novel roles for Eomes during the development of the hematopoietic lineages of the YS. These experiments demonstrate that Eomes sits at the top of a transcriptional hierarchy, functioning upstream of Runx1 expression and SCL functional activity, to promote hemogenic competence of the entire YS mesodermal lineage. These results ultimately suggest that hemogenic competence is endowed earlier during murine embryogenesis than previously appreciated and have widespread implications for the generation of HE from pluripotent stem cell sources.

CHAPTER 5 : MATERIALS AND METHODS

5.1 METHODS

5.1.1 Mouse strains and genotyping

All animal procedures were performed in accordance with Home Office (UK) regulations and approved by the Oxford Local Animal Welfare and Ethical Committee. The $Eomes^{gfp}$, Rosa26R, $Eomes^{CA/N}$;Sox2Cre and Flk-1.LacZ strains were genotyped as previously described (Arnold et al., 2008; Arnold et al., 2009; Shalaby et al., 1995; Soriano, 1999).

The $Eomes^{iCre}$, $Eomes^{CreERT2,}$ $Eomes^{CreERT2\text{-}LacZ}$ and $Eomes^{iCre\text{-}LacZ}$ alleles were generated using the same strategy as previously described (Costello et al., 2011). Briefly, the targeting vector encompassed an 8.25-kb HpaI fragment of the Eomes locus. The iCre, CreERT2, CreERT2-IRES-Lacz and iCre-IRES-LacZ coding sequences, each followed by a polyA cassette and a loxP-flanked neomycin-resistance cassette, were introduced into exon 1 between the SphI (translational start) and EagI sites, resulting in removal of ~500bp of the endogenous 5′ coding region of Exon 1. The 3' homology region of the targeting construct was flanked with a pMCI.TK negative selection cassette. Linearized vector was electroporated into CCE ESCs and drug-resistant colonies screened by Southern blot using a 5' external probe (Arnold et al., 2009) on EcoRV-digested DNA (wild-type (WT) allele; 15.2 kb; targeted allele; 10.0 kb). Correctly targeted clones were transfected with pMC1.Cre, sub-clones were subsequently screened to identify those lacking the selection cassette (6kb) using a 3' internal probe(Arnold et al., 2009). Two independent excised ESC clones were used to generate germline chimeras. Offspring were genotyped by PCR using iCre (FP: AAGGAAAGGGGCACCTACAATC, RP: TTTCCTGTTGTTCAGCTTGC (440 bp)) or

CreERT2 (FP: AAGGAAAGGGGCACCTACAATC, RP: TGCGAACCTCATCACTCGTTG (305 bp)) specific primer sets. All strains were maintained on a 129SvEv/C57Bl/6 mixed genetic background.

5.1.2 Immunostaining

E6.5/E7.5 embryos were fixed in 4% PFA at room temperature (RT) for 30 min or overnight in 1% PFA at 4ºC. Day 4 EBs were fixed in 1% PFA overnight at 4ºC. Samples were washed with 0.1% Triton-X, permeabilized with 0.5% Triton-X in PBS for 15 min, washed with 0.1% Triton-X, blocked in 5% donkey serum, 0.2% BSA and 0.1% Triton-X in PBS (embryos for 1 hr and EBs for 2 hrs), incubated with primary antibodies (embryos overnight at 4 ºC and EBs 2hrs at RT) in block solution, washed with 0.1% Triton-X, incubated with fluorophore conjugated secondary antibodies for 2 hrs at RT, washed with 0.1% Triton-X and counterstained with DAPI. Fluorescent images were captured with an Olympus FV1000. Antibodies used are listed in **Table 1, 5.2 Materials section**.

5.1.3 Whole-mount in situ hybridization and LacZ staining

E6.5-E10.5 embryos were fixed overnight in 4% PFA at 4ºC, and subject to whole-mount in situ hybridization (WISH) using standard protocols (Behringer et al., 2014) with probes against ER71(DiTacchio et al., 2012) and Eomes (Arnold et al., 2008). LacZ staining was performed according to standard protocols (Behringer et al., 2014). For histology, embryos were post-fixed in 4% PFA, dehydrated in ethanol, embedded in paraffin wax, sectioned (8.0 um) and counterstained with Nuclear FastRed. Subsequent to LacZ staining, E10.5 $Eomes^{iCre\text{-}LacZ}$ embryos were post-fixed for 2 hours in 2% PFA at room temperature,

transferred to a 16% sucrose overnight and embedded in OCT and frozen at -80ºF for cryosections.

5.1.4 ESC maintenance and differentiation

WT (CCE), Runx1-Venus (E14), SCL-mCherry (J1)(Chagraoui et al., 2018), Eomes-/- (CCE, Runx1-Venus, SCL-mCherry), SCL-null (J1)(Shivdasani et al., 1995), Runx1-null (J1)(Wang et al., 1996), Eomes-NIA(Nishiyama et al., 2009) and iRunx1 (E14)(Lancrin et al., 2009) ESC lines were maintained in feeder free culture conditions in serum + LIF as previously described (Costello et al., 2011). 48-72 hrs prior to induction of hematopoietic differentiation cells were washed with PBS and cultured in serum free ES media containing 50% Neurobasal Media (Gibco, Cat # 21103049), 50% DMEM/F12 (Gibco, Cat # 11320033), supplemented with 0.5X of both N2 (Gibco, Cat#17502048) and B27 (Gibco, Cat# 17504044), 1% Pen/Strep, 1% glutamine, 0.05% BSA (Gibco, Cat# 15260037), 1 uM PD0325091, 3 uM CHIR99021 and 1000 U/ml LIF. At D0 cells were dissociated using Trypsin-LE (Gibco) and seeded at a density of 1×10^5 ml in serum-free differentiation (SF-D) media (Nostro et al., 2008) and cultured on an orbital shaker at 70 rpm for ~18 hrs in the absence of growth factors to form EBs. At D2, EBs were split 1:3 in SF-D media containing recombinant human (rh) VEGF (5 ng ml^{-1}; R&D Systems), rhBMP4 (10 ng ml^{-1}; R&D Systems) and Activin A (5 ng ml^{-1}; R&D Systems) for 48 hr. At D4, EBs were split 1:2 in SF-D media containing rhVEGF (5 ng ml^{-1}; R&D Systems), rhBMP4 (10 ng ml^{-1}; R&D Systems) and Activin A (5 ng ml^{-1}; R&D Systems) for 24 hr. For bulk cultures, EBs were washed in IMDM (Gibco, Cat# 12440053) at D5 and D6 and cultured in SF-D media containing rhVEGF (5 ng ml^{-1}; R&D Systems) and SCF (50 ng ml^{-1}; BioLegend). From D2 onwards EBs were grown in petri dishes coated with 5% (v/v) Poly-heme solution (Sigma, Cat# P3932-10G). For EHT cultures D5 EBs were dissociated with Trypsin-LE, stained with an anti-Flk-1 (APC)

antibody (Supplementary Table 3) for 30 min on ice and Flk-1^{+} cells isolated by MACS using anti-APC microbeads (Miltenyi, Cat# 130-090-855) were plated on Matrigel (Corning, Cat# 354230) coated 96 or 12 well plates at a concentration of 5×10^{4} cells/200 µl in SF-D containing rhVEGF (5 ng ml^{-1}; R&D Systems), rhbFGF (10 ng ml^{-1}; R&D Systems) and SCF (50 ng ml^{-1};BioLegend) to form hemogenic endothelium for 72 hours. Media was changed on D6 and D7.

For Runx induction in iRunx1 EHT cultures 1 ug/mL of doxycycline, dissolved in water, was added to the culture media from either day 7-9 to or day 6-8. For Eomes-NIA cultures 0.4 ug/mL of doxycycline and 1 ug/mL of puromycin were added to culture media at all times to suppress Eomes induction. To induce Eomes in Eomes-NIA cultures EBs were washed 3 X in IMDM and subsequently cultured in media that contained 1 ug/mL of puromycin but lacked doxycycline, from either day 2-4, 4-5 or 2-5.

5.1.5 CRISPR modification of ESCs

Custom synthetic crRNA and ssODNs (Integrated DNA Technologies, USA) were resuspended in IDT duplex buffer. Sequences are provided in **Table 2, 5.2 Materials section**. All crRNA sequences were designed using the CC-Top CRISPR design tool (Stemmer et al., 2015) Cas9 ribonucleoprotein (RNP) complexes were assembled immediately prior to electroporation following the manufacturer's protocol (Alt-R CRISPR-Cas9 System:Delivery of ribonucleoprotein complexes into Jurkat T cells using the Neon® Transfection System). Briefly, 4.4 uL of 100 uM tracrRNA, 4.4 uL of 100 uM crRNA and 1.2 uL of IDT Duplex Buffer were mixed, heated at 95^{o}C for 5 min and then cooled to RT using a PCR block. The RNP complex was formed by diluting Cas9 Hifi in Buffer R to 36 uM and

mixing it 1:1 with the crRNA:tracrRNA duplex. ESC were electroporated using the Neon transfection system (Voltage = 1600V, pulse width = 10 ms, number of pulses = 3) with the appropriate ssODN (50 pmol) and RNP. If two crRNAs were used then RNPs were produced separately and mixed 1:1 prior to electroporation.

For generation of Eomes null Runx1-Venus and SCL-Cherry reporter ESCs two custom crRNAs were designed to target DNA within intron 1 and intron 5 of Eomes **(Table 2, 5.2 Materials section)** in order to delete a 2.6 kb region spanning exons 2-5 of Eomes, and recapitulate the previously described Eomes loss of function allele (Arnold et al., 2008). A ssODN was designed that contained a 5' homology arm upstream of the intron 1 DNA DS break site, followed by insertion of a new EcoRV restriction site and a 3' homology arm located downstream of the intron 5 DNA break site **(Table 2, 5.2 Materials section)**. RNPs were generated as described above using the two crRNAs. 10 uL of $2x10^4$ ESCs in Buffer R were electroporated with 1 uL of a 1:1 mix of the RNPs and 2 uL of the ssODN. Low density plating was performed after 72 hrs, and after 7-10 days clones were picked and screened using a three primer PCR strategy that simultaneously amplified the WT allele and the null allele (FP: TCTCCTCTCTAGTCACCTTCAC, RP1: CCCAATATCCACTCCTCACTTC, RP2: TCTACAGAGAGAGTTCCAGGAC (WT: 401 bp, MT: 535 bp)). Genotypes of clones were verified using Southern blotting with a 3' external probe located in exon 6 of Eomes (Arnold et al., 2009) on EcoRV digested genomic DNA.

For generation of $Eomes^{-/-}$ iRunx1 and $Eomes^{-/-}$ Eomes-NIA ESCs the same two custom crRNAs, designed to target DNA within intron 1 and intron 5 of Eomes **(Table 2, 5.2 Materials section)** in order to delete a 2.6 kb region spanning exons 2-5 of Eomes, and recapitulate the previously described Eomes loss of function allele (Arnold et al., 2008) were

used as above. Two ssODNs were designed that contained a 5' homology arm upstream of the intron 1 DNA DS break site, followed by insertion of a either a new Sph1 or Spe1 restriction site followed by a 3' homology arm located downstream of the intron 5 DNA break site **(Table 2, 5.2 Materials section)**. RNPs were generated as described above using the two crRNAs. 10 uL of $2x10^4$ ESCs in Buffer R were electroporated with 1 uL of a 1:1 mix of the RNPs and a 1:1 mix of 2 uL of both ssODNs. Low density plating was performed after 72 hrs, and after 7-10 days clones were picked and screened using the same three primer PCR strategy described above, followed by restriction enzyme digests.

For deletion of the -181kb Eomes bound Runx1 enhancer, the same CRISPR strategy described above was used with different gRNAs and ssODNs **(Table 2, 5.2 Materials section)**. A two primer PCR strategy was used to amplify the deletion allele followed by a restriction digest of the deletion product (FP: CCTCCCTCCCTGAACAATTATG, RP: CCTGTGACCCTGTAAGTGTTTAG (WT: 1580bp & Δ181: 896 bp)).

For generation of the $Eomes^{V5/V5}$ ESC lines a custom crRNA was designed to target the UAG translational stop site in exon 6 of Eomes and a ssODN was designed to insert a triple glycine V5 epitope tag (3XGly-V5) directly upstream of the UAG translational stop site of Eomes **(Table 2, 5.2 Materials section)**. An RNP was generated as described above. $2x10^4$ CCE ESCs in 10 uL of Buffer R were electroporated with 1 uL RNP and 2 uL of the ssODN as described above. Low density plating was performed after 72 hrs and clones picked after 7-10 days were screened via PCR. Homozygous insertion of the 3XGly-V5 tag at the C-terminus of the Eomes locus was assessed by PCR across the C-terminus (FP: GCAAGAGAAAGCGCCTGTC, RP: AGGATACATCAAAGGTGGAAGG (WT: 250 bp & MT: 301 bp)). In frame insertion with the correct 3XGly-V5 sequence was confirmed in

homozygously targeted clones via Sanger sequencing of a 971 bp PCR product (FP: CCTGTGACCAACAAGCTAGAC, RP: TTTAACCCTCTGGGCTGCTG) that spanned the C-terminus of Eomes. Western blotting and immunofluorescence staining were performed on day 4 EBs to confirm successful V5 tagging of the endogenous Eomes protein.

5.1.6 Hematopoietic progenitor colony assays.

EBs/EHT monolayers were dissociated at D5, D6 or D8 and single cells were plated in duplicate in Methylcellulose-Based Medium (MethoCult GF M3434; Stem Cell Technologies). Primitive erythroid colonies were scored 5 days after plating and definitive erythroid, granulocyte/macrophage and mixed colonies were counted 7-8 days after plating.

5.1.7 Flow cytometry, cell sorting and MACS.

EBs were dissociated using Trypsin-LE. For EHT cultures, floating and adherent cells were pooled, washed 3x with FACS buffer (PBS + 2% FCS), stained with antibodies for 30 min at 4ºC, washed and resuspended in FACS buffer containing DAPI (1:5000, BD Pharmigen) and analysed on either a BD Fortessa X20 or a Cytek DxP8. Cell sorting for RNA-seq and ATAC-seq was completed on a MoFlo Astrios. For MACS, dissociated cells were stained at a concentration of 10^7 cells/150 uL FACS buffer containing 3.75 uL of anti-Flk-1(APC) antibody for 30 min on ice, washed with PBE (PBS + 2mM EDTA + 0.5% BSA) and incubated in 80 uL of PBE + 20 uL of anti-APC microbeads (Miltenyi, Cat# 130-090-855) for 30 min on ice, washed with PBE and then passed over a LS magnetic column twice, as per the manufacturer's instructions (Miltenyi Biotec).

For intracellular flow cytometry day 3-5 $Eo^{V5/V5}$ EBs were dissociated using Trypsin-LE and stained with a dye for viability (Invitrogen, Cat# 65-0863-14) and the cell surface markers Flk-1 and PdgfRa prior to fixation, subsequently cells were permeabilized and V5 staining was performed using the FoxP3 Staining Buffer Set (Invitrogen, Cat# 00-5523) as per the manufacturer's instructions. For a list of antibodies used for flow cytometry see **Table 2, 5.2 Materials section**.

5.1.8 RNA isolation and quantitative RT-PCR

EBs were washed 2x in PBS and snap frozen in liquid nitrogen. Total RNA was isolated using the RNeasy Mini Kit (QIAGEN, Cat#74104) according to the manufacturer's instructions using on-column DNase treatment. Complementary DNA was generated using the SuperScriptIII kit (Invitrogen) with oligo-dT primers. RT–qPCR was performed using the Quantitect SYBRGreen PCR kit and a Rotor-gene Q (Qiagen) and analysed using the delta-delta Ct method, as described previously (Costello et al., 2011). Primer sequences are provided in **Table 3, 5.2 Materials section**.

5.1.9 RNA-seq

RNA was isolated from Flk-1^{hi}/PdgfRa^{-} and Flk-1^{-}/PdgfRa^{+} single cell suspensions ($1.5x10^5$ cells) from three independent hematopoietic differentiations of WT (CCE) and Eomes-/- (clone 6A6, CCE) cells using the RNeasy Micro Kit (QIAGEN, Cat#74004). RNA was additionally isolated from Flk-1^{+}/PdgfRa^{+} day 4 WT (CCE) EBs and day 0 WT (CCE) ES cells. Total RNA was normalized to 800ng per sample, depleted of cytoplasmic and mitochondrial ribosomal RNA sequences (Ribo-Zero Gold rRNA Removal Kit (H/M/R), Cat:

#MRZG12324) and library preparation was performed using the Illumina TruSeq Stranded Total RNA Library Prep (H/M/R) (Cat: #20020597), followed by sequencing (75-cycle paired end) on the Illumina HiSeq4000 platform.

5.1.10 RNA-seq analysis

Paired-end reads were aligned against the mm10 genome using the STAR RNA-seq aligner with default parameters outputting bam files using --outSAMtype BAM SortedByCoordinate (Dobin et al., 2013). BAM file primary alignments with a mapping quality of > 254 were treated as RNA-seq data and imported into Seqmonk 1.45.4.

(https://www.bioinformatics.babraham.ac.uk/projects/download.html#seqmonk). The RNA-seq quantitation pipeline ($p<0.05$ and multiple testing correction applied) in SeqMonk utilizing DESeq2 (Love et al., 2014) was performed to identify significantly differentially expressed genes ($p<0.05$, fold change > 1.5 and FPKM >1). PCA plots and hierarchical clustering was performed in SeqMonk.

5.1.11 scRNA-seq

Day 4/5 WT and Eomes-/- EBs were stained with Flk-1 and PdgfRa FACS antibodies **(Table 1, 5.2 Materials section)** and 10,000 Flk-1^{hi}/PdgfRa^{-} cells were sorted using a BD FACSAria III into 20 µL PBS/0.05% BSA (non-acetylated) and the volume topped up to 38 µL for loading onto the 10X Chromium Controller. Processing of samples was performed according to the 10x protocol using the Chromium Single Cell 3' library & Gel Bead Kit v3 (10x Genomics). Barcoded cell cDNAs were pooled and converted to sequence ready

libraries. Multiplexed libraries were then sequenced on Illumina Nextseq using a high output 150bp Nextseq V2.5 kit.

5.1.12 scRNA-seq analysis

Sequencing data was demultiplexed in the binary base call (BCL) format, FASTQ files were aligned to the mm10 genome using 10X Genomics Cell Ranger software (version 2.0.0) and unique molecular identifier (UMI) counts were determined. The Seurat v3 software package (Butler et al., 2018; Stuart et al., 2019) was used in R Studio to perform scRNA-seq analysis. Pre-processing was performed and cells with > 2000 RNA features and < 8 % mitochondrial RNA were used for downstream analysis. Each sample was randomly down sampled to include 3805 cells and WT and Eomes-/- samples from days 4 and 5 were merged together, normalized and 2000 variable features were identified using the VST method. Integration anchors for WT and Eomes-/- Seurat objects were identified and integration was performed using the first 20 principal component (PC) dimensions. Clusters were identified and UMAPs generated using the first 16 PC and a resolution of 0.8. Cell type identities were assigned by comparing the conserved markers from each of the 13 clusters to cell type markers previously published for cell types identified in E6.5 to E8.5 mouse embryos (Pijuan-Sala et al., 2019) **(Table 4, 5.3 Gene Lists section)**. Differentially expressed genes in the 13 Seurat clusters are listed in **Table 5, 5.3 Gene Lists section**.

Cell types annotation for the *in vitro* scRNA-seq data was performed by mapping against the mouse gastrulation atlas (Pijuan-Sala et al., 2019). Raw counts from both experiments were merged and normalised using the scater package (McCarthy et al., 2017). Then, highly variable genes were extracted from the joint data using scran's decomposeVar function(Lun

et al., 2016). Genes with an FDR lower than 0.05 were considered as highly variable and used to compute the top fifty principal components along the joint dataset. Batch correction was performed on the gastrulation atlas principal components using the fastMNN's algorithm following the exact procedure from the original publication (Pijuan-Sala et al., 2019). Integrated datasets were also corrected using fastMNN. *In vitro* cells were annotated by looking at the top 35 nearest neighbours from the atlas and selecting the most frequent cell type. A mapping score was assigned to reflect the mapped cell type frequency, where a higher score indicates a more consistent annotation. *In vitro* cells were additionally mapped back onto the force directed graph of hematoendothelial cells from the original publication (Pijuan-Sala et al., 2019) by identifying the single nearest neighbour in this manifold.

5.1.13 ATAC-seq

Tagmentation and indexing of single cell suspensions ($6x10^4$ cells) from three independent differentiations of WT (CCE) and Eomes-/- (clone 6A6, CCE) day 4 Flk-1^{hi}/PdgfRa^- and Flk-1^-/PdgfRa^+ cells was performed as previously described (Buenrostro et al., 2013), using cells from equivalent samples to those used for the RNA-seq experiments described above. To control for sequence bias of the Tn5 transposase, 100ng genomic DNA of WT (CCE) ESCs was also tagmented and indexed. Libraries were purified with two rounds of Agencourt AMPure XP bead cleanup (Agencourt, 1.5× bead:sample ratio). Library size and concentration were determined using the 2100 Bioanalyzer High Sensitivity DNA Kit (Agilent). Samples were sequenced using a 75-cycle paired end Nextera kit with custom Nextera index primers taken from Table S1 in Buenrostro et al. 2013 (Buenrostro et al., 2013) on the Illumina HiSeq4000 platform.

5.1.14 ATAC-seq analysis

Paired-end reads were aligned to the mouse genome assembly mm10 using Bowtie2 (Langmead and Salzberg, 2012) with the very-sensitive option, sorted and mitochondrial reads discarded using Samtools (Li et al., 2009) and duplicates removed using Picard (https://broadinstitute.github.io/picard/). Bigwig files were generated using deepTools2(Ramirez et al., 2016). Biological replicates were randomly downsampled to contain the same number of reads for each individual sample and peaks in each sample called using MACS2 (Zhang et al., 2008) using the Tn5 control as a control. MACS2 called peaks with a p-value < 10^{-3} were used in downstream analyses. Significant changes in ATAC-seq datasets were identified using the DiffBind package (http://bioconductor.org/packages/release/bioc/html/DiffBind.html) using bam files and an integrative bed file of all identified peaks in each sample with the following filters: FDR < 0.05, fold change > 1.5. GREAT 4.0.4 analysis (McLean et al., 2010) was performed using default basal plus extension parameters with whole genome as a background to identify peak-gene associations. Enrichment of TF motifs in differentially accessible ATAC-seq peaks was performed using the Analysis of Motif Enrichment (AME) feature in the MEME suite (McLeay and Bailey, 2010) with a background control of all ATAC-seq peaks.

Bigwig files were downloaded from GSE47085 and genomic coordinates were converted from mm9 to mm10 using Crossmap 0.2.9 (Zhao et al., 2014). An SCL peak file was downloaded from Supplementary Table S1A from Van Handel et al. 2015 (Org et al., 2015) and genomic coordinates were converted from mm9 to mm10 using UCSC LiftOver. Bedtools was used to intersect peak files and identify overlapping genomic regions(Quinlan and Hall, 2010). GREAT 4.0.4 analysis (McLean et al., 2010) was performed using default basal plus extension parameters with whole genome as a background to identify peak-gene

association. Identified genes were annotated in Seqmonk 1.45.4 for comparison of ATAC-seq and gene expression changes from RNA-seq. Changes in ATAC-seq signal were assessed using heatmaps generated in deepTools2 (Ramirez et al., 2016), and genomic snapshots visualized in IGV (Robinson et al., 2011) generated from bigwig files creates using deepTools2 (Ramirez et al., 2016).

5.1.15 ChIP-seq

Day 4 $Eomes^{V5/V5}$ (CCE) and WT (CCE) D4 EBs were dissociated using Trypsin-LE (Gibco) and ~3-4x10^7 cells were cross-linked for 10 min at RT with 1% (v/v) formaldehyde, followed by quenching with 125mM glycine. Nuclei were recovered and lysed to obtain chromatin, which was then sonicated to 200–500 bp, pre-cleared with protein G Dynabeads (Thermofisher Scientific) and ~175 ug of chromatin was immunoprecipitated with 10µg of anti-V5 (Abcam cat# ab9116, lot# GR: 322448-4) bound to protein G Dynabeads overnight on a rotator at 4ºC. Dynabeads were washed and immune complexes were eluted in IP elution buffer (1% SDS, 0.1M NaHCO3), reverse crosslinked overnight at 65ºC, RNaseA treated for 1.5hrs at 42ºC, proteinase K treated for 2hrs at 45ºC and DNA was recovered using a Zymo column kit. DNA was multiplexed and paired end sequencing was performed on a single lane of an Illumina HiSeq4000 platform.

5.1.16 ChIP-seq analysis

Paired-end reads were aligned to the mouse genome assembly mm10 using Bowtie2 (Langmead and Salzberg, 2012) with default parameters. PCR duplicates were removed using Samtools 1.9 (Li et al., 2009). Peaks were called against input DNA using MACS 2.1.2

(Zhang et al., 2008) and were considered significant if they had a fold enrichment > 2 and FDR < 0.05. Bedtools 2.27.1(Quinlan and Hall, 2010) was used to intersect the peak files from both Eomes$^{V5/V5}$ clones amd subtract peaks called in the WT control and genomic intervals located in mm10 blacklist regions (https://www.encodeproject.org/files/ENCFF547MET/@@download/ENCFF547MET.bed.gz), generating a peak file containing 338 genomic intervals used for downstream analyses. The Homer software package (Heinz et al., 2010) was used to perform motif enrichment analysis. GREAT 4.0.4 analysis (McLean et al., 2010) was performed using default basal plus extension parameters with the whole genome used as a control to identify peak-gene associations. Heatmaps and bigwig files were generated using Deeptools 3.1.3 (Ramirez et al., 2016). Bigwig files and peak files were downloaded from GSE69101 (Goode et al., 2016) and GSE128466 (Tosic et al., 2019). Data from GSE110164 (Wang et al., 2017) were downloaded and used to generate peak files and bigwig files as previously described(Senft et al., 2018).

5.2 MATERIALS

5.2.1 Antibodies

Table 1. List of antibodies

Reagent or Resource	Source	Identifier	Dilution	Application
Rabbit polyclonal anti-mouse Eomes	Abcam	Cat #ab23345	1 in 100	Immunofluorescence
Rabbit monoclonal anti-mouse Runx1	Abcam	Cat# ab92336	1 in 100	
Rabbit monoclonal anti-mouse VEGFR2 (Flk1)	Cell Signalling Technology	Cat# 2479	1 in 500	
Chicken polyclonal anti-GFP	Abcam	Cat# ab13970	1 in 1000	
Goat polyclonal anti-mouse T	SantaCruz Biotechnology	Cat# sc-17743	1 in 100	
Mouse monoclonal anti-V5 Tag	Thermo Fisher Scientific	Cat# R960-25	1 in 200	
Donkey anti-rabbit IgG AlexaFluor 488 (#670)	Life Technologies	Cat# A-21206	1 in 200	
Goat anti-Chicken AlexaFluor 488 (#722)	Life Technologies	Cat# A-11039	1 in 200	
Donkey anti-Rabbit IgG AlexaFluor 594 (#714)	Life Technologies	Cat# A-21207	1 in 200	
Donkey Anti-Mouse IgG AlexaFluor 488	Life Technologies	Cat# A-21202	1 in 400	
Donkey anti-goat IgG AlexaFluor 594 (#671)	Life Technologies	Cat# A-11058	1 in 200	
DAPI	BIOTIUM	Cat# 40043	1 in 5000	
Rat monoclonal anti-mouse Flk-1 APC	Thermo Fisher Scientific	Cat# 17-5821-81	1 in 40	Flow Cytometry
Rat monoclonal anti-mouse PdgfRa PECy7	Thermo Fisher Scientific	Cat# 25-1401-82	1 in 160	
Rat monoclonal anti-mouse CD144 APC	Thermo Fisher Scientific	Cat# 17-1441-82	1 in 160	
Rat monoclonal anti-mouse CD144 PeCy7	Thermo Fisher Scientific	Cat# 25-1441-82	1 in 160	
Rat monoclonal anti-mouse CD117 BV605	BioLegend	Cat# 105847	1 in 160	
Rat monoclonal anti-mouse CD117 APC	Thermo Fisher Scientific	Cat# 17-1172-82	1 in 160	
Rat monoclonal anti-mouse CD41a PECy7	Thermo Fisher Scientific	Cat# 24-0411-82	1 in 200	
Rat monoclonal anti-mouse CD45 PECy7	Thermo Fisher Scientific	Cat# 25-0451-82	1 in 160	
Rat monoclonal anti-mouse CD31 APC	BioLegend	Cat# 102510	1 in 80	
DAPI	BD Biosciences	Cat# 564907	1 in 5000	
V5-tag antibody - ChIP Grade	Abcam	Cat# ab9116		ChIP
Rabbit polyclonal anti-mouse Eomes	Abcam	Cat# ab23345	1 in 2000	Western Blot
Mouse monoclonal anti-V5 Tag	Thermo Fisher Scientific	Cat# R960-25	1 in 1000	
Sheep anti-mouse HRP Conjugated (#160)	GE Healthcare	Cat # NA931V	1 in 2000	
Donkey anti-rabbit HRP Conjugated (#159)	GE Healthcare	Cat# NA934V	1 in 2000	
Anti-APC Microbeads	Miltenyi Biotec	Cat# 130090855	1 in 5	MACS

Table 2. Sequence for CRISPR Reagents

Figure ID	Company	Product #	Sequence	Application
gRNA #1	Integrated DNA Technologies	Alt-R® CRISPR-Cas9 crRNA	GGTTTGCAGCAGGCGATTTGTGG	Re-generation of Eomes-null allele in Runx1-Venus and SCL-mCherry ESC lines
gRNA #2		Alt-R® CRISPR-Cas9 crRNA	AGAGGCATCCCGGCACCCTGAGG	
ssODN #1		Ultramer® DNA Oligo	C*C*CTCTTAACCTCCCTCCCCATGCCCTAAATAAACTCTATTCTATACTATTCCATCTTGTGGCTGGTCCCTCAGGGATATCGCCTGCTGCAAACCCAGGAGCCAGCGGGTCACGTAGATCTGCCCTCAAGGGTTCATTCCCAAATTTCCATC*T*C	
ssODN #2			C*C*CTCTTAACCTCCCTCCCCATGCCCTAAATAAACTCTATTCTATACTATTCCATCTTGTGGCTGGTCCCTCAGGGCATGCGCCTGCTGCAAACCCAGGAGCCAGCGGGTCACGTAGATCTGCCCTCAAGGGTTCATTCCCAAATTTCCATC*T*C	Re-generation of Eomes-null allele in Eomes-NIA and iRunx1 ESC lines
ssODN #3			C*C*CTCTTAACCTCCCTCCCCATGCCCTAAATAAACTCTATTCTATACTATTCCATCTTGTGGCTGGTCCCTCAGGACTAGTGCCTGCTGCAAACCCAGGAGCCAGCGGGTCACGTAGATCTGCCCTCAAGGGTTCATTCCCAAATTTCCATC*T*C	
gRNA #3		Alt-R® CRISPR-Cas9 crRNA	AAGGTTAAAATAATGCTCTAGGG	Generation of Eomes-V5 ESC Line
ssODN #4		Ultramer® DNA Oligo	G*T*AACCTAGGCAAAGAACACAACAAAACACCACCAGGTCCATCTGGAAAGGTTAAAGGTTAAAATAATGCTCTACGTAGAATCGAGACCGAGGAGAGGGTTAGGGATAGGCTTACCTCCTCCCTCCGGGACTTGTGTAAAAAGCATAATAAGCCCCCATGCCTTTGGAGGTGTCTTTACTGTACTCTTCAGTGTTAAT*G*T	
gRNA# 4		Alt-R® CRISPR-Cas9 crRNA	GCGAGCGACTGACTGGCATGAGG	
gRNA#5		Alt-R® CRISPR-Cas9 crRNA	TGTCGCTTACTGTTTGCCTAAGG	
ssODN #5		Ultramer® DNA Oligo	C*C*CTCTGGGCTCCTGCAAGCCTCACCTTCGCTGAGCGAGCGACTGACTGGGCATGCCCTAAGGAAGTTGGGTGCGATCTCATATGGGATTTCATGGTATCTAAA*A*A	Generation of the Runx1 (-181kb) enhancer deletion
ssODN #6		Ultramer® DNA Oligo	C*C*CTCTGGGCTCCTGCAAGCCTCACCTTCGCTGAGCGAGCGACTGACTGGACTAGTCCTAAGGAAGTTGGGTGCGATCTCATATGGGATTTCATGGTATCTAAA*A*A	
*Phosphorothioated DNA bases				

Table 3. List of qRT-PCR primers

Gene	Forward Primer (5' -> 3')	Reverse Primer #1 (5' -> 3')	Amplicon
SCL	ATAGCCTTAGCCAGCCGCTC	CGCCGCACTACTTTGGTGTG	154
Runx1	CAGCCTCTCTGCAGAACTTT	ACGGCAGAGTAGGGAACT	89
PU.1	AGCGATGGAGAAAGCCATAG	CAGCTCTGTGAAGTGGTTCT	102
Gata1	CAACAGTATGGAGGGAATTCCT	GTGTCCAAGAACGTGTTGTTGC	162
Hbb-bh1	GAAACCCCCGGATTAGAGCC	GAGCAAAGGTCTCCTTGAGGT	93
Cdh5	AGGACAGCAACTTCACCCTCA	AACTGCCCATACTTGACCGTG	70
Flk-1	CACCTGGCACTCTCCACCTTC	GATTTCATCCCACTACCGAAAG	240
Flt-1	TGGCTCTACGACCTTAGACTG	CAGGTTTGACTTGTCTGAGGTT	247
Fli1	ATGGACGGGACTATTAAGGAGG	GAAGCAGTCATATCTGCCTTGG	110

5.3 GENE LISTS

5.3.1 scRNA-seq

Table 5. Conserved markers in the Seurat clusters

Conserved Marker List (Positive Only)														
Cell Identity	Primitive Streak	Mesoderm 1	HE 1	Mesoderm 2	HE 2	HE 3	Blood 1	Blood 2	Endo 1	Endo 2	HE 4	Allantois 1	Allantois 2
Figure Cluster	1	2	3	4	5	6	7	8	9	10	11	12	13
Original ID	12	2	6	7	1	4	8	5	0	3	9	11	10
	Pou5f1	Mkrl	Lmo2	Mkrl	Lmo2	Fgf3	Ube2c	Gstal	Cldn2a	Cldn2a	Carp2	Cdkn1c	Hand1
	Fst	Krt8	Ifitm3	Tdgf1	Ube2c	Hand1	Gcsh	Rnd2	Vim	Vim	Etv2	Cavin2	Spin2c
	Tdgf1	Tdgf1	Akap12	Cenpf	Nrp2	Zfpm1	Prc1	Gcsh	Tmsb4x	Igfbp4	Tal1	Twist1	Phlda2
	T	Hand1	Upp1	Tgfb2	Exoc3l	Hist1h1b	Cenpf	Fth1	Tmsb4x	Ramp2	Map7d	Cdk2	Pmp22
	Eomes	Amot		Gpc3	Cenpf	Chtop	Rnd2	Prkar2b	Ramp2	Apoa	Mrvi1	Dlx1	Cdkn1c
	Fgf8	Gpc3		Amot	Prc1		Top2a	Hist1h1b	Gja4	Cdh5	Dok4	Ptbp1	Cavin2
	Mt1	Ifitm1		Ube2c	Ar6gv1		Zfpm1	Fth1	Sparc	Meis1	Hspa5	Spin2c	Ptbp1
	Psme2	Tgfb2		Mespz1	Cdk1		Fth1	Zfpm1	Meis1	Exoc7	Egfl7	Vcan	Cdx2
	Krt8	Mespz1		Ifitm1	Cenpa		Prkar2b	F2r	Col4a1	Gja4	Serpinh1	Tgfb2	Slc38a4
	Epcam	Wls		Ar6gv1	Etv2		Mdka1	Smtl	Egfl7	Cfl2	Hspb9b1	Sox4	Tgfb2
	Ifitm3	Dcsh		Wls	Gadd45g		Jpt1	Col18a1	Cdh5	Sparc	Krt	Map7d	Twist1
	Ldhb	T		Top2a	Top2a		Stuap1	Fgf3	Cnp2	tmr2a	Ifitm1	Slc38a4	Foxf1
	Meis1	Ckb		Hand1	Ptk1		Tacc1	Orc6l	Ctsl	Col4a1	Gpc3	Swap70	Mkx1
	Cyt25a	Prlg		Cdh1	Tpx2		Tubb4b	Apoa	tmr2a	Gstal4	Cald1	Phldb1	Ccnd2
	Krt18	Ldhb		Tcea8	Ccnb1		Ccnb1		Igfbp4	Cnp2	Tal1	Hspa5	Bambi
	Ckb	Actg1		Meg3	Bmp2		Hmmr		Hist1h1b	Igf1	Sox2	Igf2r	Sfrp1
	Ltbl1	Tpm1		Gata6	Akap12		Aurka		Tmsb10	Col18a1	Slc16a3	Spc24	Mkx2
	Aldh2			Actg1	Smc4		Ptk1		Col18a1	Tmsb10	Rhma1	Grb10	Crabp1
	Chchd10			Gja1	Cks2		Cks2		Col4a2	Etv1	Sox18	Hspb9b1	Mpv17
	Cdkn1a			Yap1	Kif20b		H2afz		Rassf1	Selenop	Pdia3	Etv2	Wnt4
	S100a11			Cenpa	Kif11		Cdk1		Exoc3l4	Col4a2	Pdia6	Ptpc1	Peg10
	Sp5			Ptk1	Mki67		Aurkb		Esam	Tm4sf	Lmo2	Ptpc3	Ppp3
	Tagln			Ptrg	Egfl7		Dstand2		Pecam1	F2r	Marf	Peg10	Sall4
	Psme1			Tpm1	Tal1		Cdca8		Atp4a1Tw	Etv2	Dusp4	Aldh	Mll3
	Ezr			Kif11	Incenp		Cenpe		Ets1	Rab	Mdk	Kdr	Baap1
	Cldn7			Smc4	Mis18bp1		Nusap1		Tuba1a	Gng2	Fam107b	Pdia3	Tceal8
	S100a10			Nusap1	Spc25		Mki67		Gng2	Rasip1	Gcc2	Sept6	Hand2
	Spnr2a3			Sgo2a	Ccnp1		Phlda1		Pgk1	Pecam1	Nrp1	Bambi	Rpgrip2
	Tmem185a			Mki67	Aurka		Ftl1		Gng11	Tmem108		Vgll4	Rhou
	Spint2			Cdc42ep5	Hmmr		Incenp		Rasgrp3	Marc2		Pxnp1	Igf2r
	Nipm3			Incenp	Bub3		Ccnf		H19	Pgk1		Hoxa7	Tbx4
	Slmo2			Cdk1	Nusap1		Tpx2		Myrap	Hsph1		Ccnjl	Slc39A1
	Pxmd8			Rtkn1	Kif23		Aspm		Hoxb2	Ginq11		Capn6	Ptprj1
	Dpysl5a			Mis18bp1	Dbf4		F2r		Isam2	Cmas		Amot	Tbx2
	Tert1			Tpx2	Ier3l		Spc25a		Crisp1	Arpc3		Shp1	Fdps5
	Phlda2			Cks2			Cksap2l		Efs3	Abhd17a		Marf	Snai1
	Psmb10			T			Antitp1		Pdia6	Man		Mdk	Rbbp7
	Mag3			Spc25			Cenpa		Atp1f1	Pdia3		H2afy2	Slc2a3
	Krt19			Kif20b			Cdc20		Sox17	Esam		Hoxa9	Ehbp1
	Eno1			St3gal6			Racgap1		Cilc1	Fstl1		Crabp1	Hoxa7
	Akap12			Nrdeg			Kif11		Swap70	Cmtm8		Hoxc9	Amot
	Tgfb2			Prc1			Kif23		Ubxn2c	Atap1l1		Tceal9	Tbx3
	Pkm2			Aurka			Kif13		Efs2	Sox17		Tceal2	Hoxb8
	Acer2			S100a11			Smc4		Ndufa8	Cldn5		Dbn1	Bmp7
	Acad9						Cdc2		Cd81	Gm45718		Baap1	Isl1
	Mt2						Anln		Cdk1	Gabarap		Sox11	Ugdh
	Ap1m2						Vat1		Ftl1	Tek		Jag1	Ptpc1
	Irf1						Birc5		Tek	Tie1		H2afy2	Ptgds
	Myl12b						Ccnd2		Cpn1	Gapc43		Rbx	Capn6
	Wfdc2						Pimreg		Mxn	Prcp		Slc2a1	Pgk1
	Tspan13								N4bp3	Gm6g		Mag3	Arhgap29
	Dstn								Pkvap	Arpc5		Mmp2	Dok4
	Dnm3os								Arhgap29	Sesn2		Rbpms2	Bex3
	Rbp1								BC028528			Hoxd9	Tbx2
	Actg1								Zfp711			Cst	Krt19
	Cdkn1								Ppp1r12			Cd24a	Rps5ka5
	Evx1os								Selenbp1			Tyrobp	Pag3
	Car2								Arpc3			Nxn	Unc5c
	Tceal3								Cd34			Wnt5a	
	Gpc3											Isl1	
	Gstc											Akap12	
	Tagln2											Rasl11	
	Pag3											Dok4	
	Gja1											Hmgb1	
	Scly												
	Atp1b1												
	Tceal8												
	Mlnm1												
	Pgp2-1												
	Cdh1												
	Slk3												
	Cox7a2												
	Igfbp2												
	Dusp6												
	Tpd52												
	Rhoc												
	Ifitm1												
	Nub1												
	Pgp4-4												
	Bex1												
	Bex4												

Table 4. Differentially expressed genes in the Seurat clusters

List of Differentially Expressed Genes in Each Cluster (FC > 1.2 & Adj. p. value < 0.05)

Cell Identity	Primitive Streak		Mesoderm 1		HE 1		Mesoderm 2		HE 2		HE 3		Blood 1		Blood 2		Endo 1		Endo 2		HE 4		Allantois 1		Allantois 2	
Cluster	1		2		3		4		5		6		7		8		9		10		11		12		13	
Gene	Log2(Ex-/-/WT)		Gene	Log2(Ex-/-/WT)	Gene	Log2(Ex-/-/WT)	Gene	Log2(Ex-/-/WT)	Gene	Log2(Ex-/-/WT)	Gene	Log2(Ex-/-/WT)	Gene	Log2(Ex-/-/WT)	Gene	Log2(Ex-/-/WT)	Gene	Log2(Ex-/-/WT)	Gene	Log2(Ex-/-/WT)	Gene	Log2(Ex-/-/WT)	Gene	Log2(Ex-/-/WT)	Gene	Log2(Ex-/-/WT)
Pou5f1	-1.82		Phlda2	-1.65	Tgfb1	-1.07	Phlda2	-1.79	Phlda2	-1.11	Phlda2	-1.14	Rasl11a	-1.18	Rasl11a	-1.02	Rasl11a	-1.45	Tgfb1	-1.32	Ucma	-1.45	Tgfb1	-1.32	Ucma	-1.45	Tgfb1	-0.98
Fst	-1.19		Tpt1	-1.01	Tgfb1	-1.01	Mki67	-1.10	Tgfb1	-1.09	Rasl11a	-1.19	Fgf8	-0.96	Tpt1	-0.91	Pcdh9	-0.89	Hspa5	-0.95	Tpt1	-0.98	Pkgcb	-0.91	Tpt1	-1.09		
Tpt1	-1.07		Mki67	-1.05	Hspa5	-0.90	Tgfb1	-1.02	S100a10	-0.96	Tpm1	-0.96	Hspa5	-0.96	Sox4	-0.88	Hspa5	-0.87	Pdia6	-0.84	Tgfb2	-0.90	Krt18	-0.72	Krt18	-0.85		
Tdgf1	-0.90		S100a10	-0.82	Dkc1	-0.79	S100a10	-1.01	Pcdc1	-0.86	Dkc1	-0.83	Pcdc6	-0.82	Exoc	-0.82	Tpm1	-0.86	Exoc	-0.88	Tpm1	-0.78	Sugt1	-0.71	Apoe	-0.83		
Mespz1	-0.86		Krt18	-0.80	Ncl	-0.76	Mki67	-0.94	Hspa5	-0.77	Tgfb	-0.77	Tpt1	-0.89	Fth1	-0.79	Exoc	-0.80	Tpt1	-0.88	Pdia2	-0.78	Zc3h10	-0.68	Hand1	-0.82		
Mrvi1	-0.84		Mkx1	-0.85	Hspa1	-0.74	Exoc	-0.87	Ncl	-0.73	Hspa1	-0.77	Gstal	-0.85	Fgf3	-0.72	Gstal	-0.76	Krt	-0.81	Fth1	-0.75	S100a10	-0.62	Etnk	-0.77		
Hspa1	-0.84		Tbx2	-0.82	Ly6d	-0.73	Krt18	-0.96	Hspa1	-0.72	Tbx2	-0.76	Fth1	-0.84	Hspa1	-0.77	Ncl	-0.76	Cavin2	-0.85	Hspa1	-0.74	Ifitm3	-0.63	Gm10039	-0.74		
Psg2	-0.79		Hspa1	-0.74	Rrs1	-0.72	Tbx3	-0.80	Fgf3	-0.72	Cdw2	-0.74	Ncl	-0.84	Phgdh	-0.75	Hspa1	-0.75	Hspa1	-0.78	Sugt1	-0.72	Lrrfip1	-0.62	Krt8	-0.74		
Tgfb2	-0.70		Meis1	-0.74	Zc3h12	-0.69	Tgfb1	-0.79	Hspa1	-0.71	Hspa1	-0.79	Exoc	-0.92	Pcdc	-0.75	Cdh5	-0.77	Sugt1	-0.77	Krt8	-0.72	Pcbd	-0.62	Sugt1	-0.79		
Hspa1	-0.70		Ccnd2	-0.74	Sugt1	-0.68	Dkc1	-0.76	Dkc1	-0.71	Phgdh	-0.71	Krt1	-0.91	Rnd3	-0.75	Snap19	-0.67	Fgf3	-0.73	Apoe	-0.72	Gm13088	-0.62	Meis1	-0.72		
Sugt1	-0.70		Lrrfip1	-0.73	Rnd3	-0.67	Meis1	-0.79	Lrrfip1	-0.67	Ncl	-0.66	Hspe1	-0.78	Hbb-bh1	-0.73	Ncl	-0.74	Dkc1	-0.74	Hspe1	-0.71	Fth1	-0.60	Fgf3	-0.69		
Meis1	-0.69		Hspe1	-0.73	S100a10	-0.65	Krt8	-0.76	Zc3h12	-0.66	Rfl	-0.68	Rapgl	-0.76	Pfn1	-0.72	Dkc1	-0.63	Dnajc10	-0.71	Dkc1	-0.69	Rcbtb2	-0.61	Phlda2	-0.67		
Ncl	-0.68		Sugt1	-0.68	Fgf3	-0.64	Hspe1	-0.70	Sugt1	-0.64	Lrrfip1	-0.67	Mpv17	-0.75	Sugt1	-0.68	Sox17	-0.73	Ncl	-0.68	Exoc	-0.68	Exoc	-0.61	Pcbd	-0.66		
Tbx3	-0.69		Exoc	-0.66	Rrm1	-0.63	Hspa1	-0.70	Pcbd	-0.63	Rbm38	-0.66	Dnajc10	-0.72	Dkc1	-0.67	Phgdh	-0.62	Rapgl	-0.67	Ncl	-0.68	Krt8	-0.61	Ifitm3	-0.64		
Lrrfip1	-0.68		Dnajc10	-0.66	Nptx1	-0.63	Lrrfip1	-0.70	Exoc	-0.62	Pcbd	-0.65	Cavin2	-0.72	Dnajc10	-0.66	Sugt1	-0.62	Sugt1	-0.66	Dnajc10	-0.66	Hspa5	-0.60	Phgdh	-0.63		
Pcbd2	-0.65		Ncl	-0.66	Tbx3	-0.63	Ncl	-0.68	Rbm38	-0.61	Exoc	-0.65	Dkc1	-0.71	Ncl	-0.69	Gm10039	-0.61	Rcn1	-0.63	Zc3h12	-0.66	Phlda2	-0.58	Mkx1	-0.62		
Csrnp3	-0.63		Phgdh	-0.64	Rcn1	-0.63	Zc3h10	-0.66	Dnajc15	-0.61	Fth1	-0.65	Ppa1	-0.69	Rrs1	-0.61	S100a10	-0.60	Dkc1	-0.63	Rnd3	-0.66	Nfatc	-0.61	Ctr1	-0.61		
Amot	-0.62		Dkc1	-0.64	Cited2	-0.63	Rrs1	-0.66	Rpl37a	-0.61	Dnajc15	-0.64	Tomm5	-0.69	Ifrd2	-0.61	Fn1	-0.60	Phgdh	-0.63	Rufy1	-0.62	Ifitm3	-0.61	Meis1	-0.60		
Fth1	-0.62		Phlda2	-0.64	Sugt1	-0.65	Cited2	-0.65	Mrps4	-0.63	Phgdh	-0.68	Gm10039	-0.61	Zc3h12	-0.60	Tmsb4x	-0.63	Rnd3	-0.62	Rbp1	-0.62	Zc3h12	-0.60				
Hand1	-0.62		Krt8	-0.63	Pcdcc	-0.61	Dnajc15	-0.65	Phgdh	-0.60	S100a10	-0.63	Commd9	-0.68	Hspe1	-0.61	Wdr12	-0.60	Wdr12	-0.61	Phgdh	-0.61	Cck	0.72	Phf1	0.61		
Dnajc15	-0.61		Zc3h12	-0.61	Cavin2	-0.61	Pcdc6	-0.64	Nufip1	-0.58	Rrs1	-0.62	Pcdcc	-0.67	Commd9	-0.61	Hspb1	-0.60	Zc3h12	-0.62	Rrs1	-0.61	Tpm3-rs7	0.62	Meis1	0.64		
Atic	-0.60		Rpl37a	-0.60	Hnrnpd	-0.61	Rpl37a	-0.63	Slc16a3	0.58	Hnrnpd	-0.60	Gclm	-0.66	Mxd1	-0.59	Exoc	0.60	Pcdcc	-0.60	Tpc	-0.59	H19	2.03	Mag3	0.69		
Eno1	-0.60		Rrs1	-0.59	Pfdn5	-0.59	Akap12	0.58	Rpl37	-0.57	Cited2	-0.64	Rpl37	-0.64	Rnd3	0.60	Mrps4	0.60	Vim	0.58					Pgp2b	0.74		
Rpl37a	-0.60		H1fx	0.60	Rdh12	-0.60	Exo1	-0.61	Ptgr1	0.60	Rrs1	-0.60	Nop58	-0.64	Limd2	0.60	Akap12	0.60	Rrs1	-0.59	Gcc2	0.59			Hoxa7	0.74		
Rpp	-0.60		Phf1	0.60	Pcbd	-0.60	Dkc1	-0.61	Zc3h13	-0.58	Sugt1	-0.59	Rbm38	-0.63	Fgfr1	-0.59	Slfn4	0.60	Rbm39	0.60	Sox18	0.58			Twsg1	0.78		
Ilvbl	-0.59		Sept11	0.61	Rpl37a	-0.59	Phgdh	-0.60	Hspa	0.61	Jun	0.59	Gm10036	-0.62	Isg15	0.61	Ifitm3	0.61	Limch1	0.60	Pkm	0.60			Tgfb3-os7	0.77		
Nop58	-0.59		Limd2	0.61	Dkc1	0.59	Pdlim2	-0.60	Krt18	0.61	Mrps4	0.59	Atic	0.62	Rtkn	0.60	Sugt1	0.60	Hbb-bh1	0.60	Eef1a1	0.60			Tbx4	0.77		
Cdh4	0.59		Exoc	0.63	Uqcr	0.60	Vldlr	-0.59	Gabarap	0.61	Ptrf	0.59	Srm	-0.61	Spacc	0.63	Slc16a3	0.62	Gpx4	0.62	Ubxd2	0.61			Pmp2	0.81		
Exoc7	0.59		Tagln	0.62	Rtkn	0.60	Efnb2	0.59	Pgk1	0.62	Rpl37	0.58	Mpv17	-0.60	Mxd1	0.62	Hnrnpd	0.59	Hmgb2	0.62	Fth1	0.60			H19	2.24		
Pkp2	0.58		Cyp26b1	0.64	Ppp1r1	0.60	Apoc1b	0.60	Rpl37	0.60	Hbb-bh1	0.58	Ppa1	-0.61	Zc3h13	-0.59	Cspg5	0.60	Hspa1	0.64	Pkp2	0.64						
Hmgb1	0.58		Ube2l	0.64	Ppp1r3	0.60	Ppa1	-0.60	Eef1a1	0.60	Eef1a1	0.58	Rpl37	-0.61	Sox17	-0.59	Rpl37	0.60	Lrrfip1	0.64	Hmgb2	0.63						
Emc9os	0.58		H2afz	0.57	Rbm3	0.58	Tpm3	0.58	Eef1a1	0.59	Tpm3	0.58	Hspb1	-0.59	Rpl37	0.59	Lrrfip1	0.64	Ube2l	0.64	H2afz	0.60						
Ldhb	0.57		Tmsb4x	0.57	Ppa1	-0.58	Ppp1r1	0.57	Ppa1	-0.58	Ppa1	-0.57	Ppa1	-0.59	Rpl37a	0.59	Ube2l	0.64	Rpl37a	0.59	Ppp1r1	0.60						
Lrrc8d	0.57		Cyp26b1	0.57	Ube2l	0.57	Ube2l	0.57	Ppp1r1	0.57	Ube2l	0.57	Rpl37a	-0.59	Ppp1r1	0.58	Rpl37a	0.59	Ppp1r1	0.59	Rpl37a	0.59						
Ppp1r1	0.56		Ppp1r1	0.56	Hmgb1	0.57	Hmgb1	0.57	Hmgb1	0.57	Hmgb1	0.57	Hmgb1	-0.58	Hmgb1	0.57	Hmgb1	0.58	Hmgb1	0.58	Hmgb1	0.58						
Tmsb4x	0.56		Hbb-bh1	0.56	Tmsb4x	0.56	Tmsb4x	0.56	Tmsb4x	0.56	Tmsb4x	0.56	Tmsb4x	-0.57	Tmsb4x	0.56	Tmsb4x	0.57	Tmsb4x	0.57	Tmsb4x	0.57						
Zeb2	0.56		Hbb-bh1	0.73	Tpm1	0.69	Limch1	0.69	Cited1	0.67	Tmsb4x	0.67	Fgfr1	0.60	Rtkn	0.71	Cited1	0.73	Cited1	0.73	Tmsb4x	0.70						
Osr2	0.56		Gpx4	0.79	Fth1	0.69	Fabp7	0.69	Rpm3-rs5	0.67	Cited1	0.66	Hbb-bh1	0.62	Cited1	0.74	Dkc1	0.74	Id1	0.71	Cited2	0.61						
Ifitm1	0.55		Meis1	0.74	Tmsb4x	0.70	Cited1	0.68	Fth1	0.66	Cited2	0.66	Ppa1	0.61	Rpm3-rs5	0.68	Ppa1	0.73	Rrs1	0.68	Hmgb2	0.71						
Sox2	0.54		Id3	0.75	Cited1	0.69	Tmsb10a	0.70	H1fx	0.66	Arg1	0.66	Smagp	0.61	Pag2	0.74	Ifitm1	0.77	Ecscr	0.73	Cldn5	0.66						
Rpm3-rs5	0.51		Ifitm2	0.76	Hmgb2	0.69	Hbb-bh1	0.69	Tpm1	0.66	Tmsb4x	0.65	Lmo2	0.60	Tmsb4x	0.77	Hmgb2	0.77	Akap12	0.72	Dkc1	0.66						
Cyp26b1	0.51		Cyp26b1	0.72	Hbb-bh1	0.68	Fth	0.70	Lmo2	0.62	Tmsb4x	0.77	Hmgb2	0.74	Akap12	0.72	Dkc1	0.66										
Ubald2	0.50		Ubald2	0.78	Tmsb4x	0.71	Ubl	0.72	Ptma1	0.70	Vtn	0.70	Fth1	0.62	Ppp1r1	0.78	Cldn5	0.78	Cldn5	0.75	Mest	0.62						
Actg1	0.50		Ifitm1	0.80	Id1	0.70	Pkp	0.70	Hmgb2	0.71	Pcdh10	0.70	H1fx	0.60	Sgk1	0.78	Sox17	0.80	Tagln	0.76	Sgk1	0.64						
Esm3	0.74		Prg	0.80	Akap12	0.76	H1fx	0.73	Cldn5	0.72	Hmgb2	0.77	Krt	0.64	Exoc	0.64	Sox18	0.81	Sox18	0.77	Ramp2	0.66						
Gpx3l	0.70		Isg15	0.81	Ifitm1	0.78	Gpx	0.72	Sparc	0.73	Ppa1	0.78	Actg1	0.62	Gpx4	0.62	Rbp1	0.82	Rbp1	0.82	Smagp	0.65						
Id1	0.70		Hmgb3	0.88	Isg15	0.77	Ubald2	0.78	Tmsb4x	0.74	Tpm1	0.81	Gabarap	0.67	Hmgb2	1.04	Pkvap	0.82	Pkvap	0.83	Tpm3-rs7	1.03						
Rpl4	0.61		Vim	0.88	Hmgb3	0.77	Isg15	0.79	Spn3rd	0.73	Rbp1	0.84	Akap12	0.69	Tpm3-rs7	1.06	Igfbp4	0.87	Meg3	1.05	Vim	0.84						
Hmgb3	0.64		Eglf7	0.90	Rbp4	0.78	Rbp3	0.80	Rbp4	0.77	Pcmt	0.84	Tpt1	0.70	Rbm3	1.09	Ramp2	1.03	Hmgb2	0.85								
Hmgb2	0.63		Cldn5	0.90	Cldn5	0.80	Hmgb3	0.82	Rbp1	0.78	Sox17	0.84	Rbp1	0.74	Igfbp4	1.29	Pmp22	1.05	Cldn5	0.87								
Rrp	0.60		Pcmt	0.92	Sept	0.81	Rbp4	0.83	Gnai1	0.79	Spn3rd	0.86	Mxd1x	0.77	Ramp2	1.07	Meg3	1.08	Gng11	0.90								
H2-K1	0.60		Igfbp4	1.06	Id2	0.85	Ecscr	0.79	Gpx	0.80	Gng11	0.90	Meg3	1.05	Meg3	1.08	Meg3	1.09	Meg3	0.94								
Cono	0.57		Ramp2	1.08	Sfrp2	0.87	Gng2	0.87	Vim	0.85	Pcmt	0.91	Pag2	0.92	Mest	1.79	Tpm3-rs7	1.17	Mest	1.00								
Lmo2	1.00		Tpm1	1.10	Rhoc	0.88	Pcmt	0.90	Ifitm1	0.86	Ramp2	1.10	Vim	0.92	H19	2.05	H19	2.17	Igfbp4	1.01								
Pcmt-rs7	1.00		Cited1	1.13	Ecscr	0.89	Eglf7	0.90	Pcmt	0.89	Tpm3-rs7	1.11	Atln	0.92					Pmp22	1.01								
Pdlr 1	1.00		Pcmt-rs	1.14	Eglf7	0.90	Vim	0.91	Ramp2	1.10	Ppp1r1	0.92	Ppp1r1	0.92					Tpm3-rs7	1.04								
Pcmt	1.00		Tpm3-rs7	1.15	Pcmt-rs	0.97	Tpm1	1.02	Meis1	0.94	Cldn5	1.30	Cldn5	0.93					Ramp2	1.07								
Tpm3-rs7	1.00		Tpm3	1.16	Tpm1	0.98	Spn3rd	1.02	Pcmt	1.00	Meg3	1.36	Vtn	0.94					H19	2.13								
Meg3	1.16		Pcmt2	1.20	Meis1	1.00	Ramp2	1.04	Ramp2	1.07	Ifitm3	1.40	Gja4	0.94														
Ifitm3	1.17		Meg3	1.29	Spn3rd	1.06	Igfbp4	1.04	Ifitm3	1.13	Igfbp4	1.44	Rhoc	0.99														
Igfbp4	1.23		Pcmt4	1.36	Ramp2	1.10	Pcmt-rs	1.12	Tpm3-rs7	1.15	Meis1	1.52	Sparc	0.94														
Isg15	1.76		H19	1.53	Pcmt4	1.18	Igfbp4	1.30	H19	2.07	Tpm3-rs7	1.42	Tpm3-rs7	1.02														
Bri2	1.79		Ifitm3	1.64	Tpm3-rs7	1.19	Pcmt2	1.18	Meg3	1.35			Ifitm3	1.02														
					Meg3	1.26	Meg3	1.24	H19	2.05			Tmsb4x	1.03														
					Igfbp4	1.27	Pcmt4	1.27					Hmgb2	1.04														
					Pcmt	1.29	Cited1	1.33					Ecscr	1.08														
					Ifitm3	1.48	H19	1.52					Igfbp4	1.14														
					H19	1.81	Ifitm3	1.71					Ramp2	1.30														
													Meg3	1.46													
													Mest	1.64													
													Cldn5	1.99													
													H19	2.26													

Table 6. Eomes-V5 bound genomic regions

Eomes-V5/V5 Bound Peaks in D4 EBs (MACS2 FC >2 and FDR < 0.05)								
338 Peaks								
Chromosome	Start	End	Chromosome	Start	End	Chromosome	Start	End
chr1	7201541	7201894	chr14	75767907	75768176	chr4	119539346	119539754
chr1	12691999	12692313	chr14	79301417	79301740	chr4	120304638	120304989
chr1	19209932	19210396	chr14	87478602	87478856	chr4	125573814	125574295
chr1	19210860	19211147	chr14	99603178	99603440	chr4	125590330	125590698
chr1	24453217	24453472	chr14	100284751	100285065	chr4	128342160	128342607
chr1	30872880	30873217	chr15	10723629	10723949	chr4	133432570	133432920
chr1	34519134	34519397	chr15	27741712	27742394	chr4	134019169	134019465
chr1	34533294	34533659	chr15	28011330	28011571	chr4	134047701	134048058
chr1	34536802	34537068	chr15	82960993	82961435	chr4	134606125	134606379
chr1	37327248	37327543	chr15	86941159	86941488	chr4	139756871	139757177
chr1	59471026	59471321	chr15	94088919	94089537	chr4	139832901	139833526
chr1	60409292	60409589	chr15	103305220	103305582	chr4	141291626	141292122
chr1	64102276	64102565	chr16	20390193	20390518	chr4	148087130	148087414
chr1	71923789	71924055	chr16	29758427	29758698	chr4	150230876	150231279
chr1	71936919	71937260	chr16	30155953	30156202	chr4	150677925	150678066
chr1	72255183	72255464	chr16	32005527	32005793	chr4	154958246	154958546
chr1	72806065	72806341	chr16	35421640	35421895	chr4	155215651	155215911
chr1	86503407	86503706	chr16	50529762	50530017	chr5	3320282	3320548
chr1	88924300	88924573	chr16	76561034	76561345	chr5	22262474	22262727
chr1	89935858	89936212	chr16	90418833	90419139	chr5	25961469	25961754
chr1	90603254	90603551	chr16	90437232	90437616	chr5	43094416	43094691
chr1	92132347	92132620	chr16	93006647	93006979	chr5	50049946	50050257
chr1	97770446	97770704	chr17	3375134	3375529	chr5	63927474	63927764
chr1	105020084	105020270	chr17	8389013	8389656	chr5	67215133	67215370
chr1	106067353	106067740	chr17	8408868	8409161	chr5	75481648	75481980
chr1	118362454	118362685	chr17	15440604	15440876	chr5	88685436	88685721
chr1	119305479	119305792	chr17	23695768	23695982	chr5	93267267	93267551
chr1	131970916	131971330	chr17	28382998	28383318	chr5	104406739	104407011
chr1	132139851	132140173	chr17	29080855	29081169	chr5	106451835	106452105
chr1	132200729	132201045	chr17	35725659	35725916	chr5	111408974	111409304
chr1	132318145	132318501	chr17	50070014	50070470	chr5	114667617	114667879
chr1	132800255	132800689	chr17	79963392	79963799	chr5	116141326	116141991
chr1	134063393	134063632	chr17	82348567	82348871	chr5	119613536	119613843
chr1	135136543	135136809	chr17	83123074	83123158	chr5	119670611	119671060
chr1	138547889	138548260	chr17	86941477	86941763	chr5	120221445	120221698
chr1	155086376	155086740	chr17	87446926	87447169	chr5	139675454	139675775
chr1	156668559	156668841	chr18	9210968	9211260	chr5	142074761	142075087
chr1	165736122	165736456	chr18	9554964	9555318	chr5	142817796	142818169
chr1	167676504	167676777	chr18	9957815	9958092	chr6	6874182	6874450
chr1	169235197	169235648	chr18	38662580	38662921	chr6	7277495	7277723
chr1	171966068	171966351	chr18	38906140	38906499	chr6	34388454	34388682
chr1	173852724	173852986	chr18	44533447	44533744	chr6	37277224	37277725
chr1	180697108	180697584	chr18	60934964	60935230	chr6	40143655	40143960
chr1	180890120	180890440	chr18	68189974	68190218	chr6	47228694	47229049
chr1	180924687	180925102	chr19	3687874	3688157	chr6	49215435	49215709
chr1	181382803	181383199	chr19	5072015	5072315	chr6	52532261	52532519
chr1	186976976	186977332	chr19	6076939	6077417	chr6	83421730	83422104
chr1	192796393	192796734	chr19	8723140	8723468	chr6	108310067	108310391
chr1	193732260	193732552	chr19	10277356	10277636	chr6	114875034	114875340
chr1	194627757	194628026	chr19	10278661	10279025	chr6	121194312	121194632
chr10	21746802	21747078	chr19	30554375	30554729	chr6	122609859	122610142
chr10	22470533	22470826	chr19	36896937	36897254	chr6	127215403	127215683
chr10	40363104	40363461	chr19	37716078	37716421	chr6	146686583	146686853
chr10	41139326	41139591	chr19	41441358	41441692	chr7	6777816	6778072
chr10	61906198	61906560	chr19	42220077	42220351	chr7	30456437	30456693
chr10	61936706	61936937	chr19	45733389	45733779	chr7	44869807	44870151
chr10	93852218	93852528	chr19	55700460	55700768	chr7	65228775	65229029
chr10	95439263	95439492	chr19	57795455	57795746	chr7	78155284	78155638
chr10	95665508	95665812	chr19	59717838	59718151	chr7	78183451	78183771
chr10	117452331	117452672	chr2	26198570	26198879	chr7	79797122	79797831
chr10	125785736	125786047	chr2	29820354	29820821	chr7	84328831	84329251
chr10	125966999	125967302	chr2	35985517	35985780	chr7	98360150	98360562
chr10	126681041	126681288	chr2	52624237	52624505	chr7	98837809	98838156
chr10	128411186	128411662	chr2	59800309	59800566	chr7	98941512	98941771
chr10	128804245	128804575	chr2	70498208	70498449	chr7	108970459	108970774
chr11	16844357	16844640	chr2	71725197	71725610	chr7	109876156	109876444
chr11	20812239	20812536	chr2	77506511	77506798	chr7	112743633	112743948
chr11	26108699	26108963	chr2	85131601	85131897	chr7	115193364	115193856
chr11	59571763	59572029	chr2	85238046	85238590	chr7	121707297	121707690
chr11	61003992	61004431	chr2	104109559	104109820	chr7	130519582	130519930
chr11	63020685	63020958	chr2	114057466	114057827	chr7	142548783	142549069
chr11	84592759	84593211	chr2	115132390	115132646	chr8	3417588	3417895
chr11	94873031	94873305	chr2	116065615	116066112	chr8	10665982	10666307
chr11	97029730	97029986	chr2	122298621	122298838	chr8	14096234	14096427
chr11	100740025	100740361	chr2	127324453	127324738	chr8	19933871	19934555
chr11	103808607	103808749	chr2	131304925	131305355	chr8	20368115	20368375
chr11	106338339	106338730	chr2	152048340	152048922	chr8	20609744	20610056
chr11	113785603	113786006	chr2	152804521	152804788	chr8	20822585	20823141
chr11	115477592	115478486	chr2	156905238	156905579	chr8	25371316	25371678
chr11	116992725	116993103	chr2	165493255	165493531	chr8	34808646	34808973
chr11	117082334	117082620	chr2	166670521	166671175	chr8	61715402	61715713
chr11	118125686	118125936	chr2	166744571	166744864	chr8	83876352	83876634
chr11	120237720	120237909	chr2	167144825	167145093	chr8	84785675	84786124
chr12	12580918	12581076	chr2	167231979	167232307	chr8	88719620	88719968
chr12	12788150	12788858	chr2	167497421	167497661	chr8	91867066	91867277
chr12	12941733	12942005	chr2	167563700	167564101	chr8	119416668	119417301
chr12	12943315	12943561	chr2	168207333	168207744	chr8	120853247	120853509
chr12	17238849	17239198	chr2	168253900	168254165	chr8	121083613	121083880
chr12	32169182	32169649	chr2	178643919	178644299	chr8	125870835	125871196
chr12	33157813	33158201	chr2	179565796	179566061	chr8	126557468	126557731
chr12	54710133	54710644	chr3	5218305	5218609	chr9	21250112	21250314
chr12	71296349	71296701	chr3	8763479	8764206	chr9	28261342	28261622
chr12	83631990	83632333	chr3	52102288	52102571	chr9	39630121	39630387
chr12	84625176	84625438	chr3	53463593	53463867	chr9	46889995	46890249
chr12	84996031	84996395	chr3	96343257	96343631	chr9	46980171	46980323
chr12	86795530	86795754	chr3	96359967	96360282	chr9	47157024	47157386
chr12	100727937	100728202	chr3	96390598	96390863	chr9	47422277	47422539
chr12	108006362	108006624	chr3	96488524	96488850	chr9	57812423	57812690
chr13	3901632	3902318	chr3	104541667	104542005	chr9	58120420	58120926
chr13	15628463	15628825	chr3	108791126	108791367	chr9	65168661	65168923
chr13	28942168	28942445	chr3	108856910	108857241	chr9	66294902	66295272
chr13	69718042	69718532	chr3	122483066	122483471	chr9	67482342	67482670
chr13	92642376	92643200	chr3	134236186	134236533	chr9	72806341	72806607
chr13	97365562	97365936	chr3	138644283	138644695	chr9	73026258	73026613
chr13	97389106	97389367	chr3	149429701	149430167	chr9	77529979	77530327
chr13	99466193	99466505	chr4	8910116	8910437	chr9	81633144	81633362
chr13	111829587	111829997	chr4	46880280	46880525	chr9	98433101	98433294
chr14	22144048	22144351	chr4	54945878	54946248	chr9	111176412	111176669
chr14	29268460	29268748	chr4	65279898	65280316	chr9	118389943	118390240
chr14	32452600	32452937	chr4	65830239	65830642	chr9	123554697	123554974
chr14	57554643	57554973	chr4	107139017	107139309	chr9	123935702	123936121
chr14	63359309	63359652	chr4	107734107	107734435	chrY	90766886	90767149
chr14	75673822	75674184	chr4	107990757	107991066			

REFERENCES

Amat, F., and Keller, P.J. (2013). Towards comprehensive cell lineage reconstructions in complex organisms using light-sheet microscopy. Dev Growth Differ *55*, 563-578.

Arnold, S.J., Hofmann, U.K., Bikoff, E.K., and Robertson, E.J. (2008). Pivotal roles for eomesodermin during axis formation, epithelium-to-mesenchyme transition and endoderm specification in the mouse. Development *135*, 501-511.

Arnold, S.J., and Robertson, E.J. (2009). Making a commitment: cell lineage allocation and axis patterning in the early mouse embryo. Nature reviews Molecular cell biology *10*, 91-103.

Arnold, S.J., Sugnaseelan, J., Groszer, M., Srinivas, S., and Robertson, E.J. (2009). Generation and analysis of a mouse line harboring GFP in the Eomes/Tbr2 locus. Genesis *47*, 775-781.

Beck, S., Le Good, J.A., Guzman, M., Ben Haim, N., Roy, K., Beermann, F., and Constam, D.B. (2002). Extraembryonic proteases regulate Nodal signalling during gastrulation. Nat Cell Biol *4*, 981-985.

Beddington, R.S., and Robertson, E.J. (1999). Axis development and early asymmetry in mammals. Cell *96*, 195-209.

Behringer, R., Gertsenstein, M., Nagy, K.V., and Nagy, A. (2014). Manipulating the Mouse Embryo: A Laboratory Manual (Cold Spring Harbor Laboratory Press).

Boiers, C., Carrelha, J., Lutteropp, M., Luc, S., Green, J.C., Azzoni, E., Woll, P.S., Mead, A.J., Hultquist, A., Swiers, G.*, et al.* (2013). Lymphomyeloid contribution of an immune-restricted progenitor emerging prior to definitive hematopoietic stem cells. Cell Stem Cell *13*, 535-548.

Boisset, J.C., van Cappellen, W., Andrieu-Soler, C., Galjart, N., Dzierzak, E., and Robin, C. (2010). In vivo imaging of haematopoietic cells emerging from the mouse aortic endothelium. Nature *464*, 116-120.

Boyle, A.P., Davis, S., Shulha, H.P., Meltzer, P., Margulies, E.H., Weng, Z., Furey, T.S., and Crawford, G.E. (2008). High-resolution mapping and characterization of open chromatin across the genome. Cell *132*, 311-322.

Buecker, C., and Wysocka, J. (2012). Enhancers as information integration hubs in development: lessons from genomics. Trends Genet *28*, 276-284.

Buenrostro, J.D., Giresi, P.G., Zaba, L.C., Chang, H.Y., and Greenleaf, W.J. (2013). Transposition of native chromatin for fast and sensitive epigenomic profiling of open chromatin, DNA-binding proteins and nucleosome position. Nat Methods *10*, 1213-1218.

Buenrostro, J.D., Wu, B., Litzenburger, U.M., Ruff, D., Gonzales, M.L., Snyder, M.P., Chang, H.Y., and Greenleaf, W.J. (2015). Single-cell chromatin accessibility reveals principles of regulatory variation. Nature *523*, 486-490.

Butler, A., Hoffman, P., Smibert, P., Papalexi, E., and Satija, R. (2018). Integrating single-cell transcriptomic data across different conditions, technologies, and species. Nat Biotechnol *36*, 411-420.

Chagraoui, H., Kristiansen, M.S., Ruiz, J.P., Serra-Barros, A., Richter, J., Hall-Ponsele, E., Gray, N., Waithe, D., Clark, K., Hublitz, P.*, et al.* (2018). SCL/TAL1 cooperates with Polycomb RYBP-PRC1 to suppress alternative lineages in blood-fated cells. Nat Commun *9*, 5375.

Chan, M.M., Smith, Z.D., Grosswendt, S., Kretzmer, H., Norman, T.M., Adamson, B., Jost, M., Quinn, J.J., Yang, D., Jones, M.G.*, et al.* (2019). Molecular recording of mammalian embryogenesis. Nature *570*, 77-82.

Chen, M.J., Yokomizo, T., Zeigler, B.M., Dzierzak, E., and Speck, N.A. (2009). Runx1 is required for the endothelial to haematopoietic cell transition but not thereafter. Nature *457*, 887-891.

Choi, K., Kennedy, M., Kazarov, A., Papadimitriou, J.C., and Keller, G. (1998). A common precursor for hematopoietic and endothelial cells. Development *125*, 725-732.

Ciruna, B.G., and Rossant, J. (1999). Expression of the T-box gene Eomesodermin during early mouse development. Mechanisms of development *81*, 199-203.

Clarke, R.L., Yzaguirre, A.D., Yashiro-Ohtani, Y., Bondue, A., Blanpain, C., Pear, W.S., Speck, N.A., and Keller, G. (2013). The expression of Sox17 identifies and regulates hemogenic endothelium. Nature cell biology *15*, 502.

Clements, W.K., and Traver, D. (2013). Signalling pathways that control vertebrate haematopoietic stem cell specification. Nat Rev Immunol *13*, 336-348.

Cook, B.D. (2014). Modeling murine yolk sac hematopoiesis with embryonic stem cell culture systems. Front Biol (Beijing) *9*, 339-346.

Costello, I., Pimeisl, I.-M., Dräger, S., Bikoff, E.K., Robertson, E.J., and Arnold, S.J. (2011). The T-box transcription factor Eomesodermin acts upstream of Mesp1 to specify cardiac mesoderm during mouse gastrulation. Nature cell biology *13*, 1084-1091.

Craft, A.M., Ahmed, N., Rockel, J.S., Baht, G.S., Alman, B.A., Kandel, R.A., Grigoriadis, A.E., and Keller, G.M. (2013). Specification of chondrocytes and cartilage tissues from embryonic stem cells. Development *140*, 2597-2610.

D'Souza, S.L., Elefanty, A.G., and Keller, G. (2005). SCL/Tal-1 is essential for hematopoietic commitment of the hemangioblast but not for its development. Blood *105*, 3862-3870.

de Bruijn, M., and Dzierzak, E. (2017). Runx transcription factors in the development and function of the definitive hematopoietic system. Blood *129*, 2061-2069.

de Bruijn, M.F., Speck, N.A., Peeters, M.C., and Dzierzak, E. (2000). Definitive hematopoietic stem cells first develop within the major arterial regions of the mouse embryo. EMBO J *19*, 2465-2474.

DiTacchio, L., Bowles, J., Shin, S., Lim, D.S., Koopman, P., and Janknecht, R. (2012). Transcription factors ER71/ETV2 and SOX9 participate in a positive feedback loop in fetal and adult mouse testis. J Biol Chem *287*, 23657-23666.

Ditadi, A., Sturgeon, C.M., and Keller, G. (2017). A view of human haematopoietic development from the Petri dish. Nat Rev Mol Cell Biol *18*, 56-67.

Dobin, A., Davis, C.A., Schlesinger, F., Drenkow, J., Zaleski, C., Jha, S., Batut, P., Chaisson, M., and Gingeras, T.R. (2013). STAR: ultrafast universal RNA-seq aligner. Bioinformatics *29*, 15-21.

Dzierzak, E., and Speck, N.A. (2008). Of lineage and legacy: the development of mammalian hematopoietic stem cells. Nat Immunol *9*, 129-136.

Eilken, H.M., Nishikawa, S., and Schroeder, T. (2009). Continuous single-cell imaging of blood generation from haemogenic endothelium. Nature *457*, 896-900.

Eliades, A., Wareing, S., Marinopoulou, E., Fadlullah, M.Z.H., Patel, R., Grabarek, J.B., Plusa, B., Lacaud, G., and Kouskoff, V. (2016). The Hemogenic Competence of Endothelial

Progenitors Is Restricted by Runx1 Silencing during Embryonic Development. Cell Rep *15*, 2185-2199.

Episkopou, V., Arkell, R., Timmons, P.M., Walsh, J.J., Andrew, R.L., and Swan, D. (2001). Induction of the mammalian node requires Arkadia function in the extraembryonic lineages. Nature *410*, 825-830.

Evans, M.J., and Kaufman, M.H. (1981). Establishment in culture of pluripotential cells from mouse embryos. Nature *292*, 154-156.

Evseenko, D., Zhu, Y., Schenke-Layland, K., Kuo, J., Latour, B., Ge, S., Scholes, J., Dravid, G., Li, X., MacLellan, W.R*., et al.* (2010). Mapping the first stages of mesoderm commitment during differentiation of human embryonic stem cells. Proc Natl Acad Sci U S A *107*, 13742-13747.

Feil, R., Brocard, J., Mascrez, B., LeMeur, M., Metzger, D., and Chambon, P. (1996). Ligand-activated site-specific recombination in mice. Proc Natl Acad Sci U S A *93*, 10887-10890.

Feil, R., Wagner, J., Metzger, D., and Chambon, P. (1997). Regulation of Cre recombinase activity by mutated estrogen receptor ligand-binding domains. Biochem Biophys Res Commun *237*, 752-757.

Ferkowicz, M.J., Starr, M., Xie, X., Li, W., Johnson, S.A., Shelley, W.C., Morrison, P.R., and Yoder, M.C. (2003). CD41 expression defines the onset of primitive and definitive hematopoiesis in the murine embryo. Development *130*, 4393-4403.

Ferkowicz, M.J., and Yoder, M.C. (2005). Blood island formation: longstanding observations and modern interpretations. Exp Hematol *33*, 1041-1047.

Frame, J.M., Fegan, K.H., Conway, S.J., McGrath, K.E., and Palis, J. (2016). Definitive Hematopoiesis in the Yolk Sac Emerges from Wnt-Responsive Hemogenic Endothelium Independently of Circulation and Arterial Identity. Stem Cells *34*, 431-444.

Friedrich, G., and Soriano, P. (1991). Promoter traps in embryonic stem cells: a genetic screen to identify and mutate developmental genes in mice. Genes Dev *5*, 1513-1523.

Gadue, P., Huber, T.L., Paddison, P.J., and Keller, G.M. (2006). Wnt and TGF-beta signaling are required for the induction of an in vitro model of primitive streak formation using embryonic stem cells. Proc Natl Acad Sci U S A *103*, 16806-16811.

Gekas, C., Dieterlen-Lievre, F., Orkin, S.H., and Mikkola, H.K. (2005). The placenta is a niche for hematopoietic stem cells. Dev Cell *8*, 365-375.

Goode, D.K., Obier, N., Vijayabaskar, M.S., Lie, A.L.M., Lilly, A.J., Hannah, R., Lichtinger, M., Batta, K., Florkowska, M., Patel, R*., et al.* (2016). Dynamic Gene Regulatory Networks Drive Hematopoietic Specification and Differentiation. Dev Cell *36*, 572-587.

Hancock, S.N., Agulnik, S.I., Silver, L.M., and Papaioannou, V.E. (1999). Mapping and expression analysis of the mouse ortholog of Xenopus Eomesodermin. Mechanisms of development *81*, 205-208.

Heinz, S., Benner, C., Spann, N., Bertolino, E., Lin, Y.C., Laslo, P., Cheng, J.X., Murre, C., Singh, H., and Glass, C.K. (2010). Simple combinations of lineage-determining transcription factors prime cis-regulatory elements required for macrophage and B cell identities. Mol Cell *38*, 576-589.

Herrmann, B.G., Labeit, S., Poustka, A., King, T.R., and Lehrach, H. (1990). Cloning of the T gene required in mesoderm formation in the mouse. Nature *343*, 617-622.

Hoodless, P.A., Pye, M., Chazaud, C., Labbe, E., Attisano, L., Rossant, J., and Wrana, J.L. (2001). FoxH1 (Fast) functions to specify the anterior primitive streak in the mouse. Genes Dev *15*, 1257-1271.

Huber, T.L., Kouskoff, V., Fehling, H.J., Palis, J., and Keller, G. (2004). Haemangioblast commitment is initiated in the primitive streak of the mouse embryo. Nature *432*, 625-630.

Ichikawa, T., Nakazato, K., Keller, P.J., Kajiura-Kobayashi, H., Stelzer, E.H., Mochizuki, A., and Nonaka, S. (2014). Live imaging and quantitative analysis of gastrulation in mouse embryos using light-sheet microscopy and 3D tracking tools. nature protocols *9*, 575-585.

Irion, S., Clarke, R.L., Luche, H., Kim, I., Morrison, S.J., Fehling, H.-J., and Keller, G.M. (2010). Temporal specification of blood progenitors from mouse embryonic stem cells and induced pluripotent stem cells. Development *137*, 2829-2839.

Izumi, N., Era, T., Akimaru, H., Yasunaga, M., and Nishikawa, S. (2007a). Dissecting the molecular hierarchy for mesendoderm differentiation through a combination of embryonic stem cell culture and RNA interference. Stem Cells *25*, 1664-1674.

Izumi, N., Era, T., Akimaru, H., Yasunaga, M., and Nishikawa, S.I. (2007b). Dissecting the molecular hierarchy for mesendoderm differentiation through a combination of embryonic stem cell culture and RNA interference. Stem Cells *25*, 1664-1674.

Jiang, S., and Mortazavi, A. (2018). Integrating ChIP-seq with other functional genomics data. Brief Funct Genomics *17*, 104-115.

Kataoka, H., Hayashi, M., Nakagawa, R., Tanaka, Y., Izumi, N., Nishikawa, S., Jakt, M.L., Tarui, H., and Nishikawa, S. (2011). Etv2/ER71 induces vascular mesoderm from Flk1+PDGFRalpha+ primitive mesoderm. Blood *118*, 6975-6986.

Kattman, S.J., Witty, A.D., Gagliardi, M., Dubois, N.C., Niapour, M., Hotta, A., Ellis, J., and Keller, G. (2011). Stage-specific optimization of activin/nodal and BMP signaling promotes cardiac differentiation of mouse and human pluripotent stem cell lines. Cell stem cell *8*, 228-240.

Keller, G. (2005). Embryonic stem cell differentiation: emergence of a new era in biology and medicine. Genes & development *19*, 1129-1155.

Kinder, S.J., Tsang, T.E., Quinlan, G.A., Hadjantonakis, A.-K., Nagy, A., and Tam, P. (1999). The orderly allocation of mesodermal cells to the extraembryonic structures and the anteroposterior axis during gastrulation of the mouse embryo. Development *126*, 4691-4701.

Kissa, K., and Herbomel, P. (2010). Blood stem cells emerge from aortic endothelium by a novel type of cell transition. Nature *464*, 112-115.

Klemm, S.L., Shipony, Z., and Greenleaf, W.J. (2019). Chromatin accessibility and the regulatory epigenome. Nat Rev Genet *20*, 207-220.

Koyano-Nakagawa, N., and Garry, D.J. (2017). Etv2 as an essential regulator of mesodermal lineage development. Cardiovasc Res *113*, 1294-1306.

Kretzschmar, K., and Watt, F.M. (2012). Lineage tracing. Cell *148*, 33-45.

Kubo, A., Shinozaki, K., Shannon, J.M., Kouskoff, V., Kennedy, M., Woo, S., Fehling, H.J., and Keller, G. (2004). Development of definitive endoderm from embryonic stem cells in culture. Development *131*, 1651-1662.

Kukurba, K.R., and Montgomery, S.B. (2015). RNA Sequencing and Analysis. Cold Spring Harb Protoc *2015*, 951-969.

Kwon, G.S., Viotti, M., and Hadjantonakis, A.K. (2008). The endoderm of the mouse embryo arises by dynamic widespread intercalation of embryonic and extraembryonic lineages. Dev Cell *15*, 509-520.

Lacaud, G., and Kouskoff, V. (2017). Hemangioblast, hemogenic endothelium, and primitive versus definitive hematopoiesis. Experimental hematology *49*, 19-24.

Lancrin, C., Mazan, M., Stefanska, M., Patel, R., Lichtinger, M., Costa, G., Vargel, O., Wilson, N.K., Moroy, T., Bonifer, C*., et al.* (2012). GFI1 and GFI1B control the loss of endothelial identity of hemogenic endothelium during hematopoietic commitment. Blood *120*, 314-322.

Lancrin, C., Sroczynska, P., Stephenson, C., Allen, T., Kouskoff, V., and Lacaud, G. (2009). The haemangioblast generates haematopoietic cells through a haemogenic endothelium stage. Nature *457*, 892-895.

Langmead, B., and Salzberg, S.L. (2012). Fast gapped-read alignment with Bowtie 2. Nat Methods *9*, 357-359.

Lee, D., Park, C., Lee, H., Lugus, J.J., Kim, S.H., Arentson, E., Chung, Y.S., Gomez, G., Kyba, M., Lin, S*., et al.* (2008). ER71 acts downstream of BMP, Notch, and Wnt signaling in blood and vessel progenitor specification. Cell Stem Cell *2*, 497-507.

Li, H., Handsaker, B., Wysoker, A., Fennell, T., Ruan, J., Homer, N., Marth, G., Abecasis, G., Durbin, R., and Genome Project Data Processing, S. (2009). The Sequence Alignment/Map format and SAMtools. Bioinformatics *25*, 2078-2079.

Li, Z., Lan, Y., He, W., Chen, D., Wang, J., Zhou, F., Wang, Y., Sun, H., Chen, X., Xu, C*., et al.* (2012). Mouse embryonic head as a site for hematopoietic stem cell development. Cell Stem Cell *11*, 663-675.

Liakhovitskaia, A., Rybtsov, S., Smith, T., Batsivari, A., Rybtsova, N., Rode, C., de Bruijn, M., Buchholz, F., Gordon-Keylock, S., Zhao, S*., et al.* (2014). Runx1 is required for progression of CD41+ embryonic precursors into HSCs but not prior to this. Development *141*, 3319-3323.

Lie, A.L.M., Marinopoulou, E., Lilly, A.J., Challinor, M., Patel, R., Lancrin, C., Kouskoff, V., and Lacaud, G. (2018). Regulation of RUNX1 dosage is crucial for efficient blood formation from hemogenic endothelium. Development *145*.

Liu, F., Kang, I., Park, C., Chang, L.W., Wang, W., Lee, D., Lim, D.S., Vittet, D., Nerbonne, J.M., and Choi, K. (2012). ER71 specifies Flk-1+ hemangiogenic mesoderm by inhibiting cardiac mesoderm and Wnt signaling. Blood *119*, 3295-3305.

Love, M.I., Huber, W., and Anders, S. (2014). Moderated estimation of fold change and dispersion for RNA-seq data with DESeq2. Genome biology *15*, 550.

Lugus, J.J., Park, C., Ma, Y.D., and Choi, K. (2009). Both primitive and definitive blood cells are derived from Flk-1+ mesoderm. Blood *113*, 563-566.

Lun, A.T., McCarthy, D.J., and Marioni, J.C. (2016). A step-by-step workflow for low-level analysis of single-cell RNA-seq data with Bioconductor. F1000Res *5*, 2122.

McCarthy, D.J., Campbell, K.R., Lun, A.T., and Wills, Q.F. (2017). Scater: pre-processing, quality control, normalization and visualization of single-cell RNA-seq data in R. Bioinformatics *33*, 1179-1186.

McGrath, K.E., Frame, J.M., Fegan, K.H., Bowen, J.R., Conway, S.J., Catherman, S.C., Kingsley, P.D., Koniski, A.D., and Palis, J. (2015a). Distinct sources of hematopoietic progenitors emerge before HSCs and provide functional blood cells in the mammalian embryo. Cell reports *11*, 1892-1904.

McGrath, K.E., Frame, J.M., and Palis, J. (2015b). Early hematopoiesis and macrophage development. Semin Immunol *27*, 379-387.

McKenna, A., and Gagnon, J.A. (2019). Recording development with single cell dynamic lineage tracing. Development *146*.

McLean, C.Y., Bristor, D., Hiller, M., Clarke, S.L., Schaar, B.T., Lowe, C.B., Wenger, A.M., and Bejerano, G. (2010). GREAT improves functional interpretation of cis-regulatory regions. Nat Biotechnol *28*, 495-501.

McLeay, R.C., and Bailey, T.L. (2010). Motif Enrichment Analysis: a unified framework and an evaluation on ChIP data. BMC Bioinformatics *11*, 165.

Metzger, D., Ali, S., Bornert, J.M., and Chambon, P. (1995). Characterization of the amino-terminal transcriptional activation function of the human estrogen receptor in animal and yeast cells. J Biol Chem *270*, 9535-9542.

Mikkola, H.K., Fujiwara, Y., Schlaeger, T.M., Traver, D., and Orkin, S.H. (2003). Expression of CD41 marks the initiation of definitive hematopoiesis in the mouse embryo. Blood *101*, 508-516.

Mitjavila-Garcia, M.T., Cailleret, M., Godin, I., Nogueira, M.M., Cohen-Solal, K., Schiavon, V., Lecluse, Y., Le Pesteur, F., Lagrue, A.H., and Vainchenker, W. (2002). Expression of CD41 on hematopoietic progenitors derived from embryonic hematopoietic cells. Development *129*, 2003-2013.

Miura, S., Davis, S., Klingensmith, J., and Mishina, Y. (2006). BMP signaling in the epiblast is required for proper recruitment of the prospective paraxial mesoderm and development of the somites. Development *133*, 3767-3775.

Murray, P.D.F. (1932). The development in vitro of the blood of the early chick embryo. Proceedings of the Royal Society of London Series B, Containing Papers of a Biological Character *111*, 497-521.

Murry, C.E., and Keller, G. (2008). Differentiation of embryonic stem cells to clinically relevant populations: lessons from embryonic development. Cell *132*, 661-680.

Naiche, L., Harrelson, Z., Kelly, R.G., and Papaioannou, V.E. (2005). T-box genes in vertebrate development. Annu Rev Genet *39*, 219-239.

Ng, E.S., Azzola, L., Sourris, K., Robb, L., Stanley, E.G., and Elefanty, A.G. (2005). The primitive streak gene Mixl1 is required for efficient haematopoiesis and BMP4-induced ventral mesoderm patterning in differentiating ES cells. Development *132*, 873-884.

Nishiyama, A., Xin, L., Sharov, A.A., Thomas, M., Mowrer, G., Meyers, E., Piao, Y., Mehta, S., Yee, S., Nakatake, Y.*, et al.* (2009). Uncovering early response of gene regulatory networks in ESCs by systematic induction of transcription factors. Cell Stem Cell *5*, 420-433.

Nostro, M.C., Cheng, X., Keller, G.M., and Gadue, P. (2008). Wnt, activin, and BMP signaling regulate distinct stages in the developmental pathway from embryonic stem cells to blood. Cell stem cell *2*, 60-71.

Nowotschin, S., Costello, I., Piliszek, A., Kwon, G.S., Mao, C.-a., Klein, W.H., Robertson, E.J., and Hadjantonakis, A.-K. (2013). The T-box transcription factor Eomesodermin is essential for AVE induction in the mouse embryo. Genes & development *27*, 997-1002.

Onodera, K., Takahashi, S., Nishimura, S., Ohta, J., Motohashi, H., Yomogida, K., Hayashi, N., Engel, J.D., and Yamamoto, M. (1997). GATA-1 transcription is controlled by distinct regulatory mechanisms during primitive and definitive erythropoiesis. Proc Natl Acad Sci U S A *94*, 4487-4492.

Org, T., Duan, D., Ferrari, R., Montel-Hagen, A., Van Handel, B., Kerenyi, M.A., Sasidharan, R., Rubbi, L., Fujiwara, Y., Pellegrini, M.*, et al.* (2015). Scl binds to primed enhancers in mesoderm to regulate hematopoietic and cardiac fate divergence. EMBO J *34*, 759-777.

Ottersbach, K., and Dzierzak, E. (2005). The murine placenta contains hematopoietic stem cells within the vascular labyrinth region. Dev Cell *8*, 377-387.

Padron-Barthe, L., Temino, S., Villa del Campo, C., Carramolino, L., Isern, J., and Torres, M. (2014). Clonal analysis identifies hemogenic endothelium as the source of the blood-endothelial common lineage in the mouse embryo. Blood *124*, 2523-2532.

Palis, J. (2014). Primitive and definitive erythropoiesis in mammals. Front Physiol *5*, 3.

Palis, J., Robertson, S., Kennedy, M., Wall, C., and Keller, G. (1999). Development of erythroid and myeloid progenitors in the yolk sac and embryo proper of the mouse. Development *126*, 5073-5084.

Papaioannou, V.E. (2014). The T-box gene family: emerging roles in development, stem cells and cancer. Development *141*, 3819-3833.

Pei, W., Wang, X., Rossler, J., Feyerabend, T.B., Hofer, T., and Rodewald, H.R. (2019). Using Cre-recombinase-driven Polylox barcoding for in vivo fate mapping in mice. Nat Protoc *14*, 1820-1840.

Peikon, I.D., Gizatullina, D.I., and Zador, A.M. (2014). In vivo generation of DNA sequence diversity for cellular barcoding. Nucleic Acids Res *42*, e127.

Peng, G., Suo, S., Cui, G., Yu, F., Wang, R., Chen, J., Chen, S., Liu, Z., Chen, G., Qian, Y.*, et al.* (2019). Molecular architecture of lineage allocation and tissue organization in early mouse embryo. Nature *572*, 528-532.

Pereira, L.A., Wong, M.S., Mossman, A.K., Sourris, K., Janes, M.E., Knezevic, K., Hirst, C.E., Lim, S.M., Pimanda, J.E., Stanley, E.G.*, et al.* (2012). Pdgfralpha and Flk1 are direct target genes of Mixl1 in differentiating embryonic stem cells. Stem Cell Res *8*, 165-179.

Pfeiffer, M.J., Quaranta, R., Piccini, I., Fell, J., Rao, J., Ropke, A., Seebohm, G., and Greber, B. (2018). Cardiogenic programming of human pluripotent stem cells by dose-controlled activation of EOMES. Nat Commun *9*, 440.

Pijuan-Sala, B., Griffiths, J.A., Guibentif, C., Hiscock, T.W., Jawaid, W., Calero-Nieto, F.J., Mulas, C., Ibarra-Soria, X., Tyser, R.C.V., Ho, D.L.L.*, et al.* (2019). A single-cell molecular map of mouse gastrulation and early organogenesis. Nature *566*, 490-495.

Pimeisl, I.M., Tanriver, Y., Daza, R.A., Vauti, F., Hevner, R.F., Arnold, H.H., and Arnold, S.J. (2013). Generation and characterization of a tamoxifen-inducible EomesCreER mouse line. genesis *51*, 725-733.

Porcher, C., Chagraoui, H., and Kristiansen, M.S. (2017). SCL/TAL1: a multifaceted regulator from blood development to disease. Blood *129*, 2051-2060.

Porcher, C., Swat, W., Rockwell, K., Fujiwara, Y., Alt, F.W., and Orkin, S.H. (1996). The T cell leukemia oncoprotein SCL/tal-1 is essential for development of all hematopoietic lineages. Cell *86*, 47-57.

Quinlan, A.R., and Hall, I.M. (2010). BEDTools: a flexible suite of utilities for comparing genomic features. Bioinformatics *26*, 841-842.

Ramirez, F., Ryan, D.P., Gruning, B., Bhardwaj, V., Kilpert, F., Richter, A.S., Heyne, S., Dundar, F., and Manke, T. (2016). deepTools2: a next generation web server for deep-sequencing data analysis. Nucleic Acids Res *44*, W160-165.

Rasmussen, T.L., Martin, C.M., Walter, C.A., Shi, X., Perlingeiro, R., Koyano-Nakagawa, N., and Garry, D.J. (2013). Etv2 rescues Flk1 mutant embryoid bodies. Genesis *51*, 471-480.

Robinson, J.T., Thorvaldsdottir, H., Winckler, W., Guttman, M., Lander, E.S., Getz, G., and Mesirov, J.P. (2011). Integrative genomics viewer. Nat Biotechnol *29*, 24-26.

Sabin, F.R. (1920). Studies on the origin of blood-vessels and of red blood-corpuscles as seen in the living blastoderm of chicks during the second day of incubation. Contrib Embryol Carneg Inst *9*, 214-262.

Sarrach, S., Huang, Y., Niedermeyer, S., Hachmeister, M., Fischer, L., Gille, S., Pan, M., Mack, B., Kranz, G., Libl, D.*, et al.* (2018). Spatiotemporal patterning of EpCAM is important for murine embryonic endo- and mesodermal differentiation. Sci Rep *8*, 1801.

Schlaeger, T.M., Mikkola, H.K., Gekas, C., Helgadottir, H.B., and Orkin, S.H. (2005). Tie2Cre-mediated gene ablation defines the stem-cell leukemia gene (SCL/tal1)-dependent window during hematopoietic stem-cell development. Blood *105*, 3871-3874.

Schutte, J., Wang, H., Antoniou, S., Jarratt, A., Wilson, N.K., Riepsaame, J., Calero-Nieto, F.J., Moignard, V., Basilico, S., Kinston, S.J.*, et al.* (2016). An experimentally validated network of nine haematopoietic transcription factors reveals mechanisms of cell state stability. Elife *5*, e11469.

Schwartzberg, P.L., Goff, S.P., and Robertson, E.J. (1989). Germ-line transmission of a c-abl mutation produced by targeted gene disruption in ES cells. Science *246*, 799-803.

Senft, A.D., Costello, I., King, H.W., Mould, A.W., Bikoff, E.K., and Robertson, E.J. (2018). Combinatorial Smad2/3 Activities Downstream of Nodal Signaling Maintain Embryonic/Extra-Embryonic Cell Identities during Lineage Priming. Cell Rep *24*, 1977-1985 e1977.

Shalaby, F., Ho, J., Stanford, W.L., Fischer, K.D., Schuh, A.C., Schwartz, L., Bernstein, A., and Rossant, J. (1997). A requirement for Flk1 in primitive and definitive hematopoiesis and vasculogenesis. Cell *89*, 981-990.

Shalaby, F., Rossant, J., Yamaguchi, T.P., Gertsenstein, M., Wu, X.F., Breitman, M.L., and Schuh, A.C. (1995). Failure of blood-island formation and vasculogenesis in Flk-1-deficient mice. Nature *376*, 62-66.

Shapiro, E., Biezuner, T., and Linnarsson, S. (2013). Single-cell sequencing-based technologies will revolutionize whole-organism science. Nat Rev Genet *14*, 618-630.

Shivdasani, R.A., Mayer, E.L., and Orkin, S.H. (1995). Absence of blood formation in mice lacking the T-cell leukaemia oncoprotein tal-1/SCL. Nature *373*, 432-434.

Soriano, P. (1999). Generalized lacZ expression with the ROSA26 Cre reporter strain. Nature genetics *21*, 70.

Srinivas, S., Watanabe, T., Lin, C.S., William, C.M., Tanabe, Y., Jessell, T.M., and Costantini, F. (2001). Cre reporter strains produced by targeted insertion of EYFP and ECFP into the ROSA26 locus. BMC Dev Biol *1*, 4.

Stemmer, M., Thumberger, T., Del Sol Keyer, M., Wittbrodt, J., and Mateo, J.L. (2015). CCTop: An Intuitive, Flexible and Reliable CRISPR/Cas9 Target Prediction Tool. PLoS One *10*, e0124633.

Strumpf, D., Mao, C.-A., Yamanaka, Y., Ralston, A., Chawengsaksophak, K., Beck, F., and Rossant, J. (2005). Cdx2 is required for correct cell fate specification and differentiation of trophectoderm in the mouse blastocyst. Development *132*, 2093-2102.

Stuart, T., Butler, A., Hoffman, P., Hafemeister, C., Papalexi, E., Mauck, W.M., 3rd, Hao, Y., Stoeckius, M., Smibert, P., and Satija, R. (2019). Comprehensive Integration of Single-Cell Data. Cell *177*, 1888-1902 e1821.

Swiers, G., Baumann, C., O'Rourke, J., Giannoulatou, E., Taylor, S., Joshi, A., Moignard, V., Pina, C., Bee, T., Kokkaliaris, K.D.*, et al.* (2013). Early dynamic fate changes in haemogenic endothelium characterized at the single-cell level. Nat Commun *4*, 2924.

Tam, P., Parameswaran, M., Kinder, S.J., and Weinberger, R.P. (1997). The allocation of epiblast cells to the embryonic heart and other mesodermal lineages: the role of ingression and tissue movement during gastrulation. Development *124*, 1631-1642.

Tam, P.P., and Loebel, D.A. (2007). Gene function in mouse embryogenesis: get set for gastrulation. Nat Rev Genet *8*, 368-381.

Tanaka, Y., Joshi, A., Wilson, N.K., Kinston, S., Nishikawa, S., and Gottgens, B. (2012). The transcriptional programme controlled by Runx1 during early embryonic blood development. Dev Biol *366*, 404-419.

Teo, A.K.K., Arnold, S.J., Trotter, M.W., Brown, S., Ang, L.T., Chng, Z., Robertson, E.J., Dunn, N.R., and Vallier, L. (2011). Pluripotency factors regulate definitive endoderm specification through eomesodermin. Genes & development *25*, 238-250.

Thambyrajah, R., Mazan, M., Patel, R., Moignard, V., Stefanska, M., Marinopoulou, E., Li, Y., Lancrin, C., Clapes, T., Moroy, T.*, et al.* (2016). GFI1 proteins orchestrate the emergence of haematopoietic stem cells through recruitment of LSD1. Nat Cell Biol *18*, 21-32.

Thurman, R.E., Rynes, E., Humbert, R., Vierstra, J., Maurano, M.T., Haugen, E., Sheffield, N.C., Stergachis, A.B., Wang, H., Vernot, B.*, et al.* (2012). The accessible chromatin landscape of the human genome. Nature *489*, 75-82.

Tosic, J., Kim, G.J., Pavlovic, M., Schroder, C.M., Mersiowsky, S.L., Barg, M., Hofherr, A., Probst, S., Kottgen, M., Hein, L.*, et al.* (2019). Eomes and Brachyury control pluripotency exit and germ-layer segregation by changing the chromatin state. Nat Cell Biol *21*, 1518-1531.

Ueno, H., and Weissman, I.L. (2006). Clonal analysis of mouse development reveals a polyclonal origin for yolk sac blood islands. Developmental cell *11*, 519-533.

Van Den Ameele, J., Tiberi, L., Bondue, A., Paulissen, C., Herpoel, A., Iacovino, M., Kyba, M., Blanpain, C., and Vanderhaeghen, P. (2012). Eomesodermin induces Mesp1 expression and cardiac differentiation from embryonic stem cells in the absence of Activin. EMBO reports *13*, 355-362.

Van Handel, B., Montel-Hagen, A., Sasidharan, R., Nakano, H., Ferrari, R., Boogerd, C.J., Schredelseker, J., Wang, Y., Hunter, S., Org, T.*, et al.* (2012). Scl represses cardiomyogenesis in prospective hemogenic endothelium and endocardium. Cell *150*, 590-605.

Wang, H., Yang, H., Shivalila, C.S., Dawlaty, M.M., Cheng, A.W., Zhang, F., and Jaenisch, R. (2013). One-step generation of mice carrying mutations in multiple genes by CRISPR/Cas-mediated genome engineering. Cell *153*, 910-918.

Wang, Q., Stacy, T., Binder, M., Marin-Padilla, M., Sharpe, A.H., and Speck, N.A. (1996). Disruption of the Cbfa2 gene causes necrosis and hemorrhaging in the central nervous system and blocks definitive hematopoiesis. Proc Natl Acad Sci U S A *93*, 3444-3449.

Wang, Q., Zou, Y., Nowotschin, S., Kim, S.Y., Li, Q.V., Soh, C.L., Su, J., Zhang, C., Shu, W., Xi, Q.*, et al.* (2017). The p53 Family Coordinates Wnt and Nodal Inputs in Mesendodermal Differentiation of Embryonic Stem Cells. Cell Stem Cell *20*, 70-86.

Wareing, S., Mazan, A., Pearson, S., Gottgens, B., Lacaud, G., and Kouskoff, V. (2012). The Flk1-Cre-mediated deletion of ETV2 defines its narrow temporal requirement during embryonic hematopoietic development. Stem Cells *30*, 1521-1531.

Winnier, G., Blessing, M., Labosky, P.A., and Hogan, B.L. (1995). Bone morphogenetic protein-4 is required for mesoderm formation and patterning in the mouse. Genes Dev *9*, 2105-2116.

Yamamoto, M., Saijoh, Y., Perea-Gomez, A., Shawlot, W., Behringer, R.R., Ang, S.L., Hamada, H., and Meno, C. (2004). Nodal antagonists regulate formation of the anteroposterior axis of the mouse embryo. Nature *428*, 387-392.

Yoshikawa, Y., Fujimori, T., McMahon, A.P., and Takada, S. (1997). Evidence that absence of Wnt-3a signaling promotes neuralization instead of paraxial mesoderm development in the mouse. Dev Biol *183*, 234-242.

Yoshimoto, M., Porayette, P., Glosson, N.L., Conway, S.J., Carlesso, N., Cardoso, A.A., Kaplan, M.H., and Yoder, M.C. (2012). Autonomous murine T-cell progenitor production in the extra-embryonic yolk sac before HSC emergence. Blood *119*, 5706-5714.

Yzaguirre, A.D., Howell, E.D., Li, Y., Liu, Z., and Speck, N.A. (2018). Runx1 is sufficient for blood cell formation from non-hemogenic endothelial cells in vivo only during early embryogenesis. Development *145*.

Zhang, Y., Liu, T., Meyer, C.A., Eeckhoute, J., Johnson, D.S., Bernstein, B.E., Nusbaum, C., Myers, R.M., Brown, M., Li, W.*, et al.* (2008). Model-based analysis of ChIP-Seq (MACS). Genome Biol *9*, R137.

Zhao, H., and Choi, K. (2017). A CRISPR screen identifies genes controlling Etv2 threshold expression in murine hemangiogenic fate commitment. Nat Commun *8*, 541.

Zhao, H., Sun, Z., Wang, J., Huang, H., Kocher, J.P., and Wang, L. (2014). CrossMap: a versatile tool for coordinate conversion between genome assemblies. Bioinformatics *30*, 1006-1007.

Zhao, H., Xu, C., Lee, T.J., Liu, F., and Choi, K. (2017). ETS transcription factor ETV2/ER71/Etsrp in hematopoietic and vascular development, injury, and regeneration. Dev Dyn *246*, 318-327.